The Astrophysical Journal Supplement Series, 150:187–237, 2004 January

PARSEC-SCALE BLAZAR MONITORING: THE DATA

Roopesh Ojha,[1] Daniel C. Homan,[2] David H. Roberts,[3] and John F. C. Wardle[3]
Physics Department, Brandeis University, MS-057, Waltham, MA 02454

and

Margo F. Aller,[4] Hugh D. Aller,[4] and Philip A. Hughes[4]
Radio Astronomy Observatory, University of Michigan, Ann Arbor, MI 48109
Received 2003 March 26; accepted 2003 September 9

ABSTRACT

We present the images and modeling data obtained from a dual frequency, six-epoch, VLBA polarization experiment monitoring a sample of 12 blazars. The observations were made at 15 and 22 GHz at evenly spaced, bimonthly intervals over 1996. The advent of the VLBA makes possible a data set with reliable calibration as well as regular and frequent temporal sampling. Detection of circular polarization, proper motion studies, and flux and polarization variability in the sample are some of the topics that such a data set makes available for robust investigation.

Subject headings: galaxies: active — galaxies: jets — galaxies: kinematics and dynamics — galaxies: Seyfert

1. INTRODUCTION

Perhaps the most distinctive feature of compact radio sources is their variability, in total flux as well as polarization (e.g., Aller et al. 1985). The most variable of these sources tend to be the more extreme members of the blazar family with typically 1–3 VLBI ''components'' emerging from their cores annually. Comprehensive observations of these components could help elucidate jet formation, evolution, and composition, as well as casting light on the still unresolved core region which includes the putative central black hole.

We have used the quick turnaround time of the National Radio Astronomy Observatory's (NRAO) Very Long Baseline Array (VLBA)[5] to monitor the milliarcsecond (mas) structure of a sample of blazars. This is the third in a series of papers where the results from this monitoring program are reported.

In Homan et al. (2001, hereafter Paper I), we presented our analysis of proper motion in these objects. Homan et al. (2002, hereafter Paper II) discusses flux density and polarization variability in this sample. In this paper we present the entire data set; all the images, total flux and polarization, as well as polarization position angle, for every epoch. We also present the modeled data in tabular form and plots illustrating variations in relevant core and jet observables. Finally, we include single-dish monitoring data from the University of Michigan Radio Astronomy Observatory (UMRAO) in order to compare activity at the two resolutions.

A major result from this observing program, the detection of circular polarization, was reported in Wardle et al. (1998) and Homan & Wardle (1999).

Section 2 describes our sample, data reduction, model-fitting procedures and our conventions and assumptions. In § 3 we present the images, tables, and plots for each observed source. We also briefly touch upon the major changes observed in each source and comment upon the reliability of its model fitting. The Appendix contains a table and plots of the core region and jet feature properties, which are analyzed in detail in Paper II.

2. OBSERVATIONS

2.1. *The Sample*

We used the VLBA to conduct a series of six experiments, each of 24 hr duration, at (close to) two month intervals during the year 1996. The observations were made at 15 GHz (λ2 cm, *U* band) (Homan 1999) and 22 GHz (λ1.3 cm, *K* band) (Ojha 1998). We observed 11 target sources for six epochs and one (J1224+21) for the latter five epochs. These sources are listed in Table 1. The epochs, labeled A through F throughout this paper, are listed in Table 2.

The sources were chosen from those regularly monitored by the UMRAO in total intensity and polarization at 4.8, 8.0, and 14.5 GHz. They were selected according to the following criteria.

1. *High total intensity.*—The weakest sources are about 1 Jy, the most powerful are as much as 22 Jy.
2. *High polarized flux*.—Typically over 50 mJy.
3. *Violently variable*.—In both total and polarized intensity. Such sources are likely to be undersampled by annual VLBI.
4. *Well distributed in right ascension*.—This allowed us to make an optimal observing schedule.

Most of the UMRAO sources meet the first three of the above criteria. The 12 actually selected were the strongest, most violently variable sources, subject to the fourth criteria. Clearly these sources do not comprise a ''complete sample'' in any sense.

2.2. *Data Calibration*

The frequency agility and high slew speeds of the VLBA antennas were used to schedule our observations to generate

[1] Current address: Australia Telescope National Facility, CSIRO, P.O. Box 76, Epping, NSW 1710, Australia; rojha@atnf.csiro.au.
[2] Current address: National Radio Astronomy Observatory, Charlottesville, VA 22901; dhoman@nrao.edu.
[3] wardle@brandeis.edu, roberts@brandeis.edu.
[4] margo@astro.lsa.umich.edu, hugh@astro.lsa.umich.edu, hughes@astro.lsa.umich.edu.
[5] The National Radio Astronomy Observatory is a facility of the National Science Foundation operated under cooperative agreement by Associated Universities, Inc.

TABLE 1
SOURCE INFORMATION

Coordinate Name (J2000.0)	Coordinate Name (B1950.0)	Other Names	Redshift	Classification
J0433+053	B0430+052	3C120, II Zw 14	0.033	Sy 1
J0530+135[a]	B0528+134	PKS 0528+134	2.060	Quasar
J0738+177	B0735+178	OI 158, DA 237, PKS 0735+178	0.424[b]	BL Lac
J0854+201[a]	B0851+202	OJ 287	0.306	BL Lac
J1224+212[a]	B1222+216	4C 21.35	0.435	Quasar
J1229+020	B1226+023	3C 273	0.158	Quasar
J1256−057[a]	B1253−055	3C 279	0.536	Quasar
J1310+323	B1308+326	OP 313	0.996	Quasar/BL Lac
J1512−090	B1510−089	OR −017	0.360	Quasar
J1751+09	B1749+096	OT 081, 4C 09.56	0.322	BL Lac
J1927+739	B1928+738	4C 73.18	0.302	Quasar
J2005+778	B2007+777		0.342	BL Lac

[a] Also observed in epoch 1997.94 (G).
[b] Lower limit.

maximal (u, v) coverage. Each observation of a source (a scan) was kept short (13 minutes for the first two epochs and 5.5 minutes for the last four) with a switch in frequency at the end of each scan. In addition, scans of neighboring sources were heavily interleaved at the cost of some additional slew time. Each source was observed for approximately 45 minutes per frequency at each epoch.

The data were correlated at the VLBA correlator in Socorro, NM. The correlator output contained 2 s integrations for all four cross-correlations (RR, RL, LR, LL), each with four IFs and 16 channels per IF. After correlation, the data were distributed on DAT tape to Brandeis University, where they were loaded into NRAO's Astronomical Imaging Processing System (AIPS; Bridle & Greisen 1994; Greisen 1988) and calibrated using standard techniques for VLBI polarization observations (e.g., Cotton 1993; Roberts, Wardle, & Brown 1994).

Here we summarize our general calibration procedures. It is important to note that VLBI calibration is highly interactive and the exact details of our calibration path differ slightly between source, frequency, and epoch. In particular, the need to confirm the detection of circular polarization in some of our sources required additional and different calibration steps as detailed in Homan & Wardle (1999).

Following a careful inspection of the data and supplied tables, the task UVFLG read in the supplied flagging information and applied the initial edits. Then the task CLCOR was used to remove the phase of the parallactic angle from the residual phases. Prior to fringe fitting, the supplied pulse calibration information was applied with the task PCCOR.[6] Global fringe fitting was performed with the AIPS task FRING, after choosing a stable, central reference antenna such as Los Alamos (LA) or Pie Town (PT). The AIPS procedure CROSSPOL then removed the multiband delay difference between the right- and left-hand systems of the array. Initial amplitude calibration was from measured system temperatures and atmospheric opacity (using the tasks ANTAB and APCAL). A bandpass correction was then determined with the task BPASS before averaging across the channels within each IF.

[6] The only exception is epoch A, where a manual phase calibration was used to align the phases across IF. "IF" is an acronym for "intermediate frequency," which in this context refers to a single signal path between a telescope and the correlator. Our total bandpass is divided into IFs that are adjacent in frequency. IFs should be distinguished from the narrow spectral channels into which they are subdivided as the geometrical and propagation errors affecting the data can be large enough to cause significant phase changes across an IF bandwidth.

TABLE 2
UT EPOCHS OF OBSERVATION

Epoch	Day	Label	Notes
1996.05	Jan 19	A	[a]
1996.23	Mar 22	B	[b]
1996.41	May 27	C	[c]
1996.57	Jul 27	D	
1996.74	Sep 27	E	[d, e]
1996.93	Dec 06	F	[f]
1997.94	Dec 07	G	[g]

[a] North Liberty antenna off-line for entire experiment.
[b] Owens Valley antenna off-line for entire experiment.
[c] No fringes found to the Kitt Peak antenna.
[d] North Liberty antenna off-line for second half of experiment.
[e] Some data loss from the Owens Valley antenna.
[f] Numerous problems spread over several antennas; poor data quality compared with the other epochs.
[g] For four sources only.

Following a short timescale, point source[7] phase calibration to improve coherence, the data were averaged in time (to 20 s at 15 GHz and 10 s at 22 GHz) and written out to the Caltech VLBI program DIFMAP (Shepherd 1997). The data were then edited in a station-based manner. Initial rounds of self-calibration and imaging were performed in DIFMAP before moving the data back to the AIPS analysis package.

After additional imaging and phase self-calibration passes in AIPS, the effects of feed leakage (D-terms) were removed from the parallel and cross-hand data. The antenna D-terms were determined from observations of the strong, compact sources J0530+13 or OJ 287, using the program LPCAL in AIPS (Leppänen, Zensus, & Diamond 1995). The amplitudes of the D-terms (i.e., the percentage of nominally orthogonally polarized flux a feed receives) ranged from approximately 1% to 5% with values close to 2% being most typical. After D-term removal, the sources were imaged in total intensity and polarization using the AIPS task IMAGR.

Calibration of the phase offset between the two orthogonal polarizations at the reference antenna, which allows determination of the polarization position angle (also known as Electric Vector Position Angle or EVPA), was done in the following manner. At each epoch and at both 15 and 22 GHz we aligned the strong jet component U1(K1) in 3C 279 to an angle of 67°. This orientation is roughly parallel to the structural position angle for this component and is within 5° of the independently calibrated observations of Leppänen et al. (1995), Taylor (1998), and Homan & Wardle (2000), whose epochs of observation bracket our own. Examination of the other sources in our sample reveals no significant Faraday rotation at these frequencies and no variation in EVPA over the period of our observations. This EVPA calibration procedure has resulted in very good internal consistency between epochs with uncertainties $\sim 2^\circ$–3° on the most robust jet features (see Appendix of Paper II).

2.3. *Modeling the Data*

Our approach to model fitting was empirical and conservative. We chose to fit the visibilities instead of modeling in the image plane, which is one step removed from the data. We fitted the visibility data with elliptical Gaussians (though point sources were used occasionally) as this made the fewest assumptions about the nature of the components. We sought to obtain the simplest possible model, i.e., the model with the least number of components that gave a good fit to the data as judged by a relative chi-squared statistic. In addition, for a fit to a source to be considered acceptable we required the components to contain $\gtrsim 95\%$ of the total flux and a convolution of the model components with the beam to be similar to the CLEAN image of the source. In some cases it was possible to fit an additional component, but we have not done so unless its presence led to a significant improvement in the quality of the fit. Several techniques were used to ensure that a fit was not a local minimum; these included trying different starting points and deliberately perturbing the final model.

No attempt was made to "drive" the fit toward previous models where such models exist in the literature. Indeed, we intentionally remained ignorant of such models to keep our work unbiased during this part of the analysis. We did try to maintain consistency between the model-fits, across both epoch and frequency of our observations; however, the primary goal was always to obtain the best representation of the data in that epoch and at that frequency.

The linear polarization was fitted in Stokes Q and U separately using the total intensity model with component positions and sizes held fixed. Linear polarization may be displaced from total intensity structure, and fitting the linear polarization in this fashion can result in a poor representation of the polarization data. However, we have found that, in general, the models for the strongly polarized structures seem to agree reasonably well with the CLEAN images. We strongly encourage readers who wish to make use of this data to closely compare model fit results with the polarization images to gauge reliability. It should be noted that our analysis of the components from epoch to epoch (in Paper II) took this issue into account by summing together nearby components, thereby greatly increasing the robustness of the results in both total intensity and polarization.

Modeling a jet with Gaussian components will work best with sources that are dominated by discrete, well-separated structures. We had the most difficulty in fitting sources that have complex morphology with a large fraction of flux in smooth, extended structures (e.g., 3C 120). As described in detail in Papers I and II, deciding which components and which properties of components are reliable tracers of changes within a source is key to the interpretation of modeling data. While we do not present physical interpretations here, we have provided notes on our impressions of the reliability of particular model components and their properties, and we refer readers to Papers I and II for examples of how these data have been interpreted.

3. RESULTS

In this section we present total intensity, polarization, and polarization position angle images of all our sources at all epochs and at both frequencies. We then present tables that contain all our model fitting data. Next we display plots comparing our 15 GHz VLBA data with single- dish monitoring data from UMRAO. We conclude by commenting briefly on the major changes seen in each source and the reliability of the model for that source. Plots of the core region and jet feature properties are in the Appendix. For a detailed discussion of proper motions see Paper I. For details on the flux and polarization variability see Paper II.

3.1. *The Images*

Figures 1–26 display the images of all 12 AGNs monitored in this program. In each figure the total intensity images are shown in the first column with $\sqrt{2}$ contours and the positions of the components marked. The zero of the abscissa corresponds to the core position. The images in the center column show polarized intensity contours with the lowest total intensity contour to indicate where the polarization lies. The tick marks show the direction of the inferred electric field component in the plane of the sky. The length of the tick marks has no significance. The images in the third column show gray-scale polarization on total intensity times 2 contours. The total intensity beam size is indicated by the cross at the end of each row. Note that in Figures 9, 10, 19, 20, 23, and 24 the total intensity, polarized intensity, and gray-scale polarization images are shown in the top, middle, and bottom rows, respectively.

[7] After epoch A, the source model from a previous epoch was used in place of a point source model for the initial phase coherence calibration.

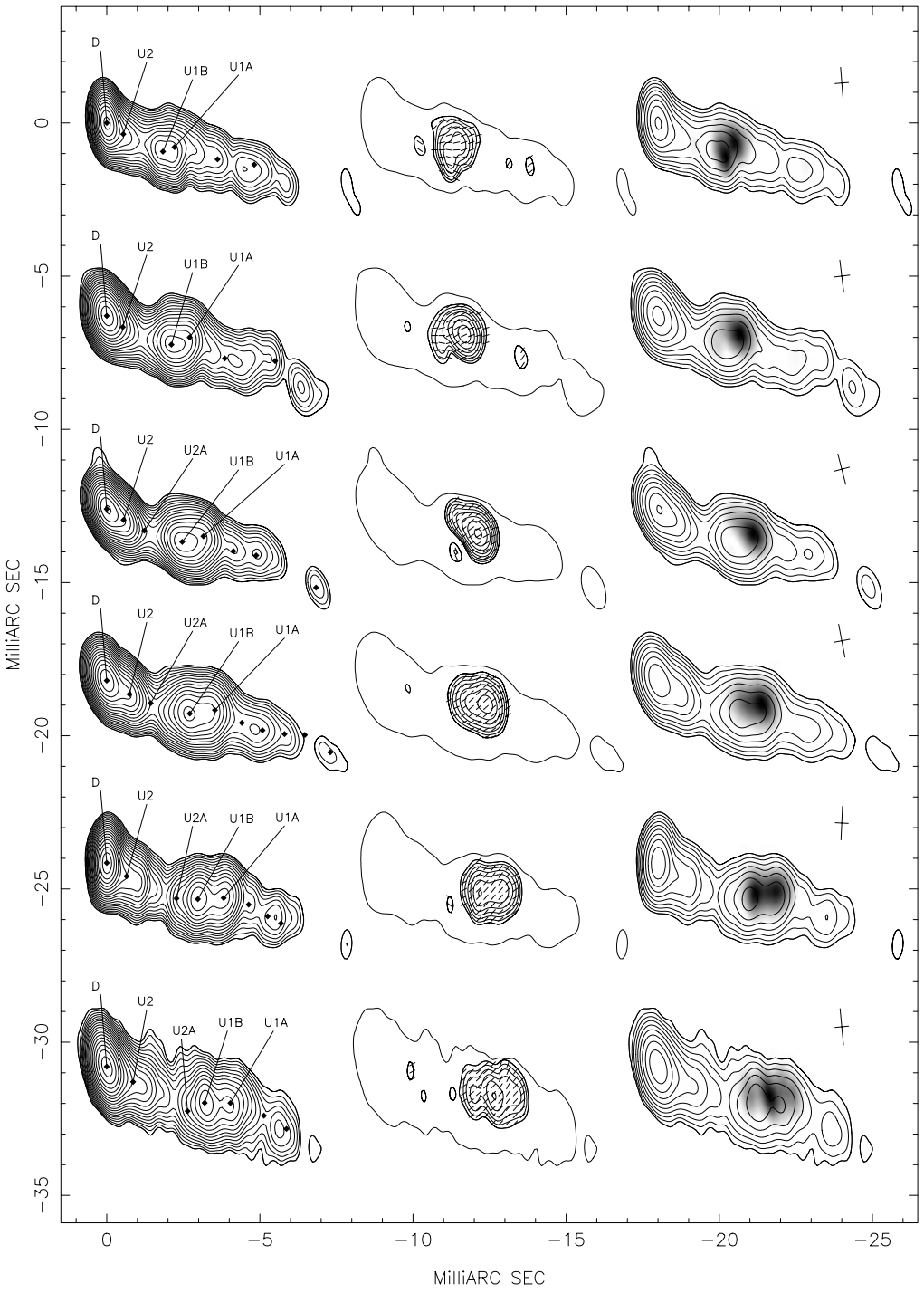

FIG. 1.—15 GHz images of 3C 120 at all six epochs. Figures are laid out as described in § 3.1. Contours in the Stokes *I* images begin at 3 mJy, and contours in the polarized images begin at 3 mJy.

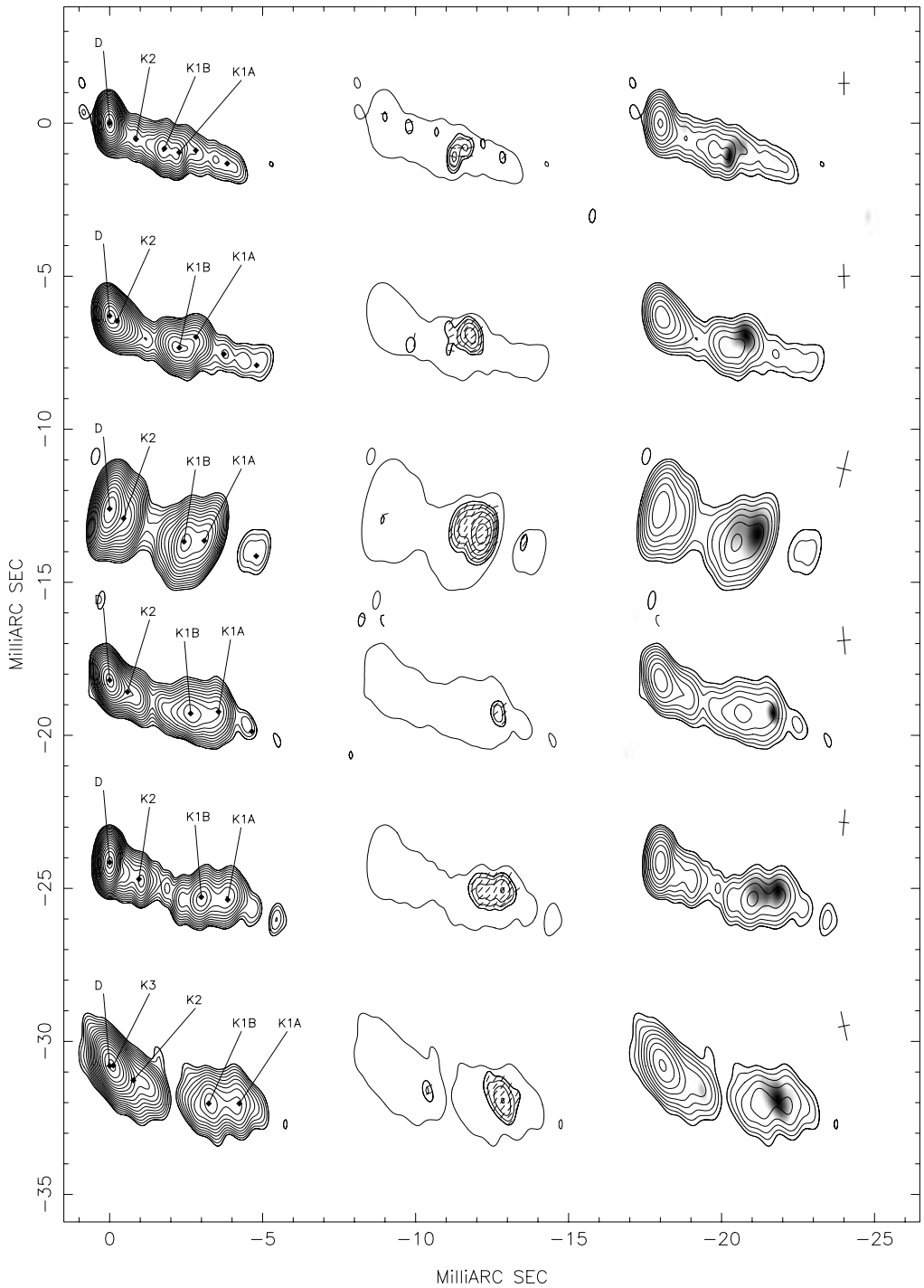

FIG. 2.—22 GHz images of 3C 120 at all six epochs. Figures are laid out as described in § 3.1. Contours in the Stokes *I* images begin at 4 mJy, and contours in the polarized images begin at 4 mJy.

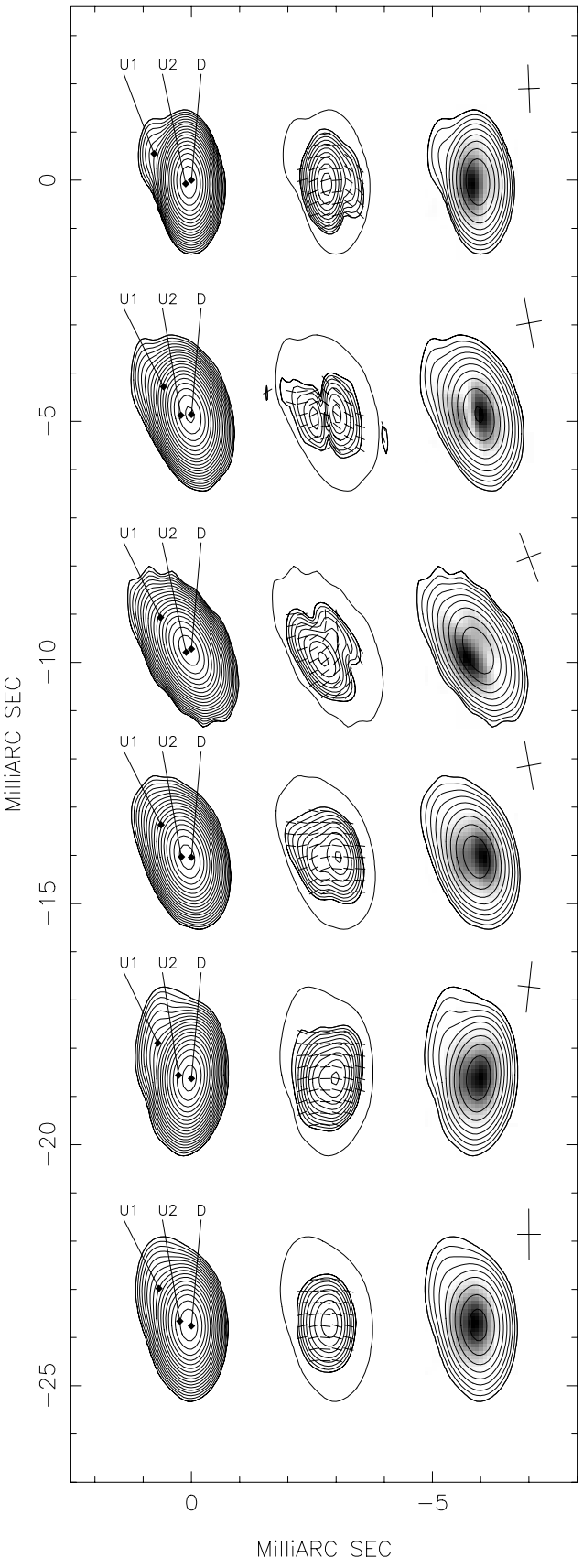

FIG. 3.—15 GHz images of J0530+135 at all six epochs. Figures are laid out as described in § 3.1. Contours in the Stokes *I* images begin at 15 mJy, and contours in the polarized images begin at 8 mJy.

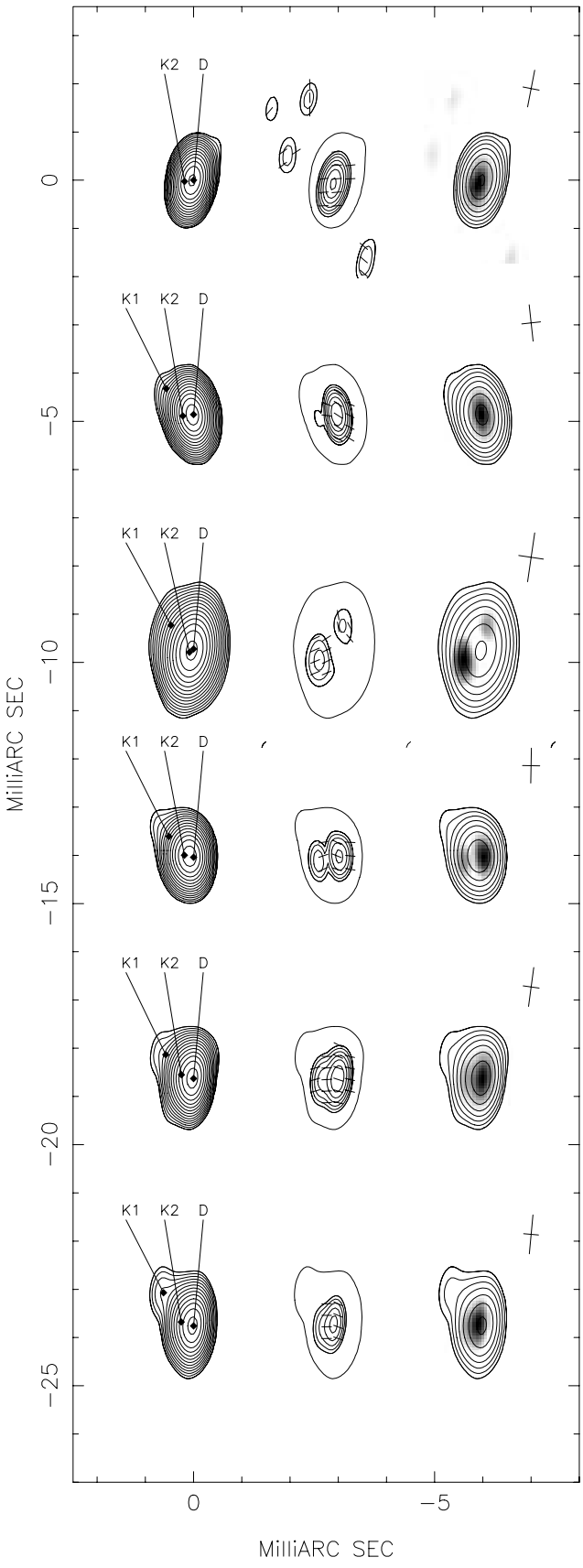

FIG. 4.—22 GHz images of J0530+135 at all six epochs. Figures are laid out as described in § 3.1. Contours in the Stokes *I* images begin at 50 mJy, and contours in the polarized images begin at 30 mJy.

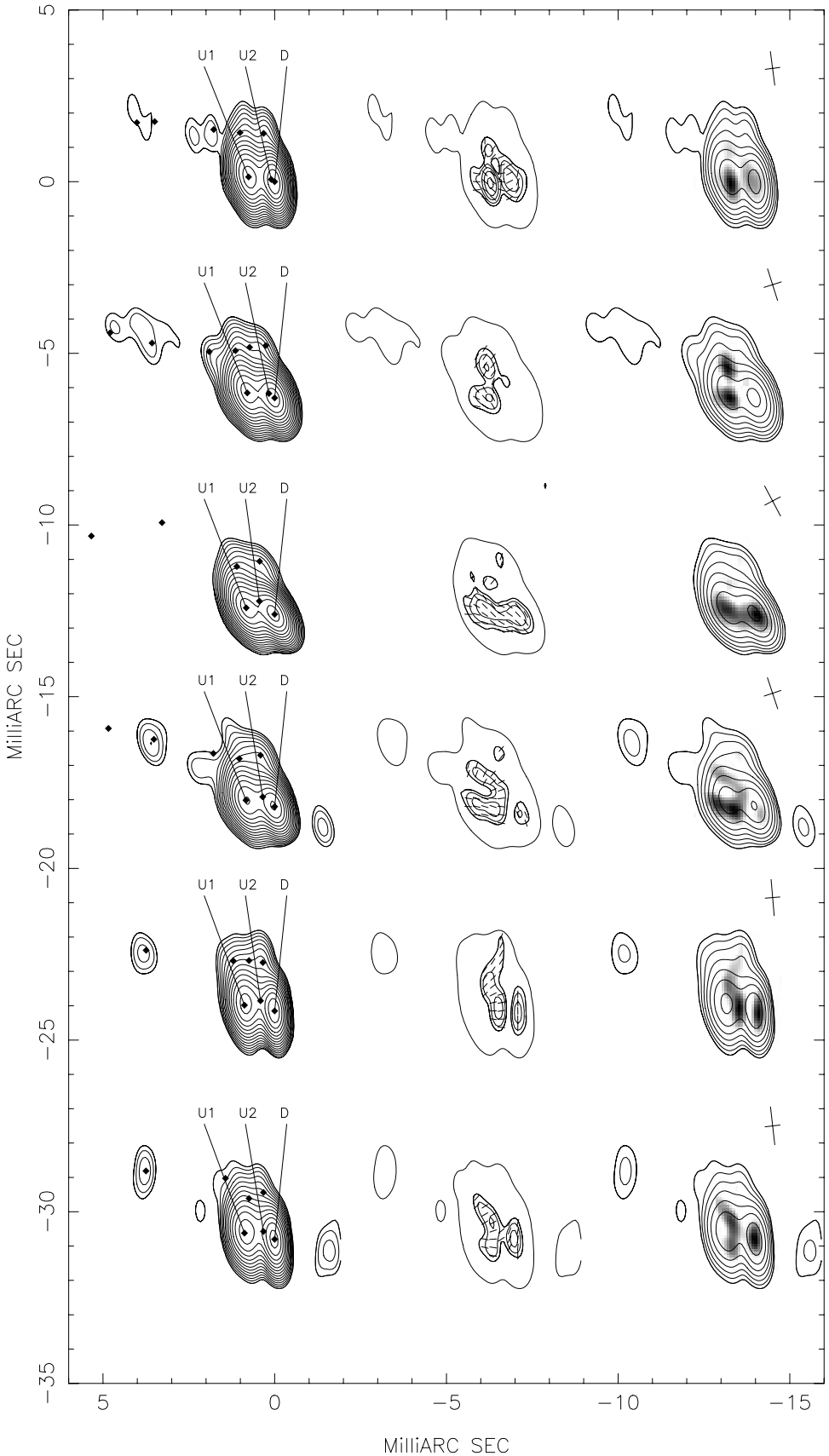

FIG. 5.—15 GHz images of J0738+177 at all six epochs. Figures are laid out as described in § 3.1. Contours in the Stokes *I* images begin at 3 mJy, and contours in the polarized images begin at 3 mJy.

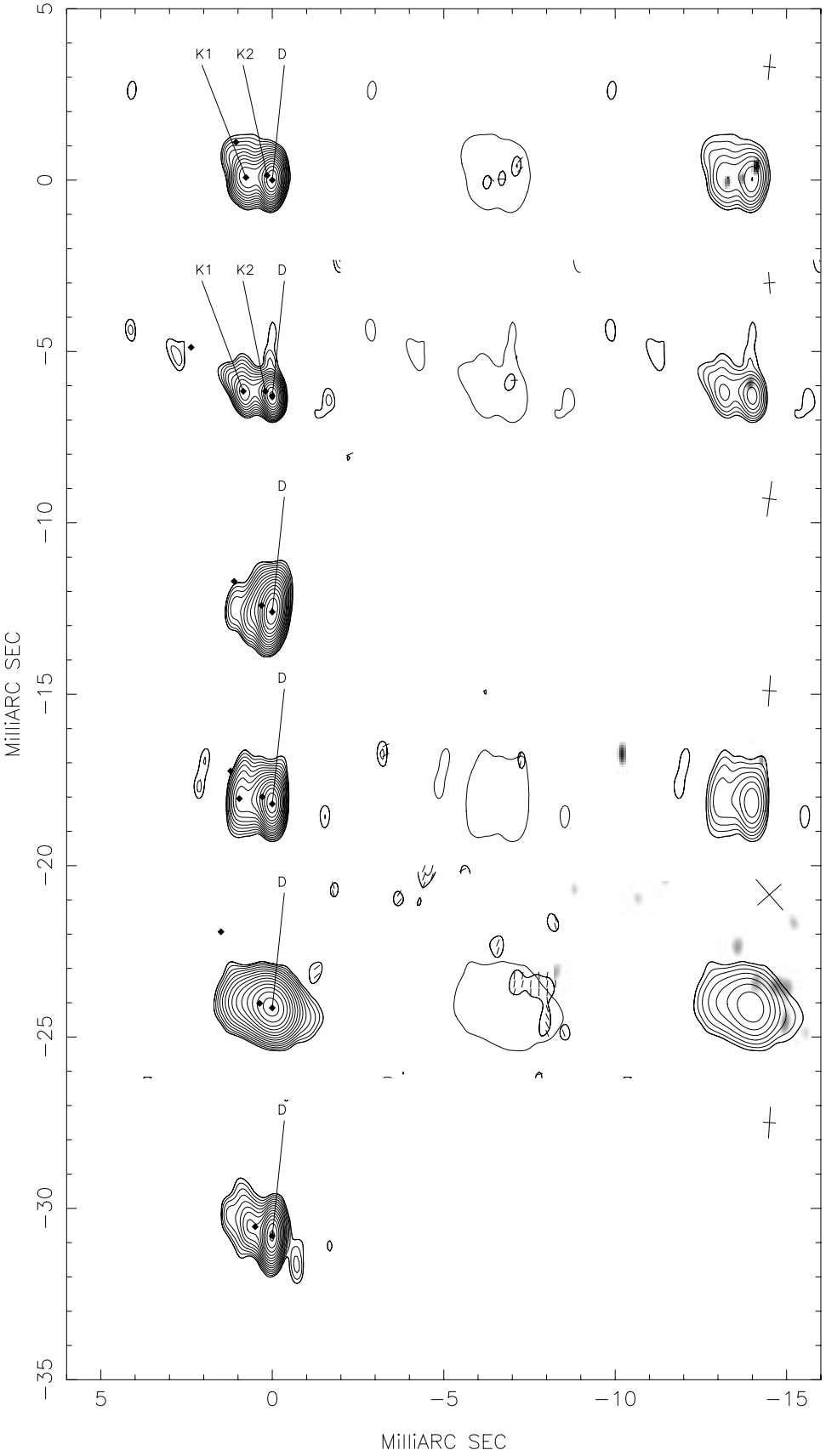

FIG. 6.—22 GHz images of J0738+177 at all six epochs. Figures are laid out as described in § 3.1. Contours in the Stokes *I* images begin at 5 mJy, and contours in the polarized images begin at 5 mJy.

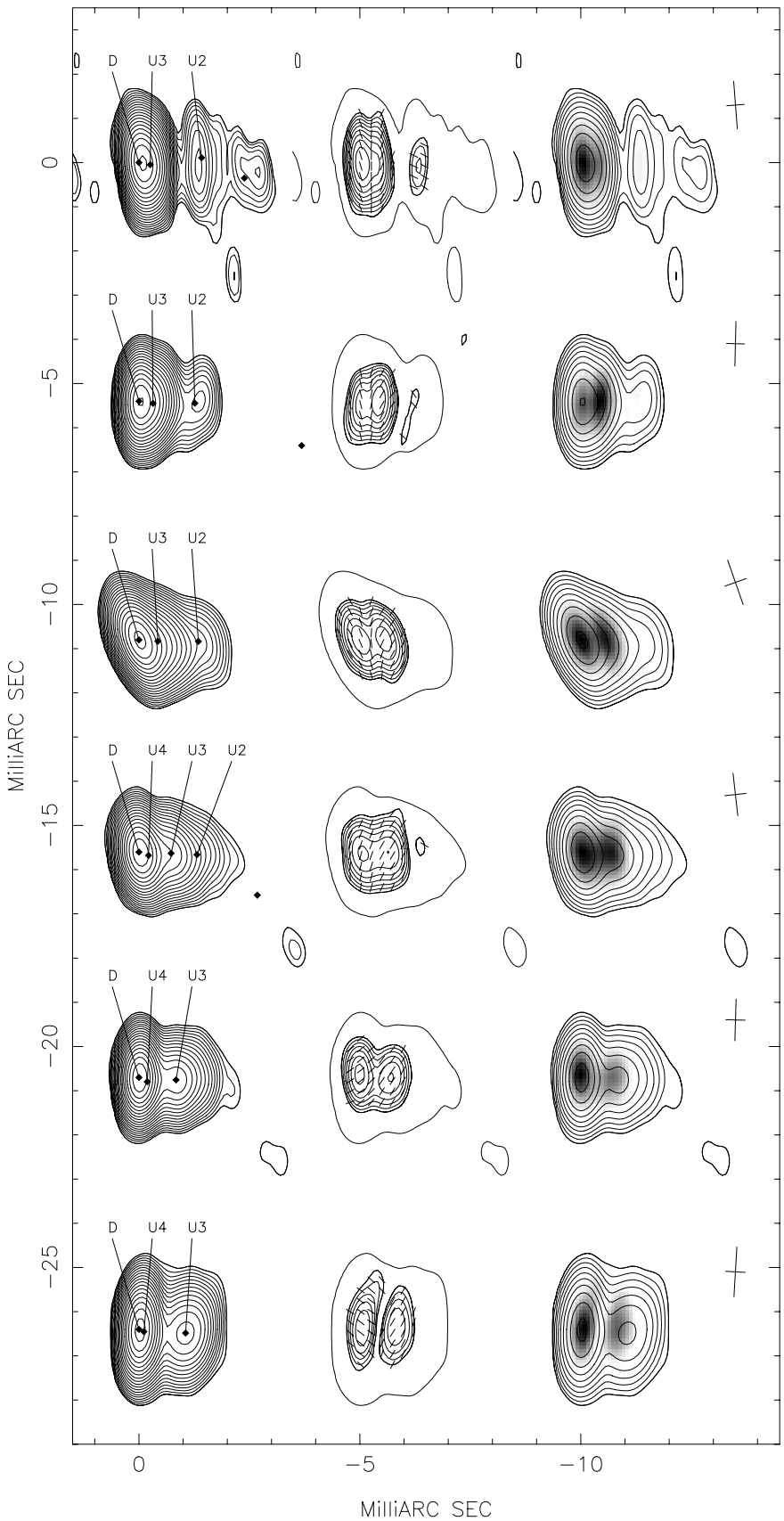

FIG. 7.—15 GHz images of OJ 287 at all six epochs. Figures are laid out as described in § 3.1. Contours in the Stokes *I* images begin at 2 mJy, and contours in the polarized images begin at 3 mJy.

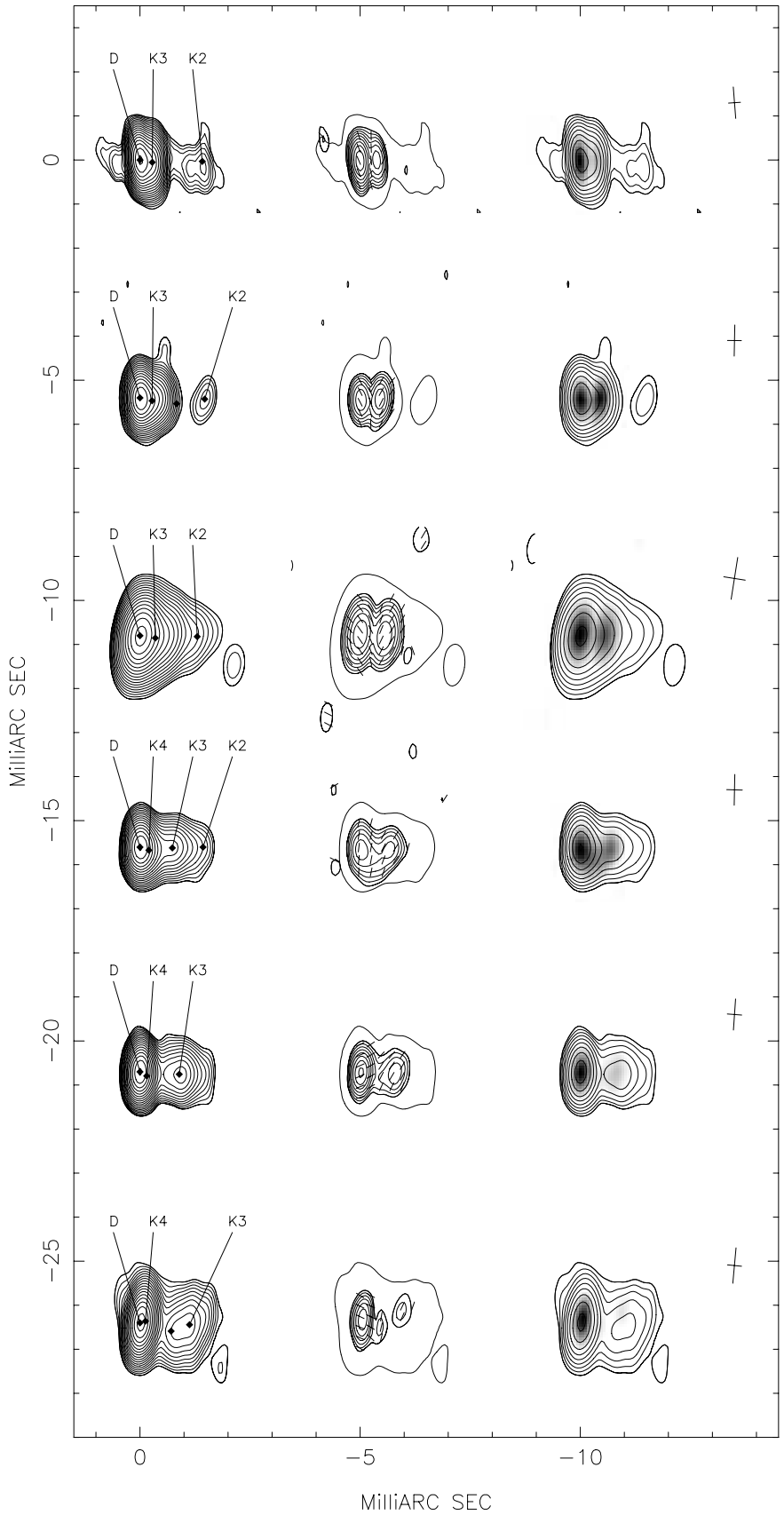

FIG. 8.—22 GHz images of OJ 287 at all six epochs. Figures are laid out as described in § 3.1. Contours in the Stokes *I* images begin at 4 mJy, and contours in the polarized images begin at 3 mJy.

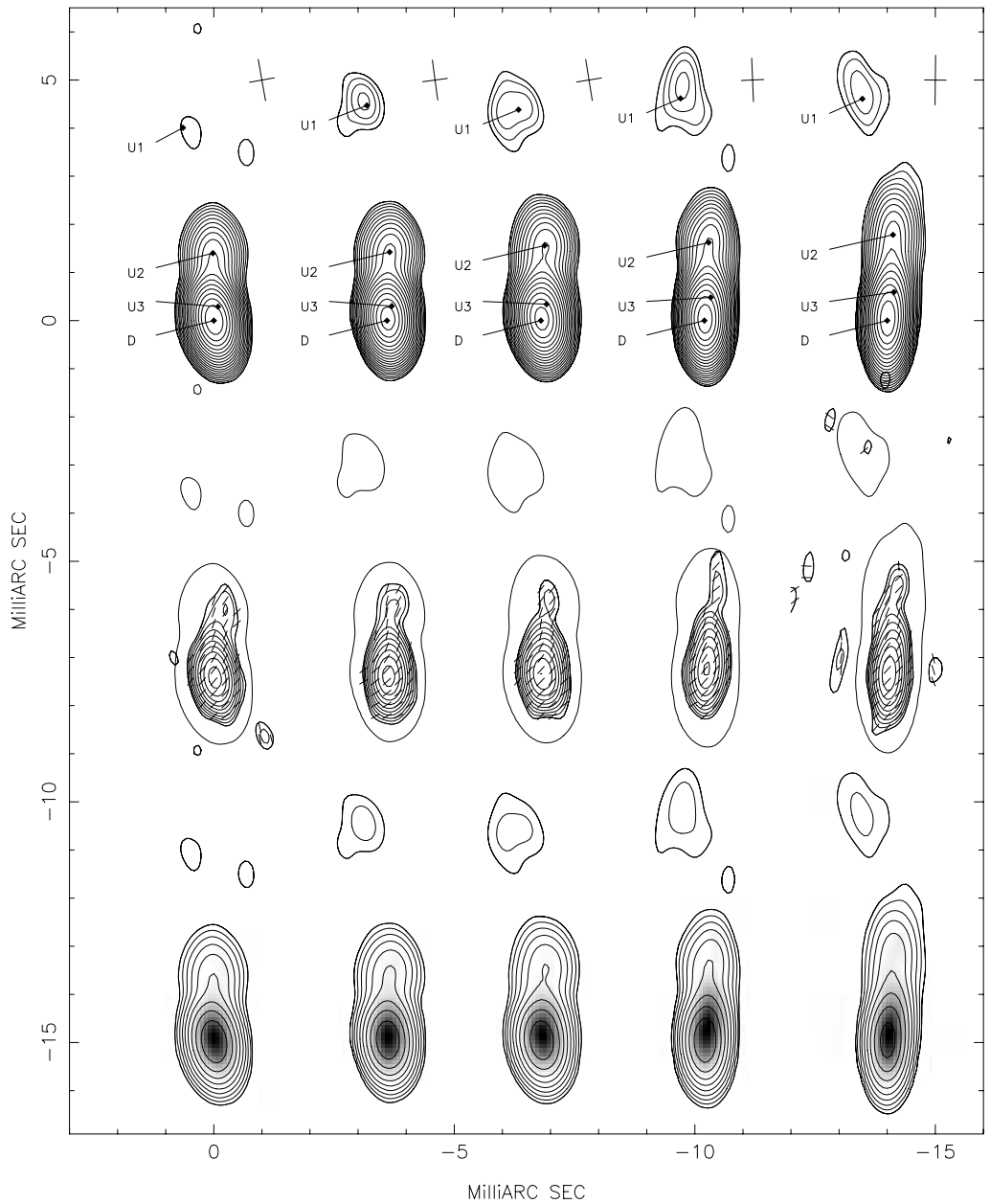

FIG. 9.—15 GHz images of J1224+212 at all six epochs. Figures are laid out as described in § 3.1. Contours in the Stokes *I* images begin at 3 mJy, and contours in the polarized images begin at 3 mJy.

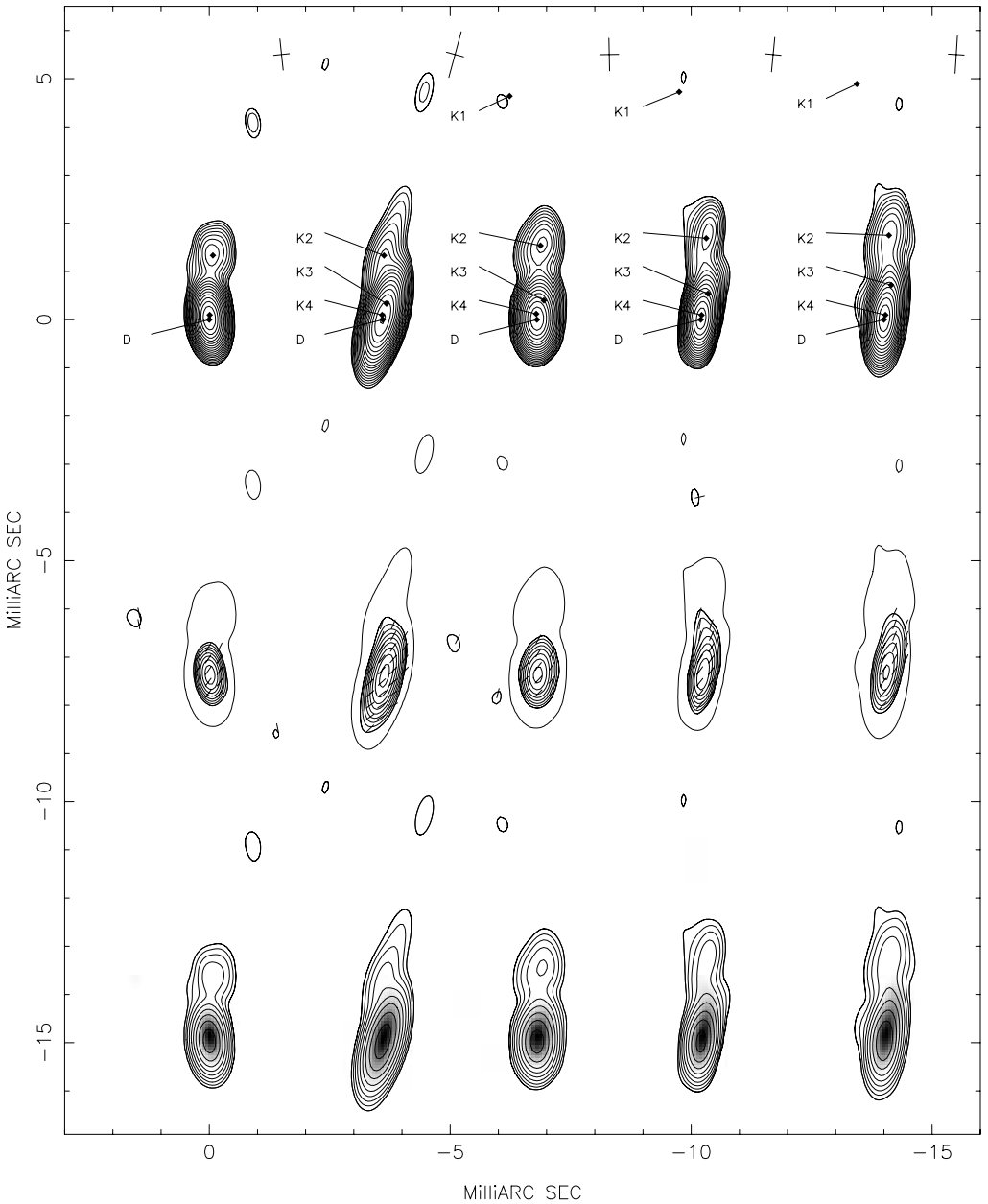

FIG. 10.—22 GHz images of J1224+212 at all six epochs. Figures are laid out as described in § 3.1. Contours in the Stokes *I* images begin at 4 mJy, and contours in the polarized images begin at 4 mJy.

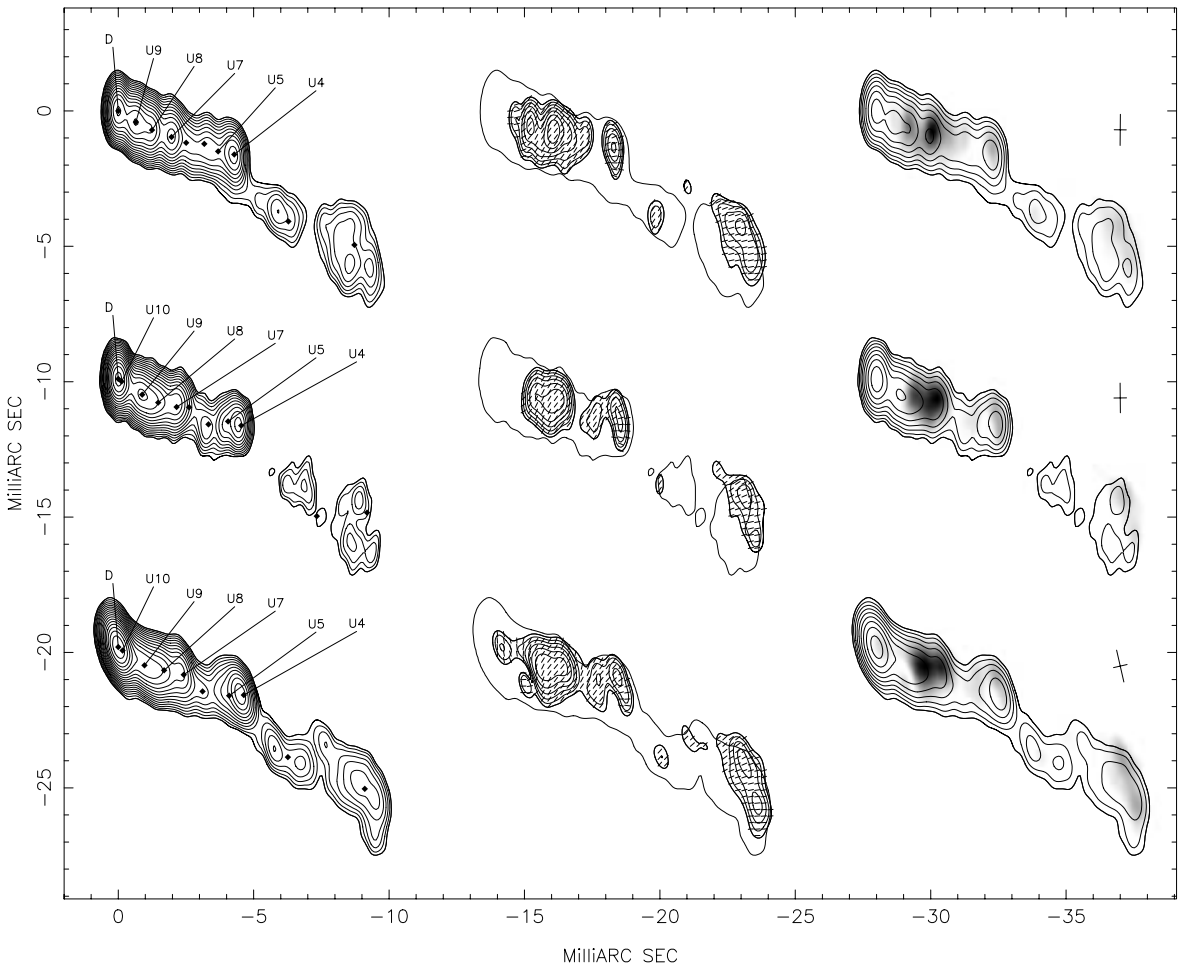

FIG. 11.—15 GHz images of 3C 273 at the first three epochs. Figures are laid out as described in § 3.1. Contours in the Stokes *I* images begin at 30 mJy, and contours in the polarized images begin at 15 mJy.

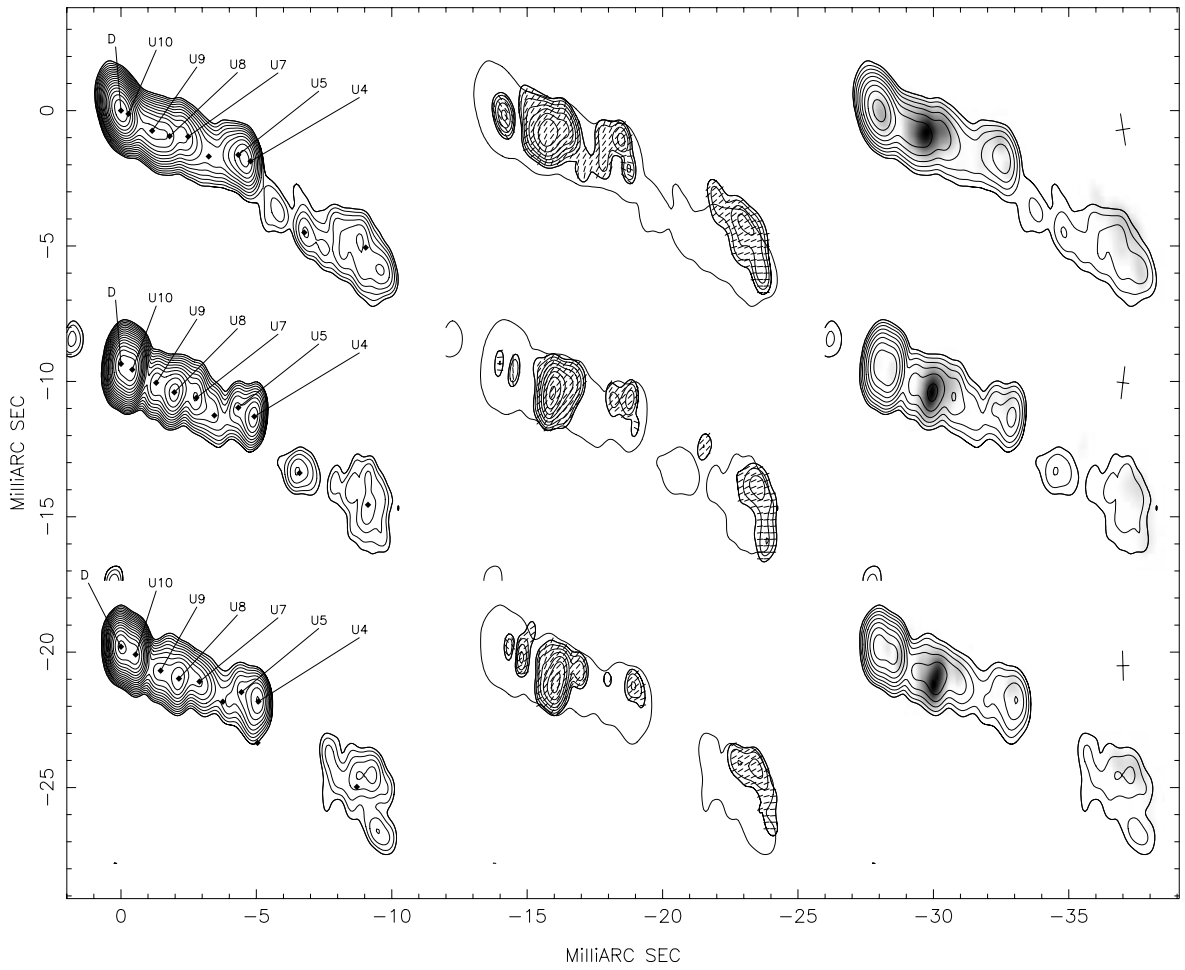

FIG. 12.—15 GHz images of 3C 273 at the latter three epochs. Figures are laid out as described in § 3.1. Contours in the Stokes *I* images begin at 30 mJy, and contours in the polarized images begin at 15 mJy.

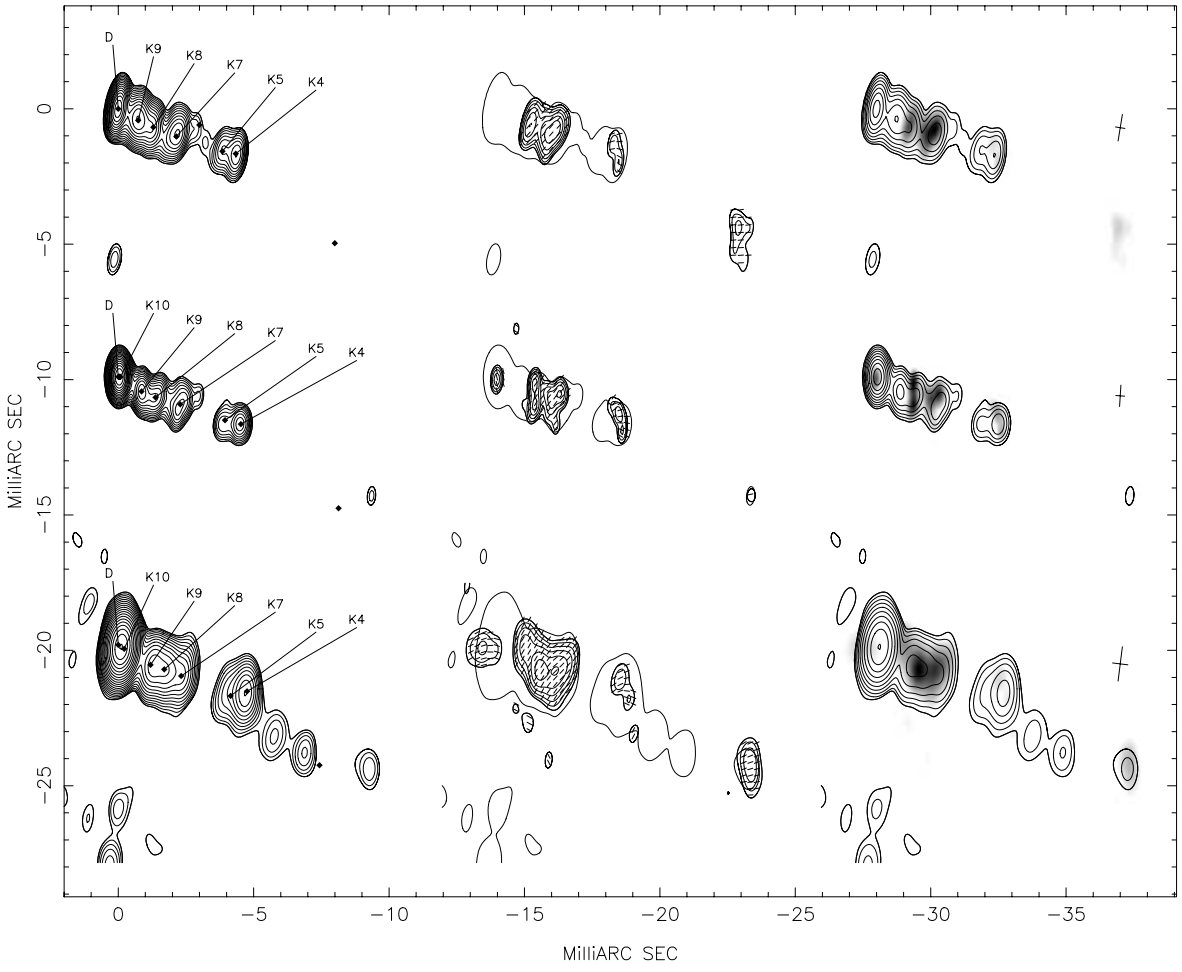

FIG. 13.—22 GHz images of 3C 273 at the first three epochs. Figures are laid out as described in § 3.1. Contours in the Stokes *I* images begin at 30 mJy, and contours in the polarized images begin at 15 mJy.

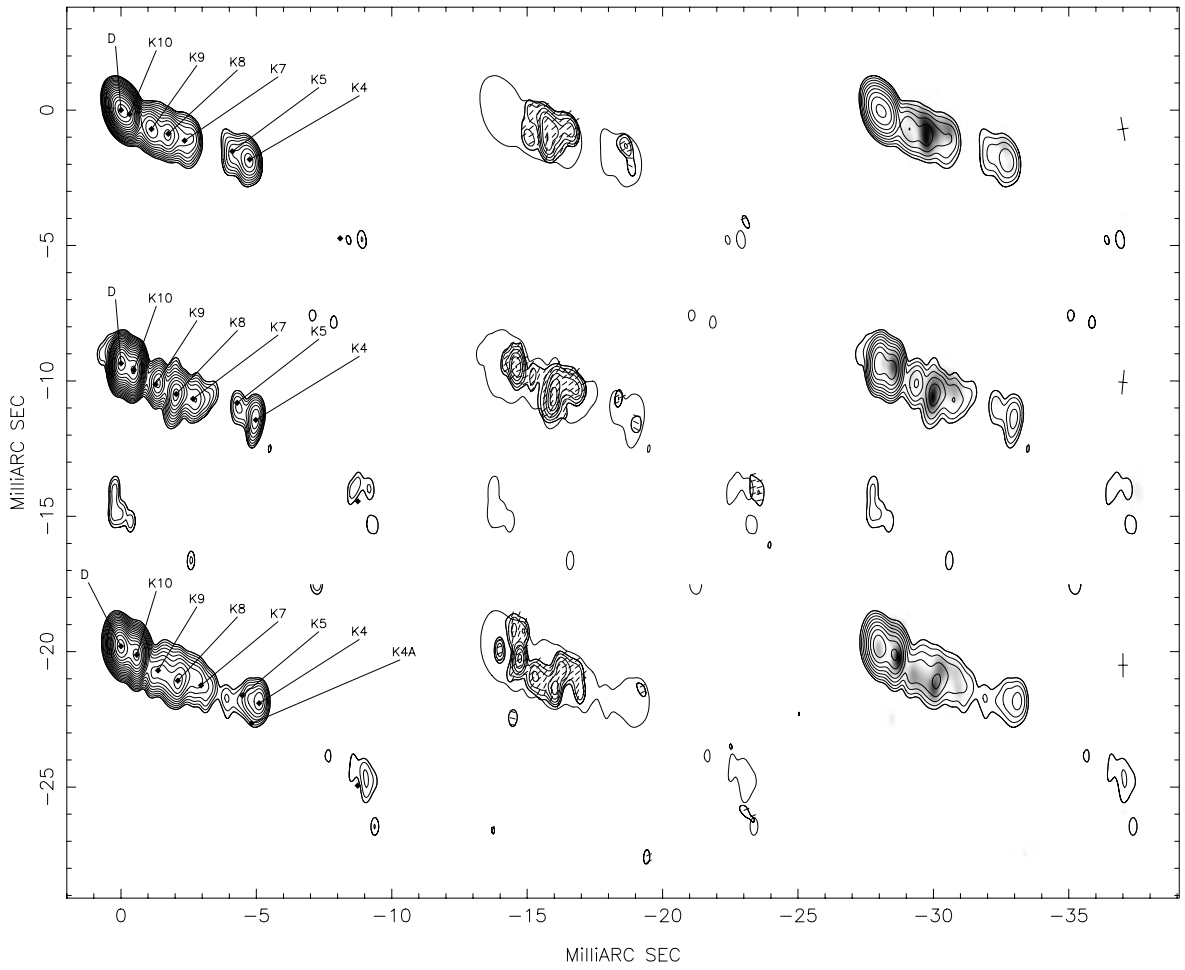

FIG. 14.—22 GHz images of 3C 273 at the latter three epochs. Figures are laid out as described in § 3.1. Contours in the Stokes *I* images begin at 30 mJy, and contours in the polarized images begin at 15 mJy.

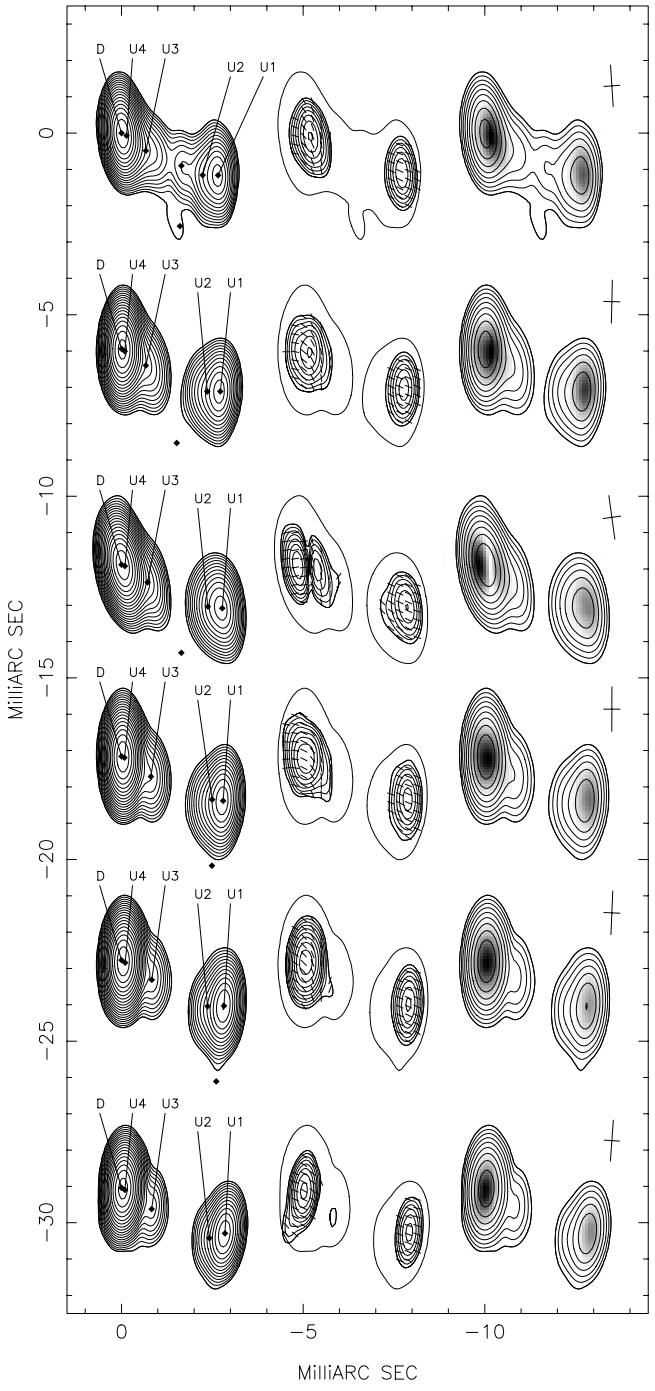

FIG. 15.—15 GHz images of 3C 279 at all six epochs. Figures are laid out as described in § 3.1. Contours in the Stokes *I* images begin at 30 mJy, and contours in the polarized images begin at 30 mJy.

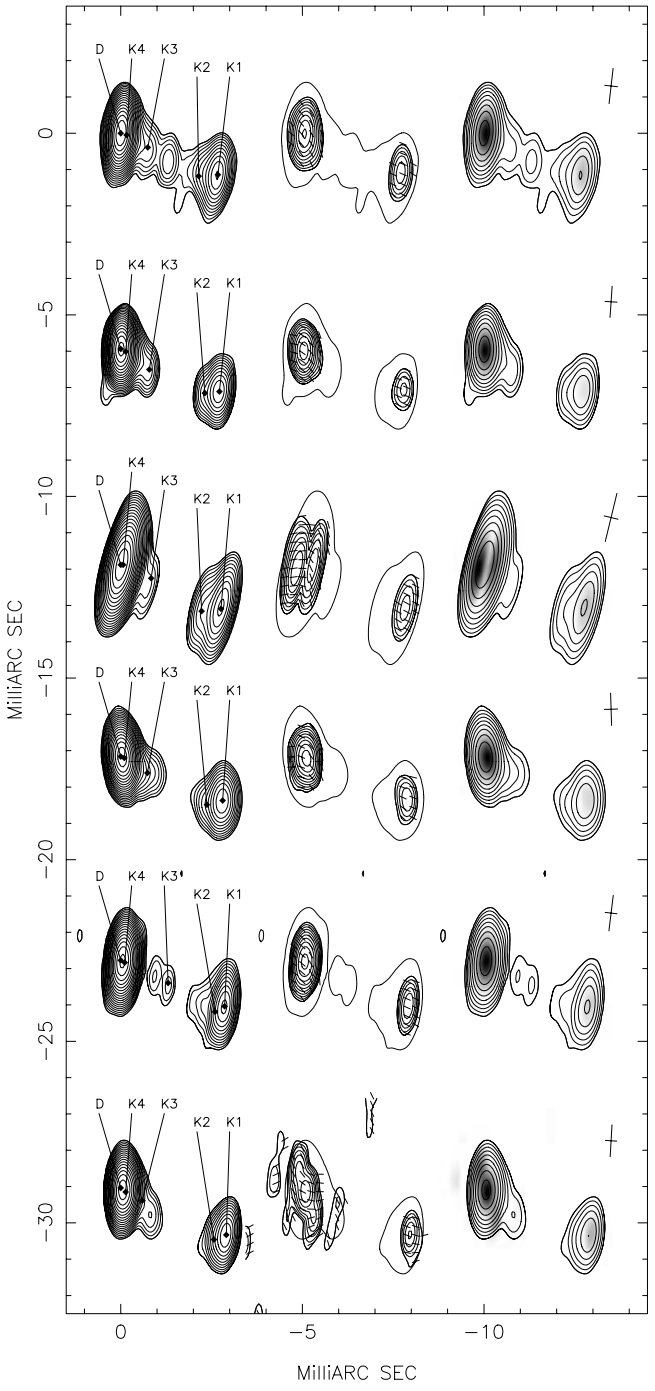

FIG. 16.—22 GHz images of 3C 279 at all six epochs. Figures are laid out as described in § 3.1. Contours in the Stokes *I* images begin at 40 mJy, and contours in the polarized images begin at 40 mJy.

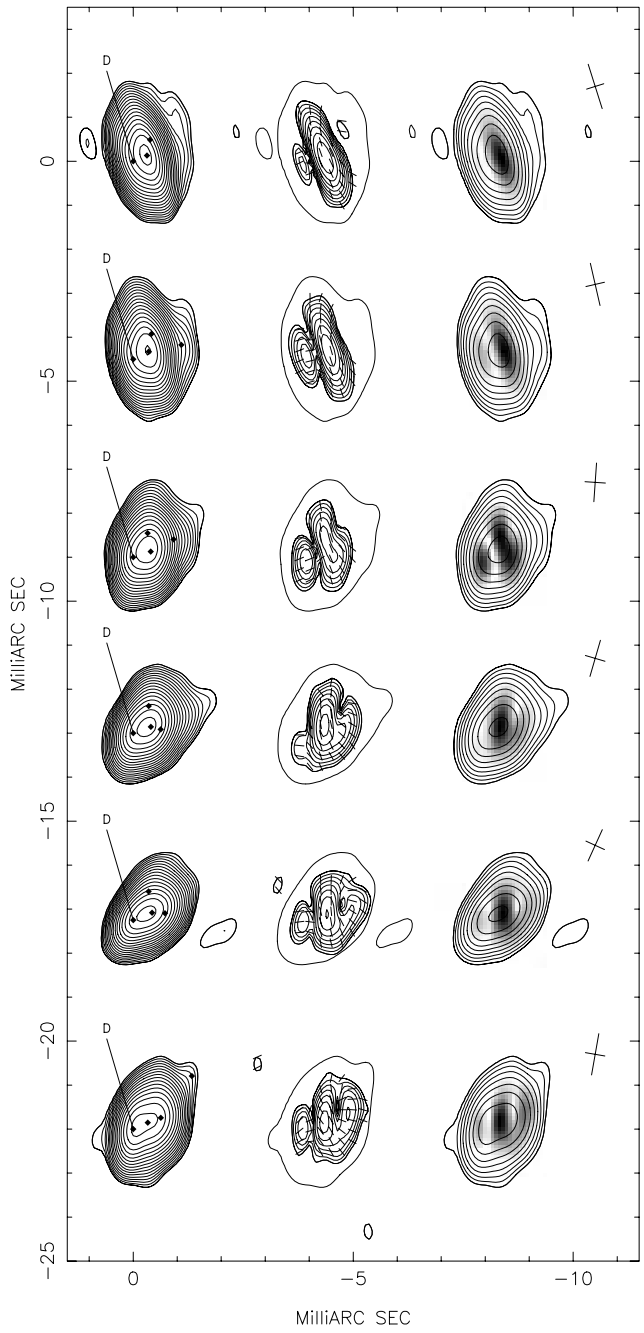

FIG. 17.—15 GHz images of J1310+323 at all six epochs. Figures are laid out as described in § 3.1. Contours in the Stokes *I* images begin at 5 mJy, and contours in the polarized images begin at 4 mJy.

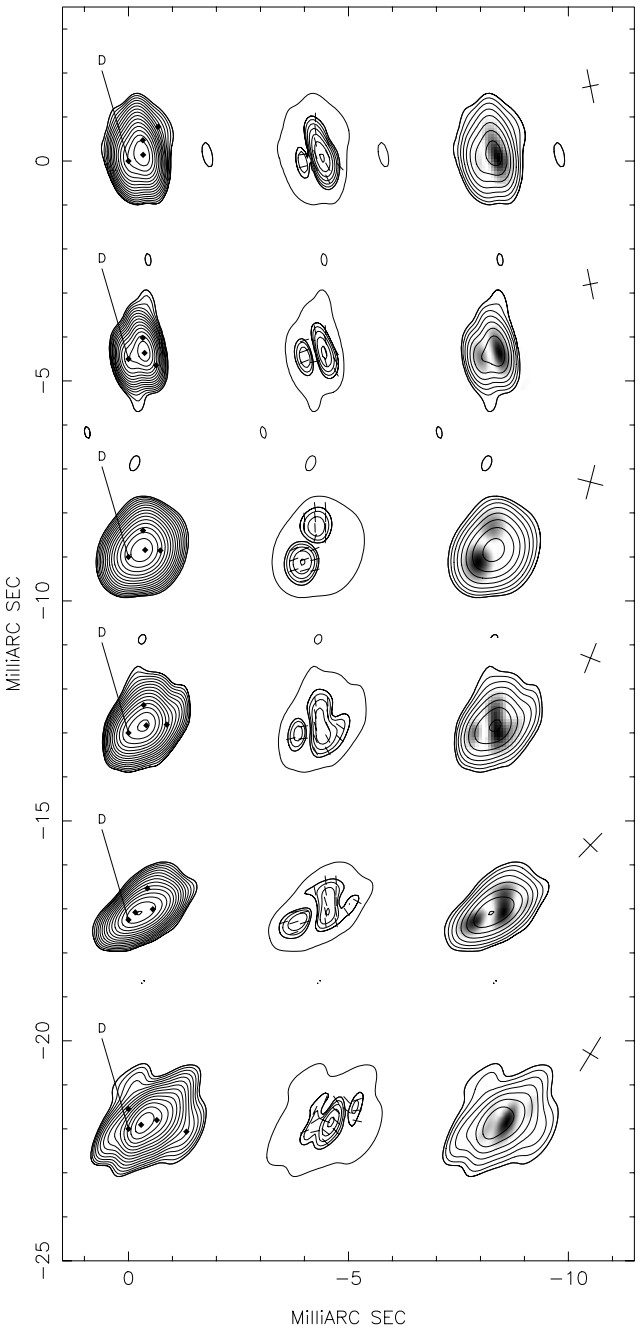

FIG. 18.—22 GHz images of J1310+323 at all six epochs. Figures are laid out as described in § 3.1. Contours in the Stokes *I* images begin at 10 mJy, and contours in the polarized images begin at 8 mJy.

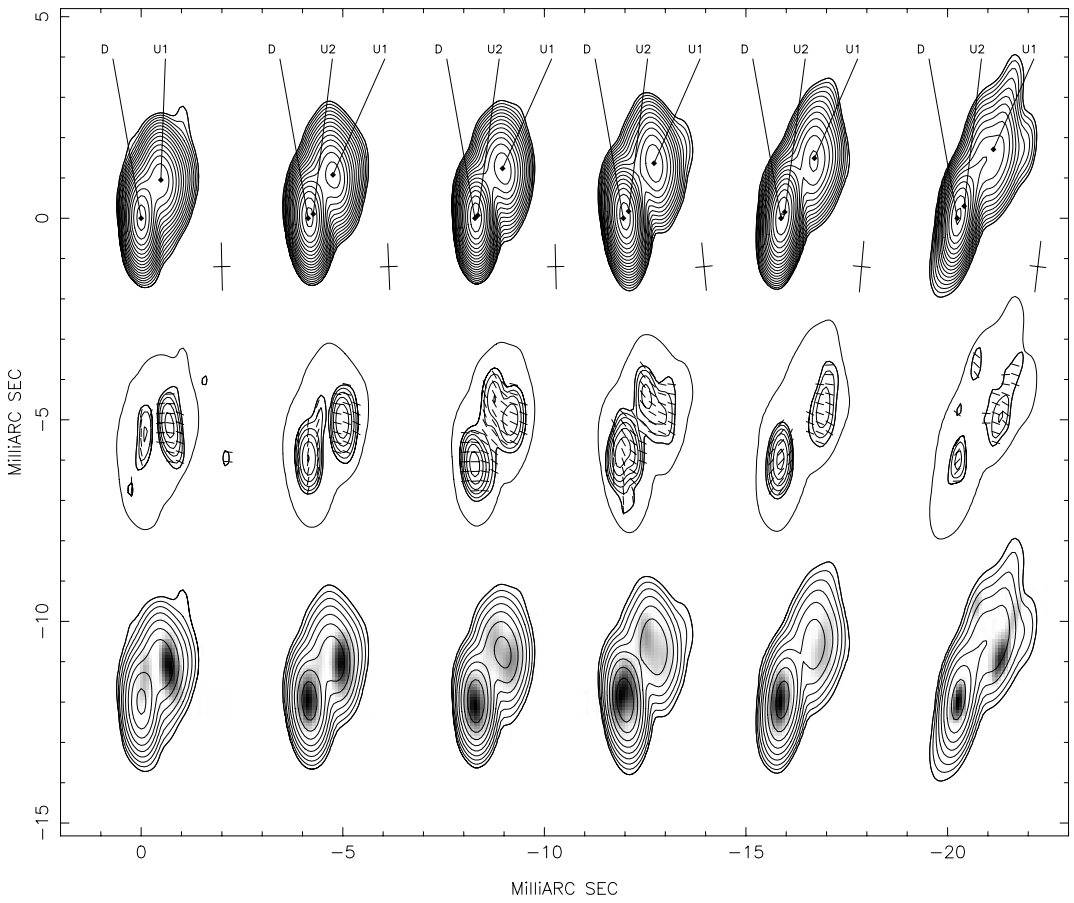

FIG. 19.—15 GHz images of J1512−090 at all six epochs. Figures are laid out as described in § 3.1. Contours in the Stokes *I* images begin at 3 mJy, and contours in the polarized images begin at 4 mJy.

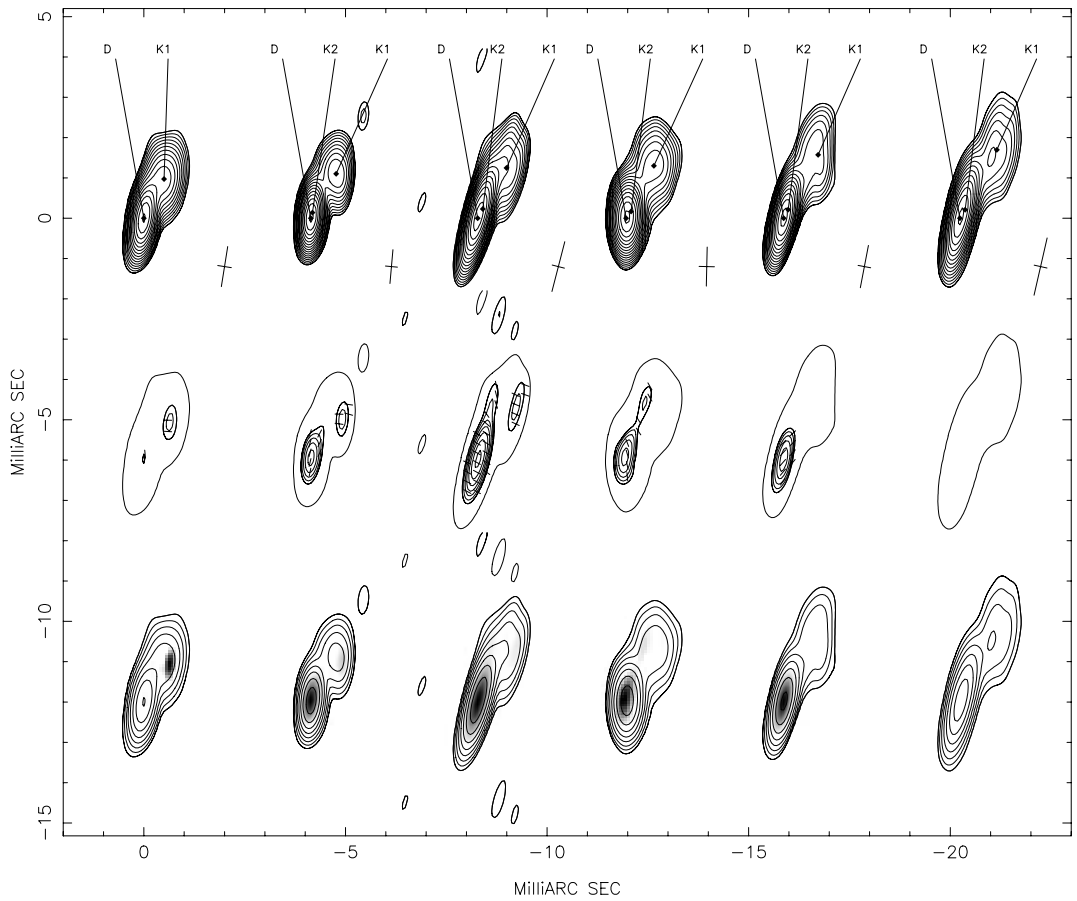

FIG. 20.—22 GHz images of J1512−090 at all six epochs. Figures are laid out as described in § 3.1. Contours in the Stokes *I* images begin at 8 mJy, and contours in the polarized images begin at 8 mJy.

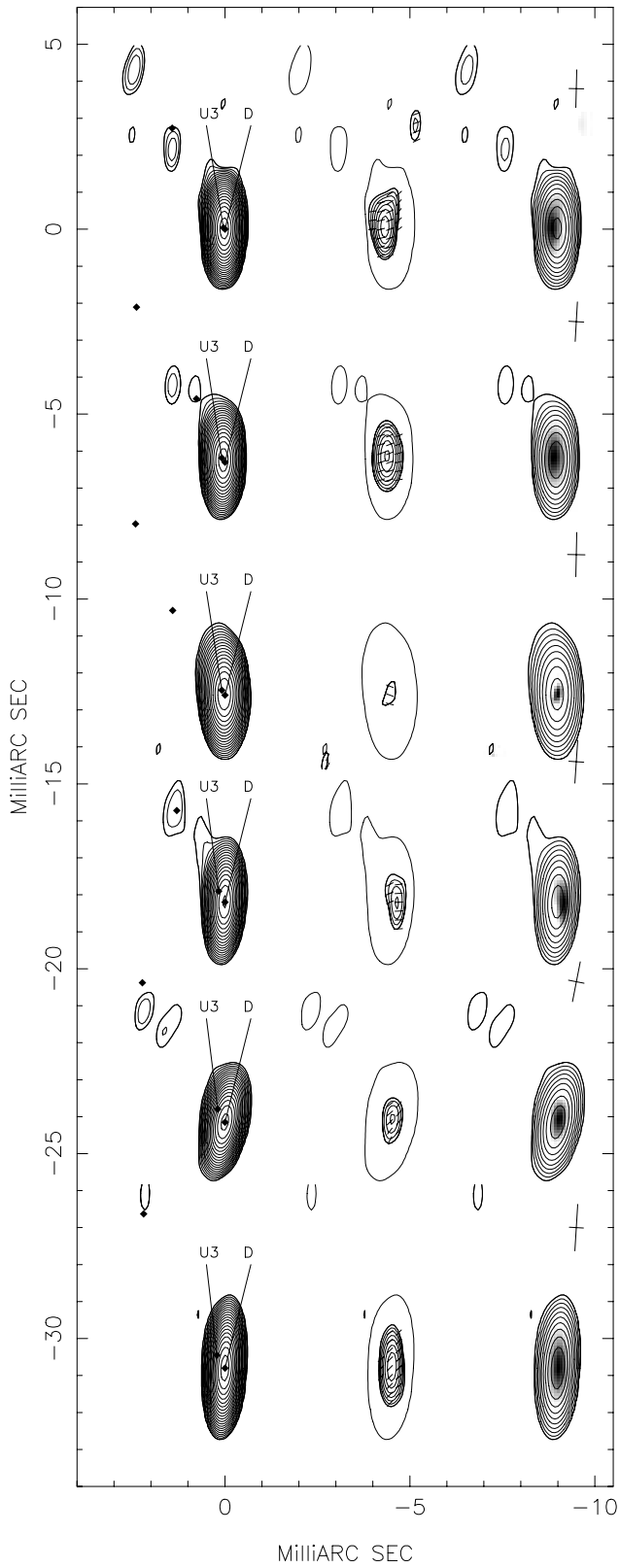

FIG. 21.—15 GHz images of J1751+09 at all six epochs. Figures are laid out as described in § 3.1. Contours in the Stokes *I* images begin at 2 mJy, and contours in the polarized images begin at 4 mJy.

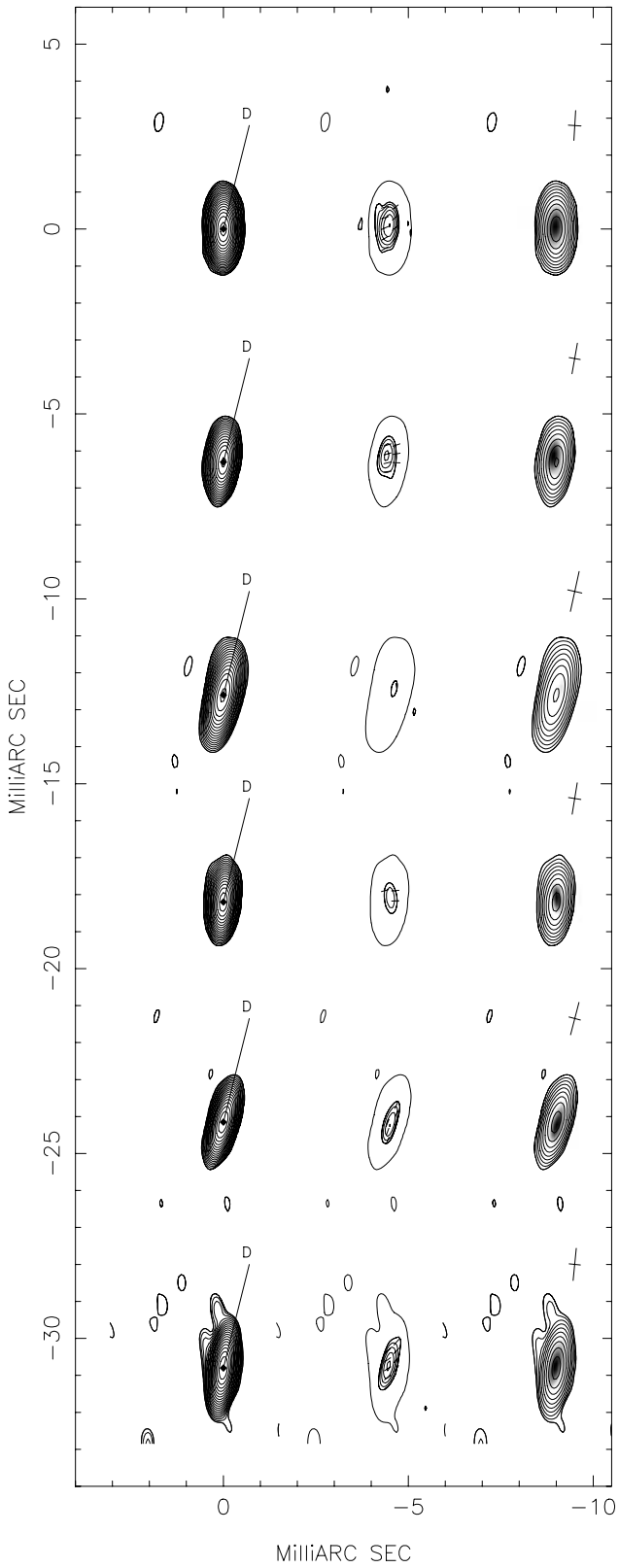

FIG. 22.—22 GHz images of J1751+09 at all six epochs. Figures are laid out as described in § 3.1. Contours in the Stokes *I* images begin at 3 mJy, and contours in the polarized images begin at 6 mJy.

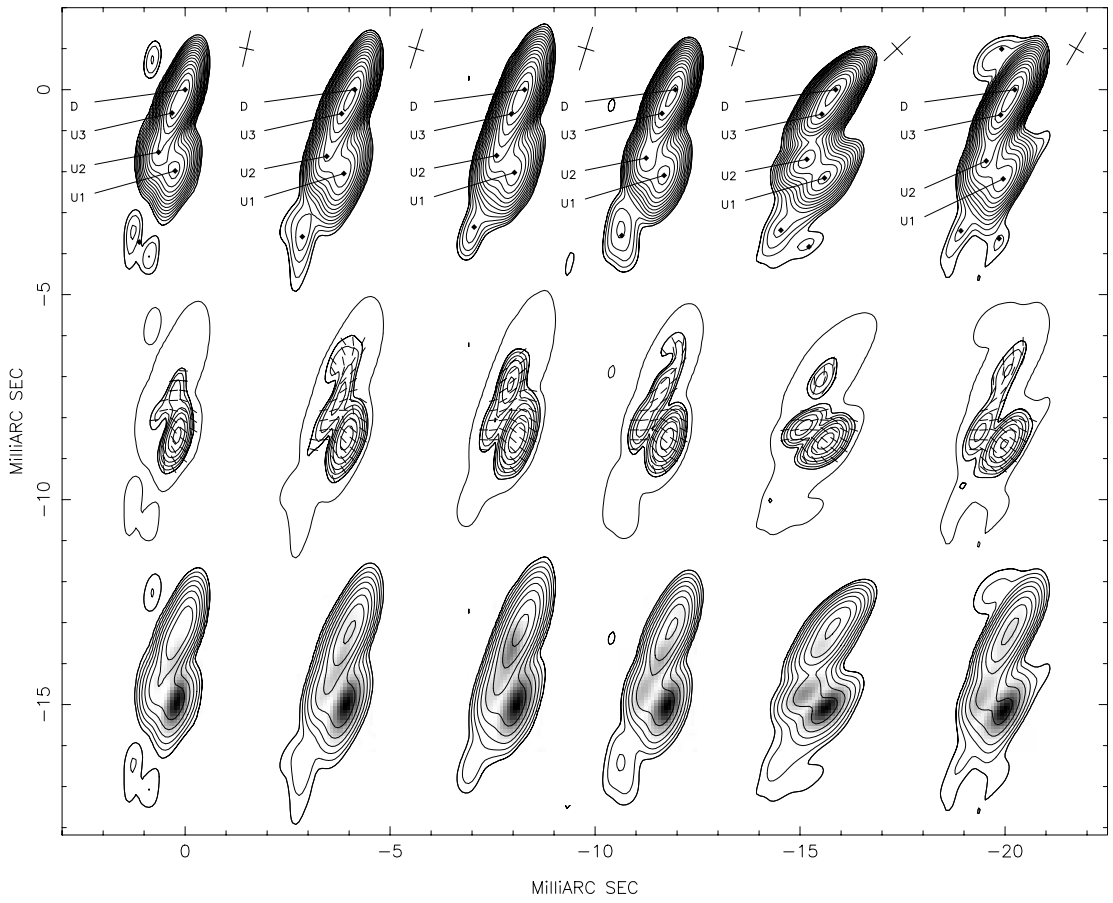

FIG. 23.—15 GHz images of J1927+739 at all six epochs. Figures are laid out as described in § 3.1. Contours in the Stokes *I* images begin at 5 mJy, and contours in the polarized images begin at 4 mJy.

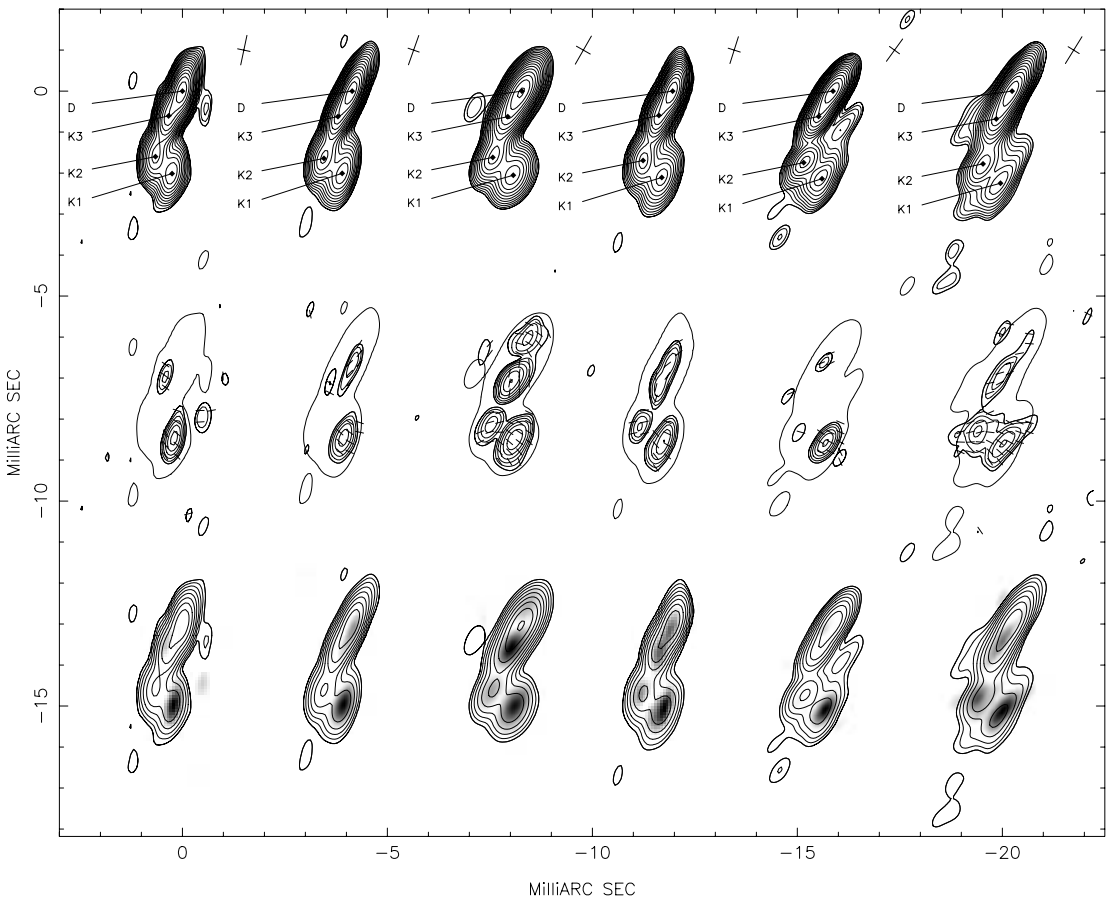

FIG. 24.—22 GHz images of J1927+739 at all six epochs. Figures are laid out as described in § 3.1. Contours in the Stokes *I* images begin at 6 mJy, and contours in the polarized images begin at 4 mJy.

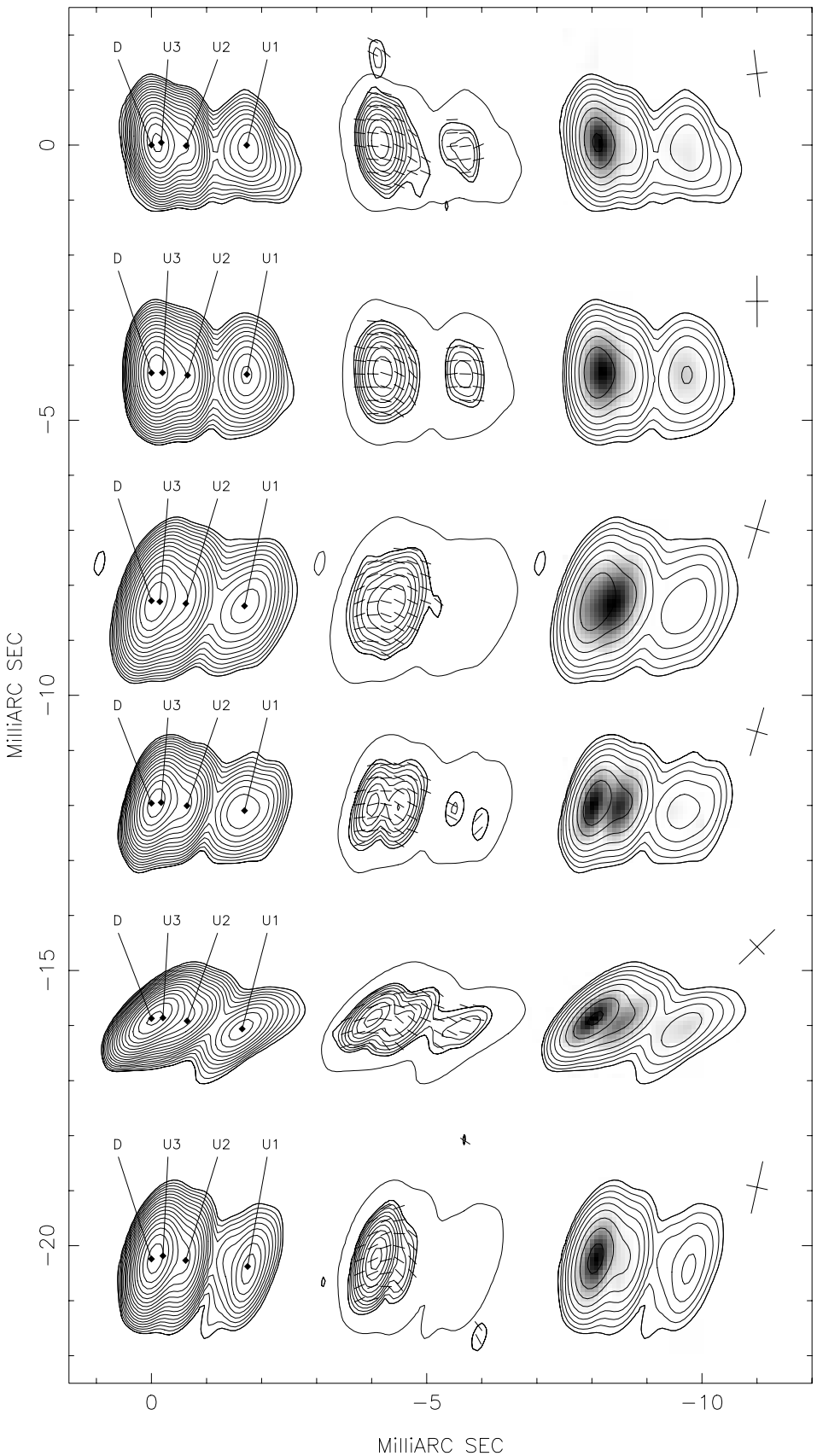

FIG. 25.—15 GHz images of J2005+778 at all six epochs. Figures are laid out as described in § 3.1. Contours in the Stokes *I* images begin at 2 mJy, and contours in the polarized images begin at 2 mJy.

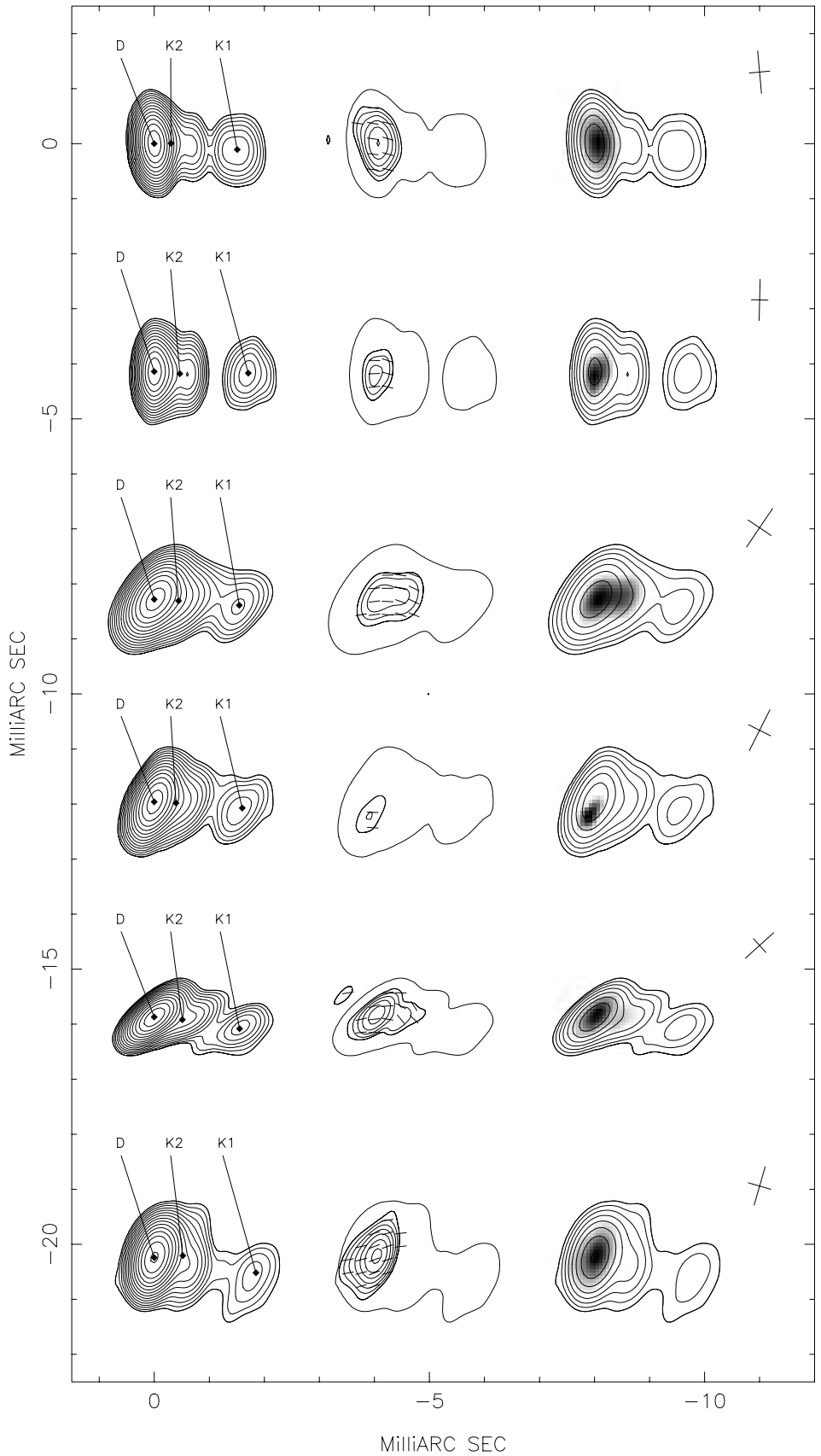

FIG. 26.—22 GHz images of J2005+778 at all six epochs. Figures are laid out as described in § 3.1. Contours in the Stokes *I* images begin at 6 mJy, and contours in the polarized images begin at 6 mJy.

3.2. *The Tables*

Tables 3–26 contain the model fit data for all 12 AGNs in our program. There are two tables per source, one for each observing frequency. Column (1) lists the epoch of observation. Column (2) lists the components. The core is labeled D. All other components that are identified over *multiple* epochs are labeled U1 (K1), U2 (K2) . . . on the 15 GHz (22 GHz) images, in order of emergence, with the earliest labeled U1 (K1). Occasionally, a component further than U1 (K1) is picked up at a later epoch, in which case it is labeled U0 (K0). Components that are only modeled at a *single* epoch (i.e., not identified at other epochs) are labeled Ux (Kx), where "x" is a lowercase letter used purely for identification and has no significance.

Column (3) lists (in mas) $R = (x^2 + y^2)^{1/2}$ where x and y denote the angular separation from the core. Column (4) shows the structural position angle θ measured with respect to north and positive east of north.

Column (5) records the total flux, I, in janskys. The fractional polarization m_L appears in column (6), while column (7) shows the polarization position angle in degrees.

Columns (8), (9), and (10) show, respectively, the length of the major axis (in mas), the length of the minor axis (in mas), and position angle of the major axis (in degrees) of the (elliptical) component. We estimate the practical limit on the measured angular size to be one-fifth of the beam width in the relevant direction.

Evaluating the reality of changes in flux and polarization in VLBI data is difficult as it is hard to obtain the real (1 σ) measurement uncertainties for the properties of source features. The data calibration path has several steps. While the uncertainties associated with some of these steps are well known, others cannot be quantified precisely. Our attempt to obtain empirical estimates of uncertainty in VLBI observables is described in Paper II.

3.3. *The Single-Dish Monitoring Plots*

Figures 27–38 display the results from single-dish monitoring of all 12 AGNs by the University of Michigan Radio Astronomy Group (UMRAO), using the 26 m diameter, parabolic reflector. These sources were generally observed weekly or more often; each day's observation consisted of a series of on-off type measurements over periods of 30 to 40 minutes, using broadband (approximately 10% of the central frequency) radiometers and prime-focus polarimeters. The

TABLE 3
COMPONENT DATA FOR 3C 120 AT 22 GHz

Epoch (1)	Component (2)	R (mas) (3)	Θ (deg) (4)	I (Jy) (5)	m_L (%) (6)	χ (deg) (7)	Major Axis (mas) (8)	Minor Axis (mas) (9)	ϕ (deg) (10)
1996.05.....	D	0.00	0.0	1.24	0.5	−64.4	0.24	...	44.0
	K2	1.01	−121.3	0.35	2.8	41.3	2.30	...	67.4
	K1B	1.97	−114.9	0.23	6.1	−60.9	0.42	0.29	−72.9
	K1A	2.46	−112.8	0.18	11.7	74.0	0.60	0.21	−26.6
	Kz	2.95	−107.5	0.04	35.3	−49.4	0.84	...	23.7
	Ky	4.06	−108.9	0.08	14.6	−40.5	1.01	...	71.0
1996.23.....	D	0.00	0.0	0.64	0.5	−79.6	0.22	...	45.3
	K2	0.29	−124.9	0.75	1.4	2.9	0.66	...	53.9
	K1B	2.50	−114.5	0.54	1.5	−70.2	0.88	0.28	74.3
	K1A	2.90	−103.7	0.12	24.7	−39.7	0.56	...	−70.6
	Kz	3.93	−108.4	0.02	6.5	−63.6	...	...	0.0
	Ky	5.06	−108.6	0.05	9.1	−30.5	0.81	0.15	57.7
1996.41.....	D	0.00	0.0	1.00	0.2	70.2	0.19	0.07	63.4
	K2	0.55	−124.8	0.42	3.2	−66.0	0.72	0.17	70.8
	K1B	2.66	−113.9	0.42	2.1	−15.0	0.46	0.36	−76.1
	K1A	3.26	−108.7	0.30	10.4	−69.0	0.76	0.34	−43.3
	Kz	5.03	−107.9	0.03	16.3	19.9	...	...	0.0
1996.57.....	D	0.00	0.0	0.88	0.3	16.9	0.20	...	58.4
	K2	0.69	−123.3	0.38	2.4	−73.6	1.13	...	60.1
	K1B	2.86	−112.3	0.48	0.2	−82.6	0.90	0.40	81.5
	K1A	3.70	−106.1	0.18	14.4	−37.3	0.82	0.33	−16.9
	Kz	4.93	−109.8	0.02	7.6	−12.9	...	...	0.0
1996.74.....	D	0.00	0.0	2.00	0.3	81.5	0.29	...	45.7
	K2	1.10	−120.0	0.54	1.3	−69.5	2.67	...	65.3
	K1B	3.20	−110.8	0.25	5.9	−51.6	0.48	0.43	−7.7
	K1A	4.05	−107.6	0.31	7.9	−50.7	0.95	0.58	−86.7
1996.93.....	D	0.00	0.0	0.27	1.4	73.8	...	...	0.0
	K3	0.12	−84.7	1.45	0.5	2.0	0.67	0.17	50.8
	K2	0.90	−121.3	0.57	3.1	−62.1	1.82	0.57	66.6
	K1B	3.46	−110.8	0.27	5.9	−14.4	0.65	0.48	29.8
	K1A	4.41	−106.2	0.25	11.6	−37.9	0.98	0.72	−75.9

TABLE 4

COMPONENT DATA FOR 3C 120 AT 15 GHz

Epoch (1)	Component (2)	R (mas) (3)	Θ (deg) (4)	I (Jy) (5)	m_L (%) (6)	χ (deg) (7)	Major Axis (mas) (8)	Minor Axis (mas) (9)	ϕ (deg) (10)
1996.05.....	D	0.00	0.0	0.88	0.6	55.0	0.26	...	43.7
	U2	0.65	−124.3	0.33	2.6	−37.0	1.00	...	56.9
	U1B	2.06	−117.1	0.40	6.1	48.2	0.87	...	67.1
	U1A	2.35	−109.6	0.26	15.7	−74.4	0.77	0.38	85.7
	Up	3.81	−108.2	0.16	10.3	−43.9	2.43	...	52.3
	Uq	5.00	−105.8	0.07	5.5	−39.6	1.03	...	66.6
	Ur	13.89	−105.2	0.05	8.3	−27.1	1.80	0.91	39.5
1996.23.....	D	0.00	0.0	1.11	0.5	−8.1	0.45	0.09	54.2
	U2	0.64	−125.0	0.28	3.5	87.2	1.14	...	60.9
	U1B	2.31	−113.9	0.53	2.1	−87.3	0.72	0.34	76.9
	U1A	2.80	−104.5	0.19	19.4	−64.9	0.53	0.22	−46.3
	Up	4.09	−109.7	0.13	5.9	−28.1	1.64	0.32	75.1
	Uq	5.69	−105.0	0.06	12.4	−32.7	2.61	0.31	50.9
	Ur	13.40	−106.1	0.10	10.2	−22.4	6.27	2.65	81.1
1996.41.....	D	0.00	0.0	0.78	0.3	55.2	0.17	...	84.8
	U2	0.65	−123.3	0.44	0.7	77.6	0.40	...	67.8
	U2A	1.41	−120.1	0.04	11.2	−50.6	...	...	0.0
	U1B	2.68	−113.6	0.61	1.0	2.7	0.70	0.38	83.5
	U1A	3.28	−105.8	0.28	21.3	−58.3	0.53	0.43	−37.5
	Up	4.36	−108.4	0.04	3.4	18.7	...	...	0.0
	Uq	5.11	−107.3	0.04	13.6	−31.2	...	...	0.0
	Ur	7.30	−110.6	0.02	9.7	1.3	...	...	0.0
1996.57.....	D	0.00	0.0	0.85	0.0	−82.4	0.43	0.07	52.6
	U2	0.86	−121.4	0.31	1.6	85.5	0.34	...	62.6
	U2A	1.61	−117.2	0.04	7.5	45.2	...	...	0.0
	U1B	2.92	−111.7	0.63	5.0	−54.7	0.88	0.49	88.2
	U1A	3.66	−105.3	0.20	15.9	−50.3	0.64	0.28	−11.3
	Up	4.62	−107.4	0.04	3.8	−14.0	...	...	0.0
	Uq	5.34	−107.7	0.04	7.3	−30.8	...	...	0.0
	Ur	6.06	−106.7	0.02	9.3	−20.9	...	...	0.0
	Us	6.70	−105.3	0.01	14.2	−52.8	...	...	0.0
	Ut	7.66	−107.8	0.01	20.1	20.0	...	...	0.0
1996.74.....	D	0.00	0.0	1.47	0.1	−72.6	0.24	...	53.5
	U2	0.78	−124.2	0.58	0.9	85.1	1.37	...	61.8
	U2A	2.55	−117.0	0.06	3.2	73.8	...	...	0.0
	U1B	3.20	−111.7	0.45	6.7	−48.4	0.54	0.36	−83.4
	U1A	3.98	−106.7	0.31	14.7	−42.6	0.68	0.48	−38.8
	Up	4.83	−106.4	0.02	13.5	−51.5	...	...	0.0
	Uq	5.53	−108.3	0.03	3.0	−18.9	...	...	0.0
	Ur	6.02	−109.1	0.02	12.5	−32.5	...	...	0.0
1996.93.....	D	0.00	0.0	1.78	0.3	−31.7	0.55	...	53.7
	U2	0.99	−120.2	0.43	2.8	−76.9	1.60	...	65.6
	U2A	3.01	−118.8	0.05	10.6	−61.5	...	...	0.0
	U1B	3.41	−110.4	0.26	6.0	−42.0	0.49	0.37	−79.2
	U1A	4.21	−106.4	0.28	14.6	−39.3	0.88	0.73	−72.3
	Up	5.38	−107.3	0.02	10.6	−42.3	...	...	0.0
	Uq	6.21	−109.1	0.03	8.8	−22.7	...	...	0.0

TABLE 5

COMPONENT DATA FOR PKS 0528+134 AT 22 GHz

Epoch (1)	Component (2)	R (mas) (3)	Θ (deg) (4)	I (Jy) (5)	m_L (%) (6)	χ (deg) (7)	Major Axis (mas) (8)	Minor Axis (mas) (9)	ϕ (deg) (10)
1996.05.....	D	0.00	0.0	7.25	3.2	79.0	0.21	...	80.3
	K2	0.19	97.7	1.41	12.6	−74.5	0.20	...	14.5
1996.23.....	D	0.00	0.0	7.99	3.1	58.2	0.18	...	72.5
	K2	0.22	97.4	1.52	1.5	−45.0	0.21	...	36.3
	K1	0.78	46.6	0.20	9.5	−65.9	0.63	0.25	3.0
1996.41.....	D	0.00	0.0	3.83	7.3	32.6	0.21	...	69.6
	K2	0.11	129.9	4.24	7.0	−58.0	0.31	0.07	88.1
	K1	0.68	43.6	0.23	9.1	−79.6	0.52	...	−21.1
1996.57.....	D	0.00	0.0	3.74	4.2	70.2	0.18	...	80.3
	K2	0.19	77.8	4.14	0.8	−29.1	0.28	0.22	89.9
	K1	0.67	49.8	0.28	18.2	−81.2	0.78	0.29	41.7
1996.74.....	D	0.00	0.0	5.87	4.4	71.1	0.20	...	67.6
	K2	0.27	72.4	1.63	4.8	−80.4	0.24	0.17	8.2
	K1	0.76	49.3	0.22	6.7	−83.5	0.50	0.08	72.5
	K0	3.19	28.3	0.04	26.0	19.8	1.23	0.25	10.8
1996.93.....	D	0.00	0.0	4.51	2.6	61.7	0.27	0.24	−14.9
	K2	0.27	72.0	1.28	8.2	−88.0	0.35	0.24	0.6
	K1	0.93	42.0	0.25	9.6	−43.9	0.46	0.23	32.3
	K0	2.03	22.1	0.04	44.9	24.2	0.37	...	53.5

TABLE 6

COMPONENT DATA FOR PKS 0528+134 AT 15 GHz

Epoch (1)	Component (2)	R (mas) (3)	Θ (deg) (4)	I (Jy) (5)	m_L (%) (6)	χ (deg) (7)	Major Axis (mas) (8)	Minor Axis (mas) (9)	ϕ (deg) (10)
1996.05.....	D	0.00	0.0	4.16	4.9	33.3	0.18	...	76.3
	U2	0.14	121.4	4.50	8.5	−68.3	0.27	...	64.2
	U1	0.95	54.7	0.10	7.3	58.3	2.21	...	−32.5
	U0	3.80	35.0	0.06	3.6	85.2	1.85	...	7.7
1996.23.....	D	0.00	0.0	7.59	1.4	47.6	0.20	...	67.1
	U2	0.22	94.0	1.60	3.6	−46.2	0.26	...	42.1
	U1	0.81	44.9	0.24	5.6	−86.1	0.78	0.25	47.8
1996.41.....	D	0.00	0.0	4.01	4.5	29.1	0.26	...	65.4
	U2	0.13	123.1	3.95	6.1	−55.1	0.32	...	74.4
	U1	0.91	44.5	0.20	5.7	75.5	0.38	...	−71.4
1996.57.....	D	0.00	0.0	4.17	4.2	71.5	0.22	...	63.9
	U2	0.21	87.4	3.58	3.0	−43.9	0.28	0.17	52.9
	U1	0.92	43.1	0.23	11.9	75.6	0.59	0.38	28.5
	U0	3.70	22.2	0.05	17.8	10.5	2.18	...	83.4
1996.74.....	D	0.00	0.0	6.35	3.2	69.8	0.23	...	69.9
	U2	0.28	75.2	1.84	6.5	−68.8	0.28	0.15	32.2
	U1	1.01	43.3	0.19	9.0	82.0	0.72	0.34	−4.8
	U0	3.97	22.7	0.05	18.7	11.9	2.56	...	76.6
1996.93.....	D	0.00	0.0	4.54	1.9	61.9	0.24	...	73.3
	U2	0.26	67.4	1.75	5.4	−82.5	0.33	0.20	39.7
	U1	1.03	40.8	0.19	3.4	80.1	0.69	0.31	1.2
	U0	4.33	24.2	0.05	30.3	33.7	4.50	...	73.9

TABLE 7
COMPONENT DATA FOR PKS 0735+178 AT 22 GHz

Epoch (1)	Component (2)	R (mas) (3)	Θ (deg) (4)	I (Jy) (5)	m_L (%) (6)	χ (deg) (7)	Major Axis (mas) (8)	Minor Axis (mas) (9)	ϕ (deg) (10)
1996.05.....	D	0.00	0.0	0.51	2.7	−19.0	...	...	0.0
	K2	0.20	48.0	0.31	7.1	−82.8	0.48	0.22	76.3
	K1	0.77	84.3	0.27	8.3	47.4	0.58	0.29	32.3
	Kz	1.53	43.8	0.07	20.2	−26.9	1.68	0.86	80.6
1996.23.....	D	0.00	0.0	0.43	2.0	6.6	...	...	0.0
	K2	0.25	55.0	0.20	5.6	−81.4	0.77	0.35	54.1
	K1	0.86	80.7	0.21	3.3	38.1	0.64	0.30	23.4
	Kz	2.76	59.0	0.02	6.5	−0.3	1.23	0.12	25.6
1996.41.....	D	0.00	0.0	0.61	2.3	20.8	0.06	...	31.0
	Kz	0.37	58.6	0.22	10.7	88.5	0.99	0.37	−45.3
	Ky	1.43	51.2	0.05	17.8	−11.5	1.49	...	−2.4
1996.57.....	D	0.00	0.0	0.59	1.6	6.8	0.10	0.06	−71.8
	Kz	0.36	54.6	0.28	5.8	81.4	0.86	0.41	−47.4
	Ky	0.98	80.8	0.08	8.4	−75.0	0.73	...	−3.9
	Kx	1.55	51.6	0.07	10.4	−12.7	1.62	0.99	−81.7
1996.74.....	D	0.00	0.0	0.44	4.0	−14.0	0.21	...	−25.6
	Kz	0.39	70.8	0.27	6.2	83.8	1.19	0.39	81.7
	Ky	2.68	34.0	0.02	39.8	−19.9	2.24	...	−43.7
1996.93.....	D	0.00	0.0	0.47	1.1	8.7	0.13	...	−9.4
	Kz	0.56	62.2	0.23	4.7	−67.3	1.44	0.77	52.5

general procedure is described by Aller et al. (1985). The flux scale was set by alternating every second or third program source observation with observations of secondary standard sources calibrated on the flux-density scale set by Ott et al. (1994). The polarization electric vectors were calibrated using a broadband source of polarized emission located at the vertex of the equatorially mounted paraboloid; the instrumental polarization was verified from daily observations of Galactic H II regions (which are believed to be unpolarized).

Each figure shows two week averages of the polarization position angle (X), polarized intensity (P), and total intensity (S). The UMRAO 14.5 GHz data are represented by crosses. For comparison, the integrated VLBA results at 15 GHz are shown as open diamonds. UMRAO 5 GHz results are also included, as open triangles, to illustrate opacity effects.

In general, there is good agreement between total fluxes and polarizations from the CLEAN maps and the single-dish values, with a near constant offset in the more extended objects. Thus, most of the variation in these sources would appear to be accounted for by the variation in their VLBI core and jet. This raises the possibility that if the VLBI components can be adequately modeled, frequently obtained single-dish values can be used as proxies to interpolate between less frequent VLBI measurements to follow the evolution of a source.

3.4. *3C 120 (J0433+05)*

In our images, 3C 120 has a strong core to the east and a jet extending several mas to the west. The core is highly variable and very slightly polarized. The jet is very complex and is fitted with a large number of components at each epoch. In Paper I, we tracked the motion of the unambiguously identifiable components U1A (K1A) and U1B (K1B). We found both components to be superluminal but moving at different speeds. In Paper II, we found that only the combination of these closely spaced components, referred to as U1A+U1B (K1A+K1B), could be robustly analyzed for variability in flux and polarization. This U1A+U1B region showed some of the largest fluctuations in total intensity for a jet feature in our sample.

Most of the polarized flux appeared to be associated with these two well-defined jet components (with U1A the more polarized) but not coincident with them. The U1A+U1B region also showed both an increase in magnetic field order as well as a rotation toward magnetic field alignment with the jet axis. There was a marked transverse asymmetry with most of the polarized flux to the north of the ridgeline. We also observed a reverse depolarization effect in this feature, with the fractional polarization being higher at the *lower* frequency (Paper II).

We see a nearly constant offset between the VLBA and single-dish flux. Almost all the observed single-dish variability is accounted for by the VLBI scale (core and jet) variation.

3.5. *J0530+135 (B0528+134)*

While the gross total intensity structure of this barely resolved source is in agreement with past VLBI images (e.g., Pohl et al. 1995), this source shows a lot of activity.

We find this source to be a barely resolved double with a weak jet at a position angle $\sim 30^\circ$. The core (D) and innermost component (U2/K2) contain almost all the flux and adequately model the total intensity structure when taken together; however, the distribution of flux and polarization between them is not robust in every epoch (Paper II). In Paper I, we fit a distinctly nonradial proper motion to U2 (K2), which we

TABLE 8

COMPONENT DATA FOR PKS 0735+178 AT 15 GHz

Epoch (1)	Component (2)	R (mas) (3)	Θ (deg) (4)	I (Jy) (5)	m_L (%) (6)	χ (deg) (7)	Major Axis (mas) (8)	Minor Axis (mas) (9)	ϕ (deg) (10)
1996.05.....	D	0.00	0.0	0.42	3.8	−12.4	...	...	0.0
	U2	0.12	57.0	0.20	13.3	−78.4	0.74	0.06	41.7
	U1	0.77	79.8	0.53	4.0	40.5	0.62	0.34	35.0
	Up	1.44	12.9	0.03	15.9	−29.3	...	...	0.0
	Uq	1.75	35.3	0.02	16.2	−25.4	...	...	0.0
	Ur	2.34	49.4	0.01	28.0	−36.6	...	...	0.0
	Us	3.91	63.4	0.01	6.7	−54.3	...	...	0.0
	Ut	4.37	66.8	0.01	7.9	−48.8	...	...	0.0
1996.23.....	D	0.00	0.0	0.37	3.8	15.2	...	...	0.0
	U2	0.21	51.7	0.15	13.0	−68.5	0.88	...	40.6
	U1	0.81	79.6	0.46	2.6	35.6	0.64	0.31	35.2
	Up	1.55	9.6	0.01	20.5	−34.9	...	...	0.0
	Uq	1.65	26.3	0.02	11.7	−50.0	...	...	0.0
	Ur	1.79	39.7	0.02	17.3	−26.9	...	...	0.0
	Us	2.34	54.8	0.01	37.2	2.9	...	...	0.0
	Ut	3.91	65.8	0.01	19.3	−47.2	...	...	0.0
	Uu	5.16	68.4	0.01	7.3	−73.6	...	...	0.0
1996.41.....	D	0.00	0.0	0.44	2.3	45.7	...	...	0.0
	U2	0.59	49.4	0.08	9.1	−63.6	0.80	0.22	−0.3
	U1	0.85	77.3	0.42	2.7	44.5	0.58	0.29	21.3
	Up	1.60	15.9	0.02	31.9	−18.5	...	...	0.0
	Uq	1.78	38.4	0.03	12.4	−18.6	...	...	0.0
	Ur	4.23	50.8	0.01	13.5	−68.5	...	...	0.0
	Us	5.80	66.9	0.01	2.9	40.3	...	...	0.0
1996.57.....	D	0.00	0.0	0.37	2.2	10.8	...	...	0.0
	U2	0.45	50.8	0.10	12.3	−77.7	0.62	0.30	11.8
	U1	0.86	77.7	0.39	1.9	71.6	0.59	0.36	17.7
	Up	1.55	15.4	0.03	20.3	−20.9	...	...	0.0
	Uq	1.73	36.4	0.02	12.0	−25.3	...	...	0.0
	Ur	2.36	49.1	0.01	18.2	−8.2	...	...	0.0
	Us	4.03	60.9	0.01	13.9	−37.5	...	...	0.0
	Ut	5.35	64.8	0.01	5.7	−2.6	...	...	0.0
1996.74.....	D	0.00	0.0	0.33	3.5	1.1	...	...	0.0
	U2	0.51	54.6	0.16	8.8	−72.5	0.90	...	52.2
	U1	0.90	79.5	0.31	1.0	89.8	0.56	0.32	35.0
	Up	1.45	13.8	0.02	15.4	−30.0	...	...	0.0
	Uq	1.64	27.1	0.02	17.1	−19.3	...	...	0.0
	Ur	1.89	39.6	0.01	18.3	−2.3	...	...	0.0
	Us	4.14	64.8	0.01	9.5	−44.8	...	...	0.0
1996.93.....	D	0.00	0.0	0.28	2.8	−2.9	...	...	0.0
	U2	0.40	55.6	0.12	8.2	−57.2	1.03	...	46.6
	U1	0.90	78.5	0.26	3.8	79.6	0.64	0.39	40.7
	Uq	1.40	13.5	0.02	11.2	−34.0	...	...	0.0
	Up	1.40	32.3	0.02	19.8	−26.9	...	...	0.0
	Ur	2.28	38.9	0.01	27.3	−23.1	...	...	0.0
	Us	4.24	62.1	0.01	11.3	−37.6	...	...	0.0

TABLE 9

COMPONENT DATA FOR OJ 287 AT 22 GHz

Epoch (1)	Component (2)	R (mas) (3)	Θ (deg) (4)	I (Jy) (5)	m_L (%) (6)	χ (deg) (7)	Major Axis (mas) (8)	Minor Axis (mas) (9)	ϕ (deg) (10)
1996.05.....	D	0.00	0.0	1.57	5.2	24.3	0.09	0.06	78.5
	K3	0.28	−100.6	0.81	3.9	−20.0	0.20	0.09	−47.8
	K2	1.41	−91.3	0.07	2.8	34.9	0.46	0.37	−14.7
1996.23.....	D	0.00	0.0	0.93	3.2	37.6	0.12	...	44.3
	K3	0.28	−103.4	0.56	5.3	−21.6	0.40	...	−79.3
	Kz	0.84	−99.0	0.01	38.0	−47.5	0.61	...	−32.5
	K2	1.47	−91.1	0.03	5.0	79.6	0.58	...	−42.9
1996.41.....	D	0.00	0.0	1.04	4.5	40.5	...	...	0.0
	K3	0.35	−98.4	0.44	10.4	−30.1	0.64	0.26	−82.0
	K2	1.30	−90.9	0.03	12.5	37.0	0.56	0.40	−4.8
1996.57.....	D	0.00	0.0	0.96	2.3	−5.9	...	...	0.0
	K4	0.22	−109.4	0.25	4.6	−15.0	0.20	0.15	41.5
	K3	0.74	−91.5	0.21	13.5	−31.3	0.56	0.29	90.0
	K2	1.43	−90.1	0.02	23.9	60.4	0.62	...	10.8
1996.74.....	D	0.00	0.0	1.40	2.4	−66.6	...	...	0.0
	K4	0.18	−122.2	0.19	5.7	−46.0	0.31	...	43.4
	K3	0.89	−93.7	0.24	8.3	−22.3	0.61	0.23	86.8
1996.93.....	D	0.00	0.0	0.95	1.6	75.8	0.08	...	−54.2
	K4	0.13	−73.6	0.48	3.1	45.0	0.41	0.20	6.3
	Kz	0.74	−105.0	0.05	15.6	−22.4	0.34	0.16	−58.5
	K3	1.13	−92.1	0.21	3.3	−26.4	0.74	0.52	−40.7

TABLE 10

COMPONENT DATA FOR OJ 287 AT 15 GHz

Epoch (1)	Component (2)	R (mas) (3)	Θ (deg) (4)	I (Jy) (5)	m_L (%) (6)	χ (deg) (7)	Major Axis (mas) (8)	Minor Axis (mas) (9)	ϕ (deg) (10)
1996.05.....	D	0.00	0.0	1.05	5.9	25.8	0.13	...	−5.7
	U3	0.26	−101.2	1.06	4.5	−16.4	0.26	...	−74.9
	U2	1.42	−85.7	0.05	9.4	87.7	0.66	0.38	−7.3
	Up	2.41	−98.4	0.03	20.4	55.2	0.78	0.38	−43.2
1996.23.....	D	0.00	0.0	0.92	2.8	30.0	0.13	...	67.3
	U3	0.32	−99.1	0.58	7.3	−26.1	0.37	0.15	−76.2
	U2	1.27	−92.2	0.06	4.0	−86.0	0.90	...	−67.4
	Up	3.82	−105.3	0.02	19.5	51.1	1.18	0.64	7.2
1996.41.....	D	0.00	0.0	1.06	4.0	34.6	0.18	...	60.3
	U3	0.43	−94.1	0.39	12.7	−29.4	0.58	0.12	−87.7
	U2	1.35	−91.5	0.04	12.0	56.8	0.57	0.39	−69.3
	Up	6.22	−106.9	0.00	10.6	11.0	0.73	...	31.7
1996.57.....	D	0.00	0.0	0.81	2.6	−13.9	...	...	0.0
	U4	0.23	−109.5	0.24	3.6	−20.4	0.24	0.16	55.1
	U3	0.73	−92.4	0.22	15.8	−31.2	0.44	0.20	81.6
	U2	1.32	−92.6	0.04	21.2	54.6	0.58	...	−74.5
	Up	2.85	−110.1	0.02	7.6	−43.8	3.50	0.49	38.1
1996.74.....	D	0.00	0.0	1.31	2.2	−56.7	...	...	0.0
	U4	0.22	−117.7	0.18	1.2	13.6	0.21	0.08	−7.4
	U3	0.84	−93.8	0.33	8.4	−29.7	0.73	0.23	−89.4
1996.93.....	D	0.00	0.0	0.83	0.8	46.7	...	...	0.0
	U4	0.12	−115.6	0.48	3.4	51.5	0.28	...	69.5
	U3	1.06	−94.6	0.28	6.4	−26.0	0.68	0.19	−84.3

TABLE 11

COMPONENT DATA FOR 4C 21.35 AT 22 GHz

Epoch (1)	Component (2)	R (mas) (3)	Θ (deg) (4)	I (Jy) (5)	m_L (%) (6)	χ (deg) (7)	Major Axis (mas) (8)	Minor Axis (mas) (9)	ϕ (deg) (10)
1996.23.....	D	0.00	0.0	0.98	2.6	84.6	...	...	0.0
	Kz	0.10	−6.1	0.66	13.0	−29.7	0.29	0.16	−14.9
	Ky	1.34	−3.3	0.12	6.6	−17.6	0.57	0.15	−50.9
1996.41.....	D	0.00	0.0	1.31	5.7	−59.6	...	...	0.0
	K4	0.10	7.9	0.18	10.6	23.8	0.45	...	−25.0
	K3	0.34	−13.4	0.07	58.5	−23.7	0.35	...	−4.3
	K2	1.33	−1.1	0.07	9.1	−0.0	0.63	0.23	−18.5
1996.57.....	D	0.00	0.0	1.26	2.7	−52.9	...	...	0.0
	K4	0.12	7.4	0.19	15.3	−25.7	0.61	...	−9.7
	K3	0.43	−19.7	0.13	13.7	−29.1	0.25	...	0.9
	K2	1.54	−2.8	0.13	2.2	−8.7	0.61	0.27	−30.3
	K1	4.67	7.0	0.03	6.7	86.5	1.72	0.70	−21.4
1996.74.....	D	0.00	0.0	1.14	2.5	−57.2	...	...	0.0
	K4	0.10	−9.3	0.17	17.5	−16.6	0.33	...	−4.9
	K3	0.56	−15.5	0.15	13.8	−32.3	0.38	...	6.3
	K2	1.69	−3.9	0.11	4.9	−18.9	0.78	0.23	−21.7
	K1	4.74	5.4	0.03	16.0	−69.9	1.93	0.50	−6.6
1996.93.....	D	0.00	0.0	0.65	0.5	−87.2	...	...	0.0
	K4	0.10	−17.2	0.46	11.3	−35.2	0.64	0.09	−16.3
	K3	0.73	−11.9	0.07	18.9	−1.8	0.49	...	25.3
	K2	1.75	−3.3	0.12	7.9	−40.2	0.79	0.32	−24.9
	K1	4.92	6.6	0.03	11.8	−64.6	1.63	1.06	−63.5

TABLE 12

COMPONENT DATA FOR 4C 21.35 AT 15 GHz

Epoch (1)	Component (2)	R (mas) (3)	Θ (deg) (4)	I (Jy) (5)	m_L (%) (6)	χ (deg) (7)	Major Axis (mas) (8)	Minor Axis (mas) (9)	ϕ (deg) (10)
1996.23.....	D	0.00	0.0	1.42	5.0	−48.4	...	...	0.0
	U3	0.30	−16.5	0.18	23.2	−15.6	0.76	...	9.5
	U2	1.40	0.8	0.12	5.5	−6.4	0.46	0.06	−59.4
	U1	4.06	9.1	0.04	9.8	−65.6	2.05	0.99	−88.1
1996.41.....	D	0.00	0.0	1.15	5.5	−60.2	...	...	0.0
	U3	0.32	−18.2	0.31	16.4	−20.6	0.32	...	9.7
	U2	1.42	−2.2	0.15	5.7	−9.6	0.59	0.28	−31.1
	U1	4.49	5.3	0.04	8.4	−82.0	1.52	0.98	60.1
1996.57.....	D	0.00	0.0	1.15	3.9	−52.5	...	...	0.0
	U3	0.36	−18.8	0.32	12.7	−27.9	0.44	0.10	2.9
	U2	1.56	−2.8	0.14	3.7	−19.7	0.59	0.26	−34.8
	U1	4.41	6.0	0.04	15.7	−72.5	1.54	0.97	20.9
1996.74.....	D	0.00	0.0	1.34	2.5	−48.6	...	...	0.0
	U3	0.50	−15.2	0.26	14.5	−23.9	0.36	...	12.4
	U2	1.62	−3.1	0.15	3.5	−25.0	0.61	0.31	−27.1
	U1	4.64	6.2	0.05	12.9	−71.6	1.37	1.07	−7.7
1996.93.....	D	0.00	0.0	1.00	5.3	−43.8	...	...	0.0
	U3	0.61	−13.3	0.19	13.2	−25.3	0.33	...	25.3
	U2	1.79	−3.8	0.12	6.2	−41.7	0.52	0.33	−39.7
	U1	4.64	6.4	0.03	12.6	−75.1	1.65	0.43	22.1

TABLE 13

COMPONENT DATA FOR 3C 273 AT 22 GHz

Epoch (1)	Component (2)	R (mas) (3)	Θ (deg) (4)	I (Jy) (5)	m_L (%) (6)	χ (deg) (7)	Major Axis (mas) (8)	Minor Axis (mas) (9)	ϕ (deg) (10)
1996.05.....	D	0.00	0.0	5.81	0.2	21.6	0.18	...	45.5
	K9	0.85	−120.4	3.70	2.2	−62.7	0.62	0.21	56.5
	K8	1.47	−117.7	1.03	13.0	−36.3	0.54	0.21	−22.0
	K7	2.38	−115.5	1.77	15.3	−39.9	0.73	0.53	−33.0
	K6	3.06	−101.3	0.26	34.0	−44.5	1.55	0.29	−18.0
	K5	4.15	−112.2	0.40	7.9	32.9	0.56	0.09	−13.5
	K4	4.65	−111.0	1.01	8.2	−82.3	0.48	0.32	6.5
	K2	9.41	−121.8	1.11	19.8	−72.7	3.15	2.25	56.6
1996.23.....	D	0.00	0.0	6.70	1.3	15.2	0.17	...	59.9
	K10	0.08	−93.9	7.04	0.4	67.4	0.26	...	46.5
	K9	1.01	−122.1	1.79	2.7	85.5	0.32	...	69.8
	K8	1.57	−118.7	1.41	12.4	−36.1	0.68	0.30	−30.8
	K7	2.51	−113.9	1.58	15.7	−40.5	0.96	0.61	−17.8
	K5	4.26	−112.1	0.45	11.1	−38.6	1.07	...	−6.2
	K4	4.85	−111.1	0.85	9.4	81.8	0.47	0.31	19.1
	K2	9.47	−120.8	1.07	21.5	−71.1	3.05	2.04	60.4
1996.41.....	D	0.00	0.0	8.84	0.2	38.8	0.37	...	−13.0
	K10	0.26	−123.2	9.25	0.2	−88.9	0.20	0.10	5.8
	K9	1.40	−121.7	1.07	4.6	−37.6	0.51	0.21	7.7
	K8	1.92	−118.0	1.31	9.0	−32.1	0.42	...	61.5
	K7	2.59	−116.2	0.69	22.2	−46.3	0.80	0.28	6.5
	K5	4.55	−114.4	0.74	13.4	−35.8	1.27	0.62	14.2
	K4	5.05	−109.8	0.84	7.0	72.4	0.87	...	4.6
	K2	8.66	−120.9	0.68	13.5	−70.8	3.95	0.69	59.0
1996.57.....	D	0.00	0.0	11.65	0.2	−7.3	0.41	0.12	59.2
	K10	0.36	−115.3	3.42	0.9	30.5	0.21	...	−12.5
	K9	1.33	−121.9	1.76	5.1	−44.1	0.57	0.42	24.3
	K8	1.95	−116.5	0.93	13.0	−27.4	0.58	...	−25.4
	K7	2.60	−115.7	1.16	17.2	−46.9	0.99	0.77	−44.3
	K5	4.38	−110.3	0.67	12.4	−28.2	1.39	0.80	3.7
	K4	5.09	−111.0	0.75	7.8	84.4	0.57	0.38	−2.9
	K2	9.38	−120.3	1.41	8.0	−80.6	4.28	2.37	46.4
1996.74.....	D	0.00	0.0	8.77	0.5	−64.7	0.27	...	60.6
	K10	0.53	−117.5	7.88	1.0	−48.1	0.32	...	65.5
	K9	1.49	−121.4	0.90	15.1	−51.8	1.19	...	4.8
	K8	2.34	−119.2	1.25	12.1	−24.5	0.48	0.28	−33.4
	K7	2.97	−116.2	1.33	15.5	−55.9	1.09	0.91	67.6
	K5	4.53	−108.8	0.24	16.6	−45.9	0.98	...	29.4
	K4	5.40	−112.8	0.93	5.7	65.6	0.93	0.33	−1.5
	K2	10.12	−120.2	1.31	15.9	−71.7	3.23	1.68	32.4
1996.93.....	D	0.00	0.0	10.11	0.6	−63.5	0.42	0.24	45.4
	K10	0.67	−118.5	5.86	2.0	−34.5	0.35	0.24	15.6
	K9	1.64	−123.1	1.09	11.0	−38.5	1.03	0.48	−39.2
	K8	2.45	−121.1	1.38	15.5	−38.6	0.73	0.47	−34.5
	K7	3.29	−116.0	0.83	15.1	−37.7	1.21	0.57	14.8
	K5	4.83	−112.0	0.48	8.9	−72.4	1.17	...	−59.3
	K4	5.52	−112.4	0.59	9.1	−47.1	0.47	0.43	68.5
	K4A	5.60	−120.7	0.12	34.3	42.8	...	...	0.0
	K2	10.14	−120.5	1.28	16.2	−66.3	3.51	1.67	41.5

TABLE 14

COMPONENT DATA FOR 3C 273 AT 15 GHz

Epoch (1)	Component (2)	R (mas) (3)	Θ (deg) (4)	I (Jy) (5)	m_L (%) (6)	χ (deg) (7)	Major Axis (mas) (8)	Minor Axis (mas) (9)	ϕ (deg) (10)
1996.05.....	D	0.00	0.0	3.11	0.7	−15.2	0.24	...	57.5
	U9	0.77	−122.5	3.84	2.6	72.5	0.48	0.13	69.8
	U8	1.43	−119.7	2.33	8.0	−35.5	0.42	0.35	−58.3
	U7	2.19	−116.1	1.51	15.9	−38.2	0.73	0.42	−9.6
	U6	2.77	−115.2	0.54	17.0	−24.7	1.25	...	41.8
	U6A	3.40	−111.0	0.53	13.9	−38.6	0.83	0.42	18.2
	U5	3.98	−112.1	0.46	2.9	−56.1	0.61	...	−66.4
	U4	4.58	−110.6	1.06	8.2	−80.4	0.60	0.25	20.4
	U3	7.49	−123.0	1.34	10.1	−21.5	6.11	0.98	51.2
	U2	10.03	−119.6	1.41	24.1	−76.0	3.02	1.50	25.9
	U1	17.34	−122.9	0.50	7.1	78.5	1.82	1.47	46.7
1996.23.....	D	0.00	0.0	3.31	0.3	−58.7	0.06	...	−82.2
	U10	0.16	−125.9	3.57	0.5	14.8	0.17	...	87.8
	U9	1.06	−123.3	3.47	1.6	−72.3	0.68	...	68.8
	U8	1.71	−120.7	1.76	9.3	−26.7	0.72	0.44	−22.8
	U7	2.39	−115.7	1.48	11.2	−33.2	0.62	0.52	−23.7
	U6	2.82	−111.8	0.31	31.4	−50.8	1.33	...	29.5
	U6A	3.73	−116.7	0.39	16.3	−19.8	1.61	...	−2.2
	U5	4.35	−111.1	0.63	8.8	−39.9	0.76	0.33	−13.9
	U4	4.85	−110.8	0.92	7.4	−85.8	0.49	0.18	10.4
	U3	8.91	−124.6	1.14	8.6	−52.3	4.77	0.49	45.2
	U2	10.43	−118.3	1.01	26.0	−72.6	2.43	0.77	30.5
	U1	17.59	−122.0	0.34	19.8	76.6	2.33	1.23	13.1
1996.41.....	D	0.00	0.0	6.03	0.6	−34.5	0.17	...	65.9
	U10	0.20	−128.4	5.76	0.9	30.0	0.24	...	69.7
	U9	1.18	−124.7	2.83	1.1	45.1	0.88	0.15	54.9
	U8	1.90	−116.9	1.87	11.5	−26.5	0.61	0.52	67.5
	U7	2.62	−112.9	0.87	15.2	−38.8	0.86	0.22	6.3
	U6	3.52	−117.7	0.52	11.4	−34.5	1.12	0.39	34.9
	U5	4.47	−113.7	0.52	16.3	−30.5	1.10	0.42	18.4
	U4	4.96	−110.9	0.99	5.5	−84.5	0.59	0.11	21.0
	U3	7.47	−123.0	0.81	10.4	−37.1	2.44	0.63	53.0
	U2	10.50	−119.9	1.30	20.6	−71.1	2.65	1.04	28.1
	U1	17.62	−123.3	0.22	13.9	84.9	2.48	...	67.4
1996.57.....	D	0.00	0.0	6.26	0.4	−29.9	0.28	...	49.8
	U10	0.30	−113.3	7.06	1.6	35.5	0.27	...	51.1
	U9	1.37	−122.8	2.26	4.1	−44.0	0.74	0.28	50.7
	U8	2.03	−117.7	1.43	15.0	−25.9	0.51	0.30	−19.9
	U7	2.66	−111.2	1.09	17.5	−43.0	0.62	0.55	21.8
	U6	3.66	−117.6	0.56	9.0	−0.9	1.36	0.76	30.2
	U5	4.63	−110.7	0.71	18.1	−38.4	0.81	0.71	−42.3
	U4	5.14	−111.4	0.74	9.7	68.4	0.51	0.20	6.9
	U3	8.13	−123.6	0.77	12.1	−23.0	4.09	0.49	45.4
	U2	10.36	−119.2	1.34	21.5	−70.0	2.89	1.03	35.7
	U1	17.81	−123.7	0.31	10.0	82.9	1.66	0.85	65.0
1996.74.....	D	0.00	0.0	6.83	0.8	85.4	0.29	...	54.3
	U10	0.47	−117.4	7.57	0.9	7.5	0.26	...	57.6
	U9	1.48	−118.4	0.87	5.8	−48.1	0.39	...	−86.7
	U8	2.24	−118.1	1.76	17.0	−35.6	0.56	0.44	−15.1
	U7	3.06	−114.3	0.88	9.5	−32.4	0.94	...	24.3
	U6	3.94	−119.0	0.49	5.1	−46.3	0.87	...	32.8

TABLE 14—*Continued*

Epoch (1)	Component (2)	R (mas) (3)	Θ (deg) (4)	I (Jy) (5)	m_L (%) (6)	χ (deg) (7)	Major Axis (mas) (8)	Minor Axis (mas) (9)	ϕ (deg) (10)
	U5	4.63	−110.5	0.42	14.2	−43.0	0.49	0.12	50.9
	U4	5.30	−111.6	0.81	2.2	−81.0	0.51	0.26	−2.3
	U3	7.73	−121.4	0.48	15.2	−31.5	1.37	0.25	56.5
	U2	10.51	−119.7	1.24	21.8	−72.0	2.71	1.42	16.9
	U1	16.85	−122.1	0.38	7.3	−76.2	2.90	...	70.3
1996.93.....	D	0.00	0.0	7.15	0.1	64.0	0.31	...	66.4
	U10	0.61	−118.1	5.65	0.3	29.3	0.29	0.16	53.1
	U9	1.71	−121.1	1.08	8.2	−34.6	0.55	0.29	−65.6
	U8	2.44	−118.8	1.28	19.1	−36.5	0.85	0.26	−14.9
	U7	3.17	−113.9	0.80	10.2	−31.5	1.00	0.47	36.3
	U6	4.28	−118.3	0.11	14.3	50.0	0.80	...	31.5
	U5	4.75	−110.6	0.54	19.3	−38.7	0.97	0.65	−23.2
	U4	5.46	−111.7	0.68	2.8	−81.3	0.51	0.26	−20.3
	U3	6.17	−125.1	0.16	6.4	23.7	1.70	0.42	18.5
	U2	10.13	−120.7	1.63	16.5	−61.5	3.47	2.01	41.0
	U1	18.00	−123.6	0.35	8.1	86.5	2.98	0.82	13.2

TABLE 15

COMPONENT DATA FOR 3C 279 AT 22 GHz

Epoch (1)	Component (2)	R (mas) (3)	Θ (deg) (4)	I (Jy) (5)	m_L (%) (6)	χ (deg) (7)	Major Axis (mas) (8)	Minor Axis (mas) (9)	ϕ (deg) (10)
1996.05.....	D	0.00	0.0	14.17	3.4	42.4	0.14	...	32.5
	K4	0.17	−107.3	1.94	25.5	26.6	0.57	...	41.0
	K3	0.84	−117.7	0.40	9.0	−38.5	0.33	0.20	−56.2
	K2	2.45	−118.8	0.70	6.4	1.1	0.65	0.61	−44.5
	K1	2.91	−113.1	1.56	18.6	67.0	0.39	0.22	−16.7
1996.23.....	D	0.00	0.0	15.66	4.2	65.1	0.16	0.06	42.3
	K4	0.16	−118.1	3.85	16.9	28.0	0.39	...	52.9
	K3	0.97	−125.8	0.43	13.0	−58.1	0.44	...	28.4
	K2	2.62	−117.6	0.50	7.7	16.4	0.58	0.33	−9.4
	K1	2.96	−113.3	1.70	12.5	67.4	0.38	0.23	−22.5
1996.41.....	D	0.00	0.0	11.97	13.3	−80.1	0.33	...	1.1
	K4	0.07	−91.8	10.51	15.1	13.8	0.32	...	54.5
	K3	0.92	−114.0	0.21	19.7	11.1	1.12	...	−15.2
	K2	2.57	−119.9	0.54	10.8	−86.5	2.23	0.21	−12.9
	K1	3.02	−113.7	1.56	11.4	66.5	0.48	0.11	−17.4
1996.57.....	D	0.00	0.0	10.46	8.7	−82.3	0.11	...	18.5
	K4	0.10	−111.9	10.54	12.6	29.1	0.26	...	55.9
	K3	0.86	−121.9	0.54	17.5	−5.6	0.76	...	70.1
	K2	2.72	−119.3	0.52	5.8	82.8	1.08	0.48	−47.1
	K1	3.06	−113.4	1.66	13.9	67.0	0.40	0.21	−38.0
1996.74.....	D	0.00	0.0	8.08	11.3	74.6	0.23	...	9.2
	K4	0.12	−121.4	11.69	11.3	18.6	0.31	...	46.7
	K3	1.45	−115.7	0.24	33.8	−23.4	1.78	...	65.1
	K2	2.96	−118.6	0.64	6.1	55.6	0.87	0.46	−29.4
	K1	3.13	−113.9	1.62	16.7	66.5	0.38	0.19	−23.2
1996.93.....	D	0.00	0.0	7.60	2.3	88.7	0.23	0.08	−10.1
	K4	0.17	−129.9	9.63	5.3	53.0	0.24	0.17	66.9
	K3	0.69	−120.3	0.64	15.9	10.7	1.72	0.25	23.4
	K2	2.93	−118.9	0.61	2.9	−34.6	0.77	0.54	−17.6
	K1	3.18	−114.0	1.55	14.9	67.4	0.41	0.14	−32.4

TABLE 16
COMPONENT DATA FOR 3C 279 AT 15 GHz

Epoch (1)	Component (2)	R (mas) (3)	Θ (deg) (4)	I (Jy) (5)	m_L (%) (6)	χ (deg) (7)	Major Axis (mas) (8)	Minor Axis (mas) (9)	ϕ (deg) (10)
1996.05.....	D	0.00	0.0	8.39	3.4	−89.1	...	...	0.0
	U4	0.15	−116.5	3.12	21.5	19.3	0.38	...	66.1
	U3	0.83	−125.8	1.17	11.6	−50.1	1.01	...	65.2
	U3A	1.88	−118.6	0.24	23.1	4.9	0.44	...	21.7
	U2	2.52	−117.4	0.47	3.1	20.5	0.61	0.22	−5.6
	U1	2.90	−113.6	1.88	16.7	66.6	0.40	0.20	−27.4
	U0	3.03	−147.9	0.10	26.5	72.3	1.07	...	53.4
1996.23.....	D	0.00	0.0	8.53	4.4	−79.8	...	...	0.0
	U4	0.11	−126.1	5.32	11.1	23.9	0.37	...	58.7
	U3	0.81	−124.2	0.91	9.1	−23.7	0.84	...	44.3
	U2	2.64	−116.5	0.76	3.1	34.7	0.53	0.46	72.6
	U1	2.96	−113.3	1.66	14.3	66.7	0.34	0.20	−22.3
	U0	3.01	−149.6	0.05	52.0	85.1	...	...	0.0
1996.41.....	D	0.00	0.0	9.23	11.0	−76.9	...	...	0.0
	U4	0.10	−114.5	6.80	13.9	14.5	0.36	...	56.3
	U3	0.87	−124.3	0.72	6.6	−50.2	0.65	...	45.4
	U2	2.64	−115.9	0.67	6.1	36.3	0.51	0.31	−32.4
	U1	3.02	−113.5	1.76	11.6	67.1	0.39	0.14	−22.1
	U0	2.93	−145.9	0.06	41.5	78.7	...	...	0.0
1996.57.....	D	0.00	0.0	7.58	10.7	−83.2	...	...	0.0
	U4	0.09	−114.5	9.19	9.9	19.1	0.34	...	53.1
	U3	0.98	−124.6	0.61	8.4	−24.6	0.48	...	51.1
	U2	2.77	−115.5	0.85	2.6	54.9	0.71	0.13	−71.1
	U1	3.05	−113.6	1.67	13.7	66.8	0.37	0.09	−34.5
	U0	3.90	−140.4	0.05	46.7	21.0	...	...	0.0
1996.74.....	D	0.00	0.0	7.08	11.6	74.8	0.11	...	27.3
	U4	0.12	−124.9	9.90	10.0	6.8	0.30	...	62.0
	U3	0.99	−123.0	0.43	10.4	−30.7	0.48	...	48.4
	U2	2.69	−118.2	0.53	2.5	6.3	0.66	...	−63.0
	U1	3.09	−114.1	2.21	14.1	67.2	0.40	0.17	−31.1
	U0	4.24	−142.0	0.05	18.7	46.9	...	...	0.0
1996.93.....	D	0.00	0.0	6.90	6.0	81.0	0.16	...	30.8
	U4	0.11	−120.2	8.15	4.4	29.4	0.34	...	59.0
	U3	1.02	−125.2	0.32	10.3	−8.7	0.27	...	15.5
	U2	2.79	−119.8	0.39	3.5	−16.4	0.56	...	59.9
	U1	3.11	−113.8	2.02	12.3	67.4	0.30	...	−58.4

take to be only a lower limit on the true velocity. The polarization behavior is extremely complex and, together with the complex nature of the observed proper motion and flux, strongly suggests the source is more complicated than our simple two-component model fit.

The combined flux of D and U1 (K1) rises from the first to second epoch before declining, in close step with UMRAO single-dish monitoring data at 14.5 GHz. The total polarizations from our images also agree with the UMRAO measurements at all epochs.

3.6. *J0738+177 (B0735+178)*

The structure of this source is extremely complicated, with the VLBI core to the west and jet components extending to the east at a range of position angles from $\sim 40^\circ - 80^\circ$. In general, our model fits are inconsistent across epoch and frequency. There is a faint parallel "bar" of emission about 1.5 mas north of the ridge line to which no fits were possible. Thus, the behavior of J0738+177 is best addressed in a qualitative fashion, by examining the images.

In Paper I, We could follow only one jet component, U1 (K1), for proper motion analysis. In Paper II, no components met our criteria for robust variability analysis. The linear polarization structure is most clearly detected at the lower (more sensitive) frequency. It is not only complex in its distribution, but also undergoes changes in magnitude and position angle that appear unrelated to changes in the total intensity structure. The integrated polarization is low.

The total fluxes of the core and jet decline in step over the year. With a constant offset, this change is tracked by the 15 GHz UMRAO data.

3.7. *J0854+201 (OJ 287, B0851+202)*

This source has a strong core and a short jet extending about 2 mas due west. It is fitted with deceptive simplicity at individual epochs by two or three components. As described in

TABLE 17
COMPONENT DATA FOR J1310+32 AT 22 GHz

Epoch (1)	Component (2)	R (mas) (3)	Θ (deg) (4)	I (Jy) (5)	m_L (%) (6)	χ (deg) (7)	Major Axis (mas) (8)	Minor Axis (mas) (9)	ϕ (deg) (10)
1996.05.....	D	0.00	0.0	0.83	3.1	−81.4	0.25	0.16	−2.3
	K3	0.36	−67.4	1.76	4.8	30.2	0.28	0.14	41.9
	K2	0.57	−34.6	0.42	7.0	−21.2	0.53	0.19	25.2
	K1	1.03	−40.9	0.06	8.8	56.5	0.83	...	51.5
1996.23.....	D	0.00	0.0	0.59	5.6	−73.3	0.15	...	−37.9
	K3	0.39	−69.7	1.20	2.0	25.9	0.20	0.11	78.9
	K2	0.58	−34.2	0.31	7.4	−6.6	0.43	0.20	24.0
	K1	0.65	−103.1	0.09	23.6	32.3	1.10	...	−39.1
1996.41.....	D	0.00	0.0	0.65	6.0	−68.3	0.20	...	75.1
	K3	0.41	−67.2	1.46	0.5	39.5	0.29	0.06	80.6
	K2	0.69	−28.9	0.22	13.0	−1.0	0.27	...	−20.1
	K1	0.74	−78.5	0.19	10.0	53.2	0.60	0.27	−31.5
1996.57.....	D	0.00	0.0	0.72	3.5	−80.1	0.19	0.13	−49.0
	K3	0.44	−67.2	1.44	3.0	15.0	0.27	0.17	−79.8
	K2	0.72	−28.6	0.22	9.5	−5.2	0.43	0.22	−57.2
	K1	0.89	−77.7	0.19	13.1	70.0	0.83	...	−33.4
1996.74.....	D	0.00	0.0	0.42	7.2	−71.1	0.56	...	−73.1
	K4	0.23	−42.0	0.70	1.2	69.8	...	...	0.0
	K3	0.60	−66.5	1.03	4.2	10.2	0.47	0.21	−55.1
	K2	0.84	−30.7	0.14	8.9	6.1	0.61	...	−66.5
1996.93.....	D	0.00	0.0	0.26	8.1	75.8	1.31	...	−66.1
	K4	0.30	−72.6	0.72	6.3	−58.4	...	...	0.0
	K2	0.45	−0.0	0.13	19.1	1.8	1.02	0.39	−17.2
	K3	0.68	−72.7	1.08	5.9	41.0	0.65	0.41	−60.9
	K1	1.32	−92.8	0.06	19.0	−62.9	0.48	0.13	−27.4

Paper I, it is only the close spacing of the epochs and the availability of polarization information that allowed its kinematics to be understood. We found that OJ 287 has two stationary components, one very near the VLBI core and another at approximately 1.5 mas from it. Between these two stationary features, we followed another component, U3 (K3), with very rapid superluminal motion, which was confirmed by our polarization data.

For the variability analysis in Paper II, the core region, components D + U4(K4), is treated as one component and the superluminal component U3 (K3) as another. The core region of OJ 287 is the only one in our sample that showed a significant linear trend in fractional polarization: a decay of 3%–4% over the year. It is also one of only two cores that had a very large ($\sim$180°) apparent rotation in their polarization position angle. The total flux of the jet feature, U3 (K3), decayed rapidly and showed the largest flux variation (about a linear decline) seen in jet features in our sample. U3 (K3) also shows the highest rise and fall in fractional polarization (4%) of any component.

The 15 GHz single-dish UMRAO data show the total and polarized flux declining during the first half of the year before rising slightly. This behavior is reflected in our VLBA data.

3.8. *J1224+212 (B1222+216, 4C 21.35)*

This source has a dominant core with a north-south jet. Apart from the core, four components are fitted, of which three jet components K1 (U1), K2 (U2), and K3 (U3) are fitted well enough to derive proper motions in Paper I.

For variability analysis (Paper II), a "core region" consisting of D+U3 (D+K4+K3) was used. It had a steady fractional polarization of about 5% and modest change in EVPA. It showed only a slight decline in total flux over five epochs which is consistent with the sparse UMRAO data for this source.

3.9. *3C 273 (J1229+02)*

This source has a bright core that undergoes an almost fivefold increase in flux during the first four epochs. There is a complex jet at a position angle of −110° for the first 6 mas, where the inner jet terminates at a strong component, before bending to a position angle $\sim$−135°. The inner jet had five components fitted well enough for proper motions to be measured (Paper I).

For variability analysis in Paper II, three regions were used: the "core region" D+U10 (D+K10), the jet region U9+U8+U7 (K9+K8+K7) and the bright jet knot U5+U4 (K5+K4). The core region had a decrease in spectral index, suggesting a shift toward more optically thin radiation. This coincided with the birth of a new component and the appearance of circular polarization in mid-1996 (Homan & Wardle 1999). The change in the fractional polarization ratio of the jet region U9+U8+U7, at our two frequencies, strongly suggested that this component is emerging from behind a Faraday screen (Paper II; R. Ojha et al. 2004, in preparation). This is the only such component in our sample.

TABLE 18

COMPONENT DATA FOR J1310+32 AT 15 GHz

Epoch (1)	Component (2)	R (mas) (3)	Θ (deg) (4)	I (Jy) (5)	m_L (%) (6)	χ (deg) (7)	Major Axis (mas) (8)	Minor Axis (mas) (9)	ϕ (deg) (10)
1996.05.....	D	0.00	0.0	0.84	2.6	−75.0	0.18	...	−50.3
	U3	0.34	−67.4	1.97	5.3	23.9	0.25	0.13	40.5
	U2	0.62	−37.9	0.31	4.7	−30.5	0.59	...	48.2
1996.23.....	D	0.00	0.0	0.69	5.0	−72.8	0.07	...	−7.3
	U3	0.39	−63.7	1.99	3.3	22.9	0.31	0.20	46.3
	U2	0.71	−35.8	0.33	8.1	−10.2	0.55	...	49.6
	U1	1.14	−73.4	0.05	21.6	67.7	0.94	...	−8.0
1996.41.....	D	0.00	0.0	0.71	4.1	−67.9	0.20	...	−22.1
	U3	0.42	−72.2	1.70	2.1	26.4	0.33	0.08	−84.8
	U2	0.64	−30.9	0.38	7.1	0.2	0.30	...	77.7
	U1	1.00	−66.1	0.07	16.2	77.3	0.81	...	−86.2
1996.57.....	D	0.00	0.0	0.69	1.7	89.1	0.22	...	−39.8
	U3	0.43	−70.2	1.61	4.5	4.6	0.39	0.18	−77.0
	U2	0.63	−82.2	0.22	28.2	67.4	1.10	0.37	−60.9
	U2	0.71	−29.6	0.23	9.9	−11.8	0.34	...	82.8
	U0	5.80	−73.9	0.01	14.8	27.1	...	...	0.0
1996.74.....	D	0.00	0.0	0.71	4.7	88.6	0.14	...	−32.9
	U3	0.46	−68.5	1.62	5.2	2.5	0.44	0.16	−80.5
	U2	0.74	−77.9	0.17	24.0	78.3	0.70	0.41	−43.4
	U2	0.74	−28.1	0.18	13.0	4.8	0.34	...	−45.3
1996.93.....	D	0.00	0.0	0.75	4.8	−68.7	0.10	...	−48.9
	U3	0.36	−66.2	0.79	11.5	24.7	0.44	0.35	19.5
	U2	0.68	−67.7	0.72	5.4	−75.4	0.39	0.09	70.2
	U1	1.80	−47.8	0.01	4.5	−84.1	0.41	...	−51.3

TABLE 19

COMPONENT DATA FOR PKS 1510−089 AT 22 GHz

Epoch (1)	Component (2)	R (mas) (3)	Θ (deg) (4)	I (Jy) (5)	m_L (%) (6)	χ (deg) (7)	Major Axis (mas) (8)	Minor Axis (mas) (9)	ϕ (deg) (10)
1996.05.....	D	0.00	0.0	1.11	1.7	8.9	0.19	0.07	−4.7
	K1	1.09	−27.3	0.43	4.5	82.7	0.52	0.35	47.1
1996.23.....	D	0.00	0.0	1.17	2.1	−8.9	...	...	0.0
	K2	0.14	−17.1	0.54	5.5	−22.5	0.37	0.18	−15.9
	K1	1.27	−29.7	0.39	5.4	86.1	0.62	0.36	21.9
1996.41.....	D	0.00	0.0	1.52	4.6	59.7	...	...	0.0
	K2	0.26	−28.7	0.36	1.6	58.4	0.18	...	−12.8
	K1	1.44	−29.7	0.31	4.8	42.7	0.76	0.37	21.1
1996.57.....	D	0.00	0.0	1.32	4.1	1.3	...	...	0.0
	K2	0.21	−36.3	0.37	8.3	69.2	0.09	...	14.6
	K1	1.47	−27.9	0.32	6.7	52.6	1.00	0.61	−9.8
1996.74.....	D	0.00	0.0	0.99	4.3	−41.3	...	...	0.0
	K2	0.24	−27.2	0.26	2.1	43.7	0.89	...	−26.9
	K1	1.79	−28.5	0.19	9.4	57.5	1.39	0.40	9.6
1996.93.....	D	0.00	0.0	0.60	0.8	84.2	...	...	0.0
	K2	0.25	−31.6	0.28	3.3	−8.1	0.75	0.14	−21.8
	K1	1.93	−28.4	0.20	8.6	57.9	1.31	0.75	4.5

TABLE 20
COMPONENT DATA FOR PKS 1510−089 AT 15 GHz

Epoch (1)	Component (2)	R (mas) (3)	Θ (deg) (4)	I (Jy) (5)	m_L (%) (6)	χ (deg) (7)	Major Axis (mas) (8)	Minor Axis (mas) (9)	ϕ (deg) (10)
1996.05.....	D	0.00	0.0	0.96	1.0	6.9	0.21	...	−25.8
	U1	1.07	−27.2	0.61	3.4	88.3	0.56	0.47	10.8
1996.23.....	D	0.00	0.0	0.97	3.2	−8.9	...	...	0.0
	U2	0.16	−50.3	0.35	1.0	−39.8	0.40	...	3.2
	U1	1.24	−29.7	0.57	4.4	78.5	0.72	0.45	23.5
1996.41.....	D	0.00	0.0	1.01	4.8	−76.7	...	...	0.0
	U2	0.10	−43.8	0.53	5.5	26.8	0.31	...	−28.0
	U1	1.41	−28.9	0.48	6.6	50.5	0.80	0.49	21.2
1996.57.....	D	0.00	0.0	0.99	3.9	−2.0	...	...	0.0
	U2	0.22	−36.9	0.50	7.9	61.6	0.23	...	−6.3
	U1	1.56	−29.2	0.37	7.6	59.5	0.94	0.56	7.1
1996.74.....	D	0.00	0.0	0.71	4.6	−46.6	...	...	0.0
	U2	0.18	−31.0	0.47	1.8	29.5	0.28	...	−31.2
	U1	1.70	−29.1	0.30	7.2	61.4	1.04	0.55	1.7
1996.93.....	D	0.00	0.0	0.51	2.1	−40.9	...	...	0.0
	U2	0.35	−29.8	0.16	2.3	18.2	0.21	...	−61.0
	U1	1.93	−27.7	0.28	6.8	65.7	1.41	0.66	−9.1

There is a roughly constant offset in both total and polarized intensity between the UMRAO single-dish and the VLBA data.

3.10. *3C 279 (J1256−05)*

Only the inner 3 mas of the jet is seen at our frequencies. It is essentially a double with a strong core and a jet at a position angle of -115° terminating in a bright component. Four jet components are identified, of which U1 (K1) and U4 (K4) are followed reliably enough for proper motion study in Paper I.

For variability analysis (Paper II) we used the two distinct features: the core region D+U4 (D+K4) and the strong, superluminal jet feature U1+U2 (K1+K2). Though U4 had to be lumped with D for studying total flux, it is clear that it is a distinct component with different polarization properties. From later observations (Homan & Wardle 2000, epoch 1997.94) we know it emerges from the core.

The core region sharply increased in flux before starting a steady decay. As in 3C 273, this region had a decrease in spectral index pointing to a shift toward more optically thin radiation and this appears linked to the formation of a new component (Paper II). Variability in fractional polarization and EVPA is significant with a discontinuity at the third epoch. These large changes in the core region have little effect on the region U1+U2, which exhibits minimal variation. As described above, U1 was used to calibrate our EVPAs.

This is another of our sources showing a near constant offset between the VLBA and UMRAO monitoring data.

3.11. *J1310+323 (B1308+326, OP 313)*

This barely resolved source has a bright asymmetric core with an extension along $\theta \sim -55^\circ$. Though fitted with multiple components at individual epochs, no robust identification

TABLE 21
COMPONENT DATA FOR J1751+09 AT 22 GHz

Epoch (1)	Component (2)	R (mas) (3)	Θ (deg) (4)	I (Jy) (5)	m_L (%) (6)	χ (deg) (7)	Major Axis (mas) (8)	Minor Axis (mas) (9)	ϕ (deg) (10)
1996.05.....	D	0.00	0.0	2.73	1.6	−61.5	0.20	...	36.0
1996.23.....	D	0.00	0.0	1.00	2.6	−81.3	0.28	...	34.6
1996.41.....	D	0.00	0.0	0.85	0.6	55.8	0.19	...	0.3
1996.57.....	D	0.00	0.0	1.04	1.2	−79.7	0.09	...	27.3
1996.74.....	D	0.00	0.0	1.06	1.6	−24.3	...	...	−30.7
1996.93.....	D	0.00	0.0	2.32	1.1	−14.1	0.25	...	−21.9

TABLE 22

COMPONENT DATA FOR J1751+09 AT 15 GHz

Epoch (1)	Component (2)	R (mas) (3)	Θ (deg) (4)	I (Jy) (5)	m_L (%) (6)	χ (deg) (7)	Major Axis (mas) (8)	Minor Axis (mas) (9)	ϕ (deg) (10)
1996.05.....	D	0.00	0.0	1.25	9.3	14.6	...	...	0.0
	U3	0.06	44.1	1.48	10.8	−74.3	0.28	0.05	36.0
	Up	3.08	27.5	0.03	18.7	18.3	3.02	0.43	−2.1
1996.23.....	D	0.00	0.0	0.41	3.5	35.5	...	...	0.0
	U3	0.14	36.6	0.64	8.3	−66.2	0.34	...	35.9
	Up	1.88	24.2	0.02	15.0	13.7	1.60	0.78	37.8
	Uq	4.82	29.7	0.02	14.3	−4.5	2.52	1.91	21.9
1996.41.....	D	0.00	0.0	0.54	1.2	38.2	...	...	0.0
	U3	0.16	32.2	0.24	3.0	−72.8	0.53	0.10	27.6
	Up	2.69	31.7	0.01	23.3	12.8	1.15	0.25	26.6
	Uq	5.22	27.6	0.01	5.5	−1.6	2.28	1.34	−51.7
1996.57.....	D	0.00	0.0	0.74	1.4	−88.2	...	...	0.0
	U3	0.34	29.6	0.06	8.2	−42.0	0.26	...	5.8
	Up	2.80	27.7	0.03	14.7	29.1	3.98	1.07	30.5
1996.74.....	D	0.00	0.0	0.83	1.2	−39.1	0.06	...	57.7
	U3	0.40	28.7	0.04	5.0	86.4	0.45	0.10	5.7
	Up	4.38	30.6	0.02	15.5	15.1	2.67	1.30	33.6
1996.93.....	D	0.00	0.0	1.82	2.3	−46.2	0.05	...	55.3
	U3	0.41	31.9	0.02	3.4	−73.5	0.52	...	10.5
	Up	4.71	27.8	0.02	9.7	33.1	2.99	1.82	18.2

TABLE 23

COMPONENT DATA FOR J1927+73 AT 22 GHz

Epoch (1)	Component (2)	R (mas) (3)	Θ (deg) (4)	I (Jy) (5)	m_L (%) (6)	χ (deg) (7)	Major Axis (mas) (8)	Minor Axis (mas) (9)	ϕ (deg) (10)
1996.05.....	D	0.00	0.0	1.56	0.2	−45.5	0.29	...	−21.4
	K3	0.69	150.9	0.81	0.4	60.7	0.31	0.10	−17.2
	K2	1.73	157.7	0.32	3.3	−88.6	0.34	...	56.2
	K1	2.03	172.9	0.25	15.6	43.6	0.33	0.18	−30.9
1996.23.....	D	0.00	0.0	1.54	0.9	−36.1	0.29	...	−21.2
	K3	0.71	150.8	0.70	0.6	−58.7	0.31	0.07	−5.8
	K2	1.78	157.3	0.31	2.3	75.2	0.31	...	71.6
	K1	2.02	173.2	0.29	13.1	52.5	0.51	0.26	−19.3
1996.41.....	D	0.00	0.0	1.74	0.2	64.8	0.34	0.05	−25.3
	K3	0.71	151.3	0.63	6.3	−12.6	0.15	...	9.6
	K2	1.77	156.4	0.26	8.5	−72.2	0.23	...	18.2
	K1	2.06	174.2	0.27	19.5	49.5	0.37	0.31	46.1
1996.57.....	D	0.00	0.0	1.55	1.1	−56.0	0.26	...	−18.9
	K3	0.68	150.5	0.83	2.8	−20.9	0.33	0.12	−13.3
	K2	1.84	156.9	0.35	6.6	−75.0	0.37	0.24	5.9
	K1	2.12	172.8	0.32	14.4	51.4	0.61	0.31	−29.0
1996.74.....	D	0.00	0.0	1.69	0.4	−64.5	0.37	...	−23.4
	K3	0.71	150.4	0.71	0.5	−2.4	0.26	...	−5.7
	K2	1.88	157.7	0.31	7.0	−77.5	0.37	0.24	−31.6
	K1	2.15	172.8	0.34	14.8	47.8	0.65	0.31	−27.7
1996.93.....	D	0.00	0.0	1.75	0.7	−88.4	0.45	...	−20.1
	K3	0.78	150.4	0.70	2.2	−43.5	0.26	...	20.6
	K2	1.91	158.2	0.32	6.8	−85.1	0.56	0.25	−9.1
	K1	2.27	172.8	0.27	15.5	54.8	1.05	0.29	−31.3

TABLE 24
COMPONENT DATA FOR J1927+73 AT 15 GHz

Epoch (1)	Component (2)	R (mas) (3)	Θ (deg) (4)	I (Jy) (5)	m_L (%) (6)	χ (deg) (7)	Major Axis (mas) (8)	Minor Axis (mas) (9)	ϕ (deg) (10)
1996.05.....	D	0.00	0.0	1.21	0.2	−46.3	0.36	...	−28.2
	U3	0.65	150.8	0.86	1.2	−87.9	0.20	...	6.8
	U2	1.66	157.0	0.44	3.4	−69.4	0.40	0.29	1.3
	U1	2.00	173.0	0.42	14.6	42.0	0.62	0.28	−28.7
	Up	3.88	163.3	0.05	18.5	80.5	1.09	...	42.7
	Uq	8.59	163.8	0.09	8.7	82.7	7.36	0.77	−16.7
1996.23.....	D	0.00	0.0	1.18	0.7	−16.7	0.33	...	−25.7
	U3	0.67	151.1	0.99	0.7	−48.3	0.32	0.12	−16.6
	U2	1.76	157.2	0.41	4.1	−73.2	0.36	0.29	−5.3
	U1	2.06	172.6	0.43	14.0	44.7	0.66	0.29	−22.3
	Up	3.81	160.3	0.06	18.9	70.7	1.29	0.54	−0.6
	Uq	9.90	165.3	0.10	9.1	81.6	6.19	1.21	−9.3
1996.41.....	D	0.00	0.0	1.40	0.2	−4.8	0.36	...	−26.7
	U3	0.68	151.4	0.85	3.4	−57.9	0.31	...	−3.1
	U2	1.75	157.0	0.37	4.9	−79.2	0.29	0.08	52.5
	U1	2.04	173.1	0.39	15.1	49.8	0.47	0.30	−30.3
	Up	3.57	159.9	0.06	16.2	84.8	1.15	0.52	−19.7
	Uq	9.07	164.8	0.04	21.8	84.9	1.92	0.87	7.8
1996.57.....	D	0.00	0.0	1.35	0.4	−1.7	0.31	...	−21.2
	U3	0.67	150.5	0.96	1.5	−50.6	0.33	0.09	−6.3
	U2	1.81	156.9	0.38	5.4	−74.9	0.34	0.25	4.4
	U1	2.11	172.5	0.41	14.4	50.2	0.65	0.31	−25.1
	Up	3.79	159.8	0.06	15.2	89.0	1.01	0.38	15.4
	Uq	10.08	164.9	0.06	15.4	81.6	5.11	1.08	−5.4
1996.74.....	D	0.00	0.0	1.52	0.4	−22.3	0.36	...	−22.2
	U3	0.69	150.4	1.00	1.0	−14.3	0.26	0.07	−1.7
	U2	1.84	157.5	0.39	6.7	−78.3	0.38	0.22	3.8
	U1	2.17	172.7	0.36	15.8	51.3	0.48	0.29	−28.6
	Up	3.68	158.7	0.06	16.4	73.2	1.06	0.56	−33.4
	Uq	3.89	170.4	0.02	9.8	−25.6	0.83	...	−70.0
	Ur	10.10	164.6	0.09	15.0	85.6	4.82	1.32	−5.3
1996.93.....	D	0.00	0.0	1.38	0.9	−5.5	0.43	...	−20.6
	U3	0.71	150.8	0.98	0.6	−28.7	0.34	...	−7.8
	Up	1.04	18.0	0.03	5.6	36.3	...	...	0.0
	U2	1.87	158.1	0.33	6.5	−76.7	0.40	0.26	−19.9
	U1	2.19	172.5	0.31	17.0	50.9	0.64	0.28	−36.5
	Uq	3.65	173.9	0.03	14.4	−9.2	1.08	...	36.8
	Ur	3.69	159.1	0.02	30.6	66.2	0.67	0.10	−9.5
	Us	9.44	165.6	0.11	19.0	86.3	9.69	1.48	−4.1

of these components was possible between epochs and no proper motion information could be obtained (Paper I).

For variability analysis the entire image was summed over. The total intensity decreased monotonically, and this decrease was mirrored in the UMRAO monitoring data. The total VLBA polarization flux also closely agrees with the UMRAO values. However, the polarization images carry a wealth of detail. They show a clear double that may be a core-jet structure with the core to the east and the jet roughly along the extension in total intensity. The core and jet polarizations beat to depress the polarized flux between them and probably exaggerate the distance between them. A ''pinched'' edge is clearly visible on the northwest edge of the jet component, suggesting the presence of another polarized component. The ''jet'' component itself appears to be expanding to the southwest.

3.12. *J1512−090 (B1510−089, OR−017)*

This source has a strong core and a single jet component to the northwest along a position angle $\sim -25^\circ$. Two jet components were fitted and their proper motions analyzed in Paper I. Startlingly, the very fast jet component, U1 (K1), is growing in size at a rate almost as fast as its outward motion! The implications of this are discussed in J. F. C. Wardle et al. (2004, in preparation).

For the variability analysis in Paper II, we considered a core region D+U3 (D+K3) and a jet component U1 (K1). While the fractional polarization of the core region varied irregularly, its flux showed a large rise and fall. It had the largest rotation in polarization angle seen in our sample, with a slope of -350° per year (Paper II).

TABLE 25

COMPONENT DATA FOR J2005+77 AT 22 GHz

Epoch (1)	Component (2)	R (mas) (3)	Θ (deg) (4)	I (Jy) (5)	m_L (%) (6)	χ (deg) (7)	Major Axis (mas) (8)	Minor Axis (mas) (9)	ϕ (deg) (10)
1996.05.....	D	0.00	0.0	0.68	4.9	85.1	0.14	...	−13.8
	K2	0.31	−89.1	0.17	25.6	61.5	1.02	0.23	88.4
	K1	1.51	−94.1	0.09	9.6	−48.6	0.52	0.28	−56.2
1996.23.....	D	0.00	0.0	0.58	3.7	88.1	0.18	0.09	87.9
	K2	0.47	−95.0	0.23	5.1	60.5	0.58	0.20	87.5
	K1	1.71	−91.0	0.09	7.6	66.1	0.52	0.27	−70.0
1996.41.....	D	0.00	0.0	0.62	2.3	−71.2	0.12	...	−53.3
	K2	0.44	−93.7	0.18	16.4	65.2	0.62	0.23	−87.8
	K1	1.55	−94.0	0.05	5.1	66.7	0.52	0.29	−35.9
1996.57.....	D	0.00	0.0	0.66	1.8	−69.9	0.11	0.06	−59.1
	K2	0.40	−93.2	0.18	9.1	68.2	0.67	0.18	−86.2
	K1	1.60	−94.0	0.07	3.6	7.4	0.70	0.39	−59.6
1996.74.....	D	0.00	0.0	0.74	4.6	−80.4	0.19	...	−67.4
	K2	0.51	−95.3	0.15	14.0	44.2	0.65	0.13	−81.4
	K1	1.57	−97.8	0.06	5.3	69.0	0.41	0.13	−86.7
1996.93.....	D	0.00	0.0	0.89	7.9	−72.4	0.22	0.16	−42.5
	K2	0.52	−86.3	0.17	7.0	43.7	0.78	0.09	39.1
	K1	1.87	−98.6	0.05	9.1	81.3	0.75	0.22	28.3

TABLE 26

COMPONENT DATA FOR J2005+77 AT 15 GHz

Epoch (1)	Component (2)	R (mas) (3)	Θ (deg) (4)	I (Jy) (5)	m_L (%) (6)	χ (deg) (7)	Major Axis (mas) (8)	Minor Axis (mas) (9)	ϕ (deg) (10)
1996.05.....	D	0.00	0.0	0.29	4.2	−83.4	...	...	0.0
	U3	0.18	−76.1	0.41	11.9	74.6	0.19	0.06	48.4
	U2	0.63	−91.2	0.24	6.2	51.4	0.32	0.15	59.3
	U1	1.73	−90.1	0.13	9.3	−84.0	0.60	0.17	−86.9
1996.23.....	D	0.00	0.0	0.28	4.4	−68.8	...	...	0.0
	U3	0.20	−88.5	0.34	10.3	69.6	0.20	0.05	88.9
	U2	0.66	−93.7	0.19	4.8	48.0	0.26	...	80.3
	U1	1.73	−90.9	0.13	10.4	85.0	0.57	0.31	−77.8
1996.41.....	D	0.00	0.0	0.27	8.1	−48.2	...	...	0.0
	U3	0.15	−96.9	0.28	10.6	65.3	0.22	...	−86.6
	U2	0.63	−94.7	0.18	9.1	65.7	0.25	0.15	−66.6
	U1	1.69	−93.2	0.12	3.6	85.9	0.78	0.31	−78.7
1996.57.....	D	0.00	0.0	0.25	8.2	−63.3	...	...	0.0
	U3	0.18	−85.6	0.32	4.7	64.1	0.26	0.12	−79.8
	U2	0.65	−94.0	0.15	11.1	61.7	0.20	0.17	−31.8
	U1	1.70	−94.6	0.10	3.0	−77.4	0.76	0.31	−86.2
1996.74.....	D	0.00	0.0	0.40	7.4	−63.5	...	...	0.0
	U3	0.21	−86.8	0.25	6.1	60.8	0.24	0.13	−62.4
	U2	0.65	−94.0	0.14	10.5	46.2	0.15	...	53.0
	U1	1.66	−96.5	0.10	9.5	79.6	0.61	0.32	−73.6
1996.93.....	D	0.00	0.0	0.47	8.3	−59.9	...	...	0.0
	U3	0.22	−74.8	0.29	8.2	−82.2	0.26	0.06	−22.3
	U2	0.62	−92.5	0.16	6.2	40.9	0.34	0.14	7.5
	U1	1.75	−94.5	0.07	4.9	−88.0	0.55	0.49	−39.6

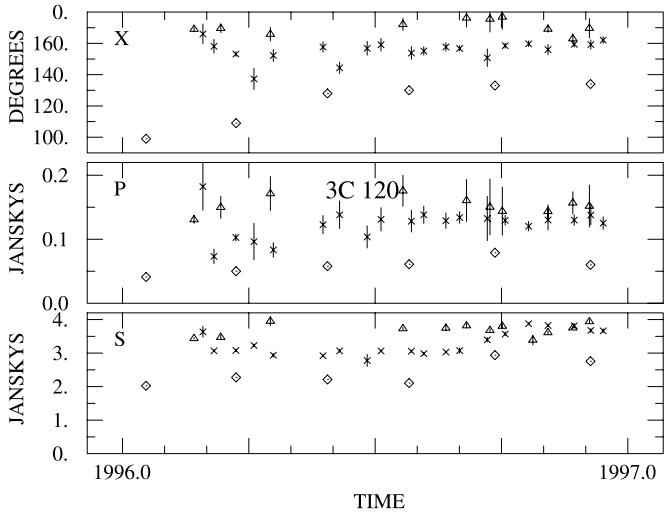

FIG. 27.—Single-dish monitoring data for 3C 120 for the year 1996. Plots are laid out as described in § 3.3.

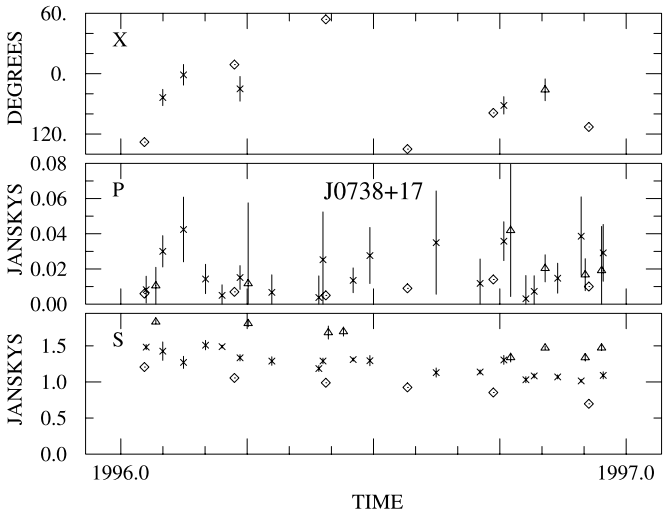

FIG. 29.—Single-dish monitoring data for J0738+171 for the year 1996. Plots are laid out as described in § 3.3.

All changes in the VLBA data are closely tracked by changes in the single-dish UMRAO data, with a constant offset in total flux.

3.13. *J1751+09 (B1749+096, OT 081, 4C 09.56)*

J1751+09 has a strong core and a very weak jet to the northeast. At 22 GHz we only fitted a single core component, but at 15 GHz another component, U3, was fitted close to the core. As U3 faded rapidly, its proper motion may have been confused (Paper I). The northeast extension is too faint to allow a convincing fit.

We consider only the core region, D+U3 (D at 22 GHz) for variability analysis (Paper II). It showed two sudden large changes between neighboring epochs, a sharp drop in flux density between the first two and a sharp rise between the last two. This region also had a distinct increase in spectral index, suggesting a shift toward more optically thick radiation. This shift may be connected with particle injection at the start of a new outburst.

The total and polarized flux from our CLEAN maps agree with the UMRAO values at all six epochs.

3.14. *J1927+739 (B1928+738, 4C 73.18)*

This source was fitted with a core and three convincing jet components that lie on different structural position angles and are all moving radially away from the core, implying different angles of ejection for each (Paper I).

For variability analysis in Paper II, three features were used: D+U3 (D+K3), and the two jet components U2 (K2) and U1 (K1). U1 (K1) was the only jet feature in our sample beyond a projected radius of 5 pc that showed significant fluctuations in flux. Both U1 (K1) and U2 (K2) had an increasing spectral index. This simultaneous change in these two almost side by side components may have resulted from particle reacceleration in a standing shock at their position in the jet (Paper II).

The total flux from our CLEAN maps shows a near constant offset from the single-dish UMRAO flux.

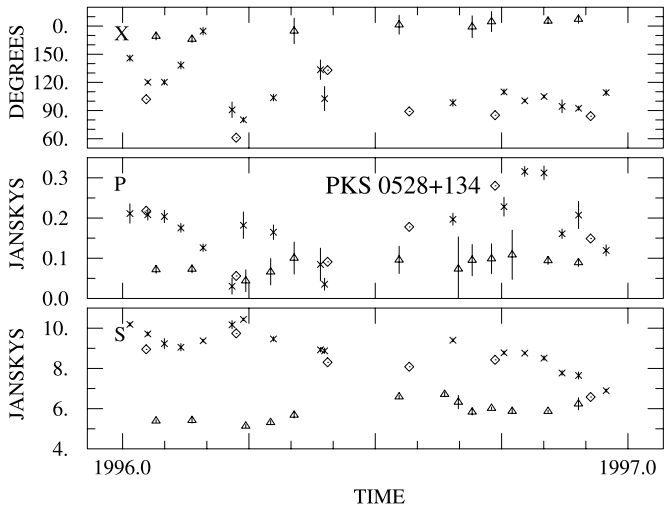

FIG. 28.—Single-dish monitoring data for J0530+135 for the year 1996. Plots are laid out as described in § 3.3.

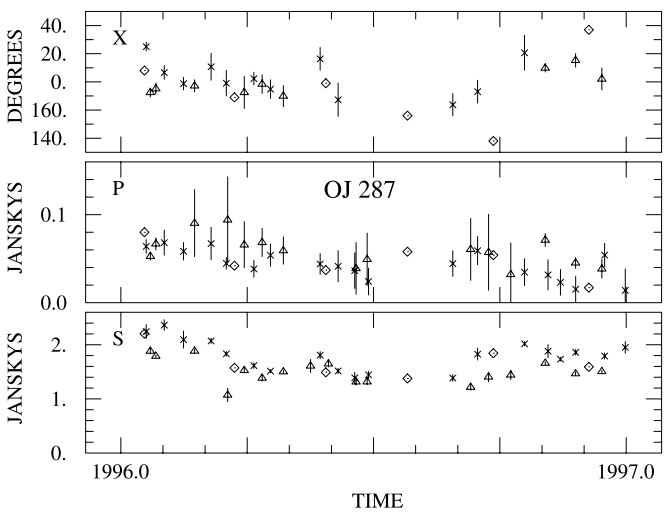

FIG. 30.—Single-dish monitoring data for J0854+201 for the year 1996. Plots are laid out as described in § 3.3.

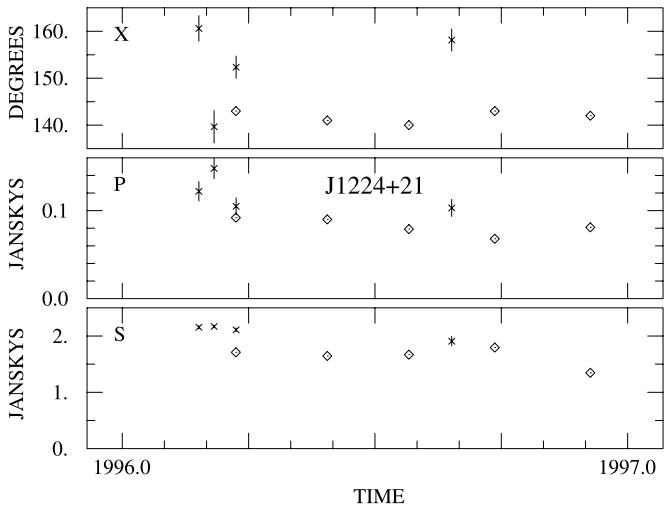

FIG. 31.—Single-dish monitoring data for J1224+212 for the year 1996. Plots are laid out as described in § 3.3.

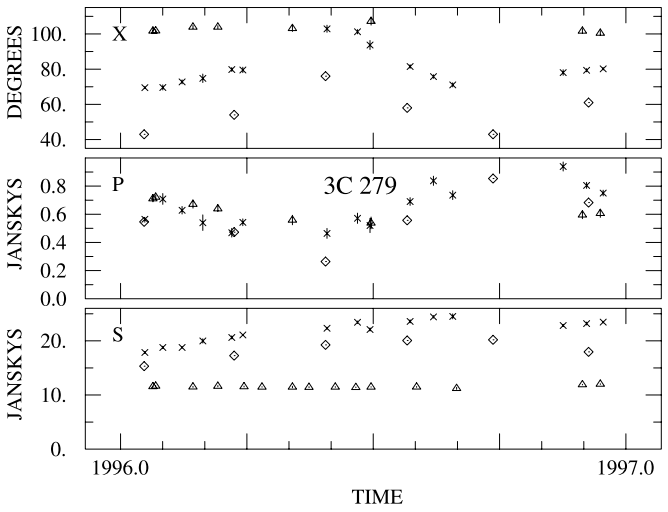

FIG. 33.—Single-dish monitoring data for 3C 279 for the year 1996. Plots are laid out as described in § 3.3.

3.15. *J2005+778 (B2007+777)*

J2005+778 has a short jet extending ∼2.5 mas to the west. It was well fitted by three jet components (two at 22 GHz). Uniquely, in our sample the jet features of this source had no detectable proper motion (Paper I), although U1 (K1) had a very significant flux decay (Paper II).

For the variability analysis in Paper II, we used the core region D+U3+U2 (D+K2) and the jet component U1 (K1). The core region showed a gentle fall in flux followed by a rise. Like J1751+09, this core region had a distinct increase in spectral index, implying a shift toward more optically thick radiation; a shift that may be connected with particle injection at the start of a new outburst.

There is a roughly constant offset between the total and polarized flux from our VLBA images and the single-dish UMRAO flux.

4. CONCLUSIONS

Twelve blazars were monitored at regular, bimonthly intervals for a year. They were observed at two high (15 and 22 GHz) frequencies by the VLBA. Both polarized and total intensity data were calibrated and modeled.

The quick turnaround time of the VLBA made it practical to monitor the milliarcsecond polarization and total intensity structures of these rapidly varying sources both regularly and more frequently than previous, quasi-annual, VLBI observations. Frequent temporal sampling is vital for understanding the properties of extragalactic radio sources given that they are often variable on timescales of months, weeks, and indeed, in some cases, days. We saw changes in all our sources at our shortest (two month) observation intervals.

At the high observing frequencies (15 and 22 GHz) of this program, extra care in calibration and self-calibration as

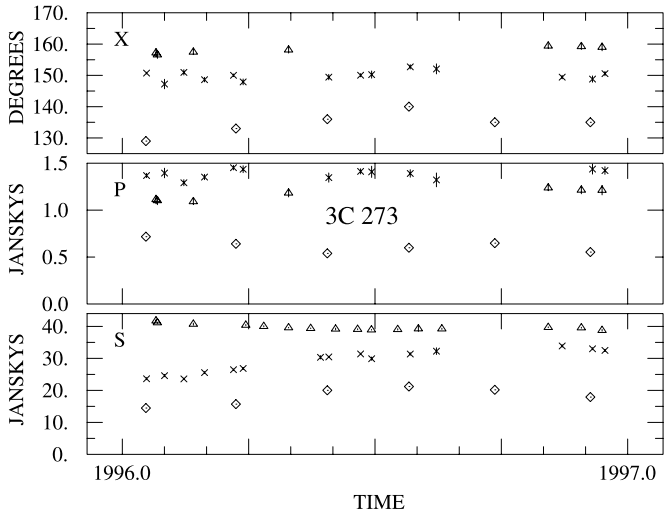

FIG. 32.—Single-dish monitoring data for 3C 273 for the year 1996. Plots are laid out as described in § 3.3.

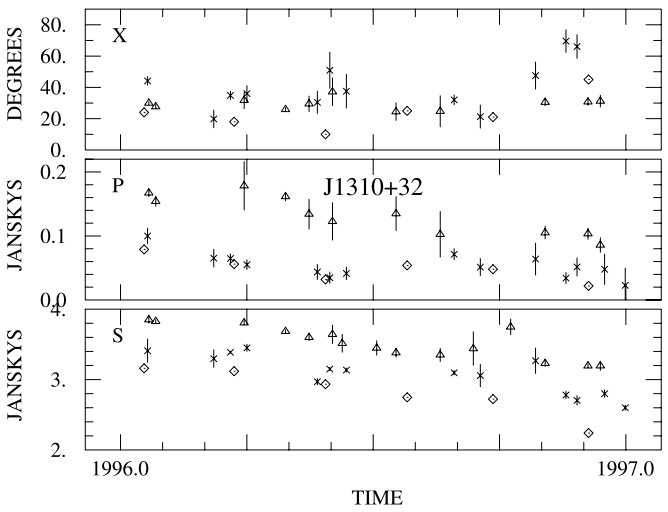

FIG. 34.—Single-dish monitoring data for J1310+323 for the year 1996. Plots are laid out as described in § 3.3.

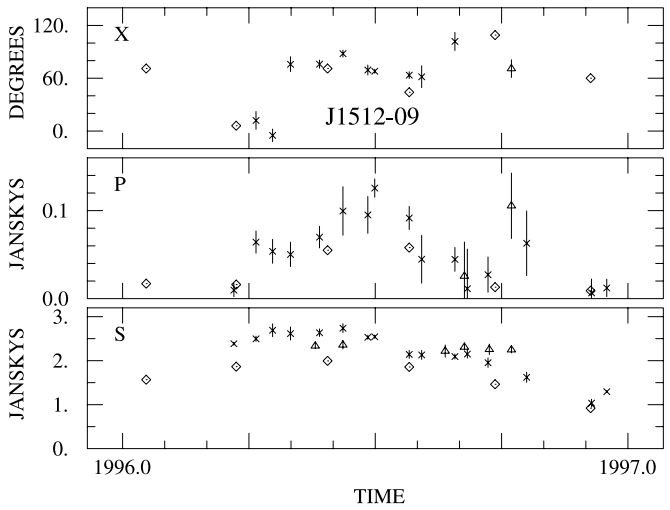

FIG. 35.—Single-dish monitoring data for J1512−090 for the year 1996. Plots are laid out as described in § 3.3.

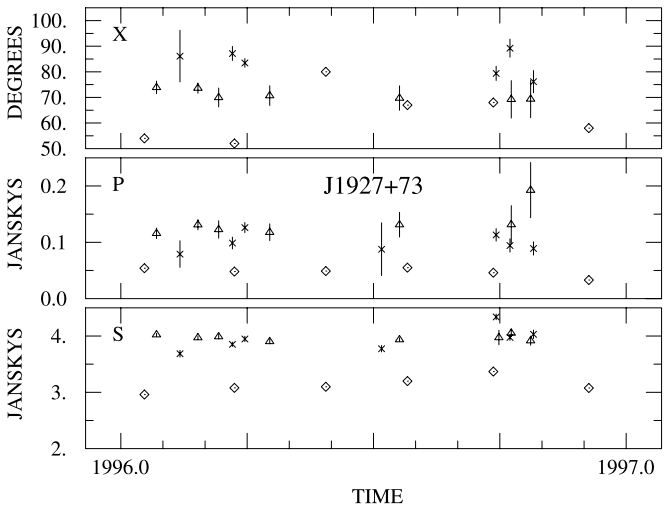

FIG. 37.—Single-dish monitoring data for J1927+739 for the year 1996. Plots are laid out as described in § 3.3.

changes in the atmosphere occur on shorter timescales and opacity corrections were needed. This extra work was justified as the higher frequencies gave us better resolution, made us more sensitive to outbursts (outbursts have a higher amplitude at shorter wavelengths), and the effects of Faraday rotation are minimal.

Observing at two closely spaced frequencies allowed us to disentangle Faraday effects from changes in magnetic field order. It allowed us to study spectral evolution of source components and to deduce empirical estimates for the uncertainties in measuring properties of jet features (Paper II, Appendix).

Finally, polarization information not only allowed us to investigate the properties of the magnetic field structures and the kinematics of the jet that they trace (Paper II), but also provided a means of unambiguously identifying jet features that was crucial to a robust study of proper motions (Paper I).

We thank C. C. Cheung and G. Sivakoff for their assistance in the initial organization of the model fit data. This work has been supported by NASA grants NGT-51658 and NGT5-50136 and NSF grants AST 91-22282, AST 92-24848; AS T94-21979, AST 95-29228, AST 98-02708, and AST 99-00723. This research has made use of the NASA/IPAC Extragalactic Database (NED), which is operated by the Jet Propulsion Laboratory, California Institute of Technology, under contract with the National Aeronautics and Space Administration. This research has made use of NASA's Astrophysics Data System Abstract Service. R. O. dedicates this paper to L. L.

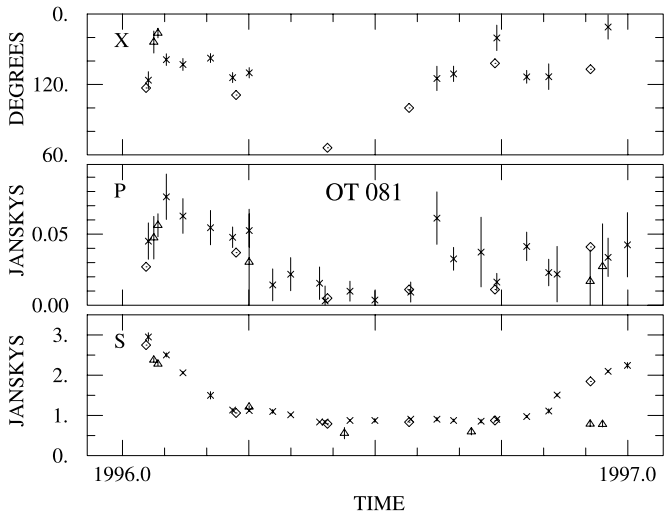

FIG. 36.—Single-dish monitoring data for J1751+09 for the year 1996. Plots are laid out as described in § 3.3.

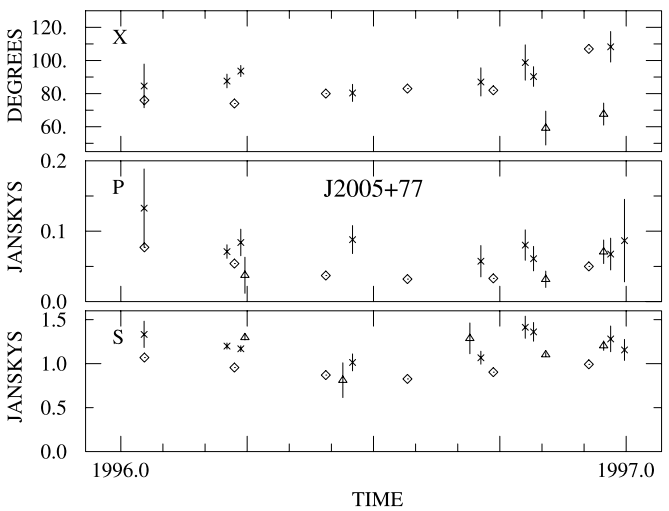

FIG. 38.—Single-dish monitoring data for J2005+778 for the year 1996. Plots are laid out as described in § 3.3.

APPENDIX

PLOTS OF CORE REGION AND JET FEATURE PROPERTIES

In this Appendix we present plots of the core region and jet feature properties, which are analyzed in detail in Paper II. These core regions and jet features were formed by simply summing the flux of model components that we could not confidently treat as separate units. Table 27 lists the core regions and jet features analyzed in Paper II and lists the model components which comprise them. The plots appear in Figure 39 and are included here as a service to the reader; they are not discussed or analyzed in this paper.

TABLE 27
CORES AND JET FEATURES

Object	Core and Jet Feature	$\langle R \rangle$ (pc)	$\langle \theta \rangle$ (deg)	N_I	N_P
3C 120	KD+K3+K2/UD+U2	0.13	−121.5	6	...
	K1A+K1B/U1A+U1B	1.99	−110.3	6	6
J0530+13	KD+K2/UD+U2	0.50	91.3	6	5
J0738+17	KALL/UALL	2.23	65.4	6	...
OJ 287	KD+K4/UD+U4	0.09	−106.1	6	6
	K3/U3	2.76	−94.7	6	5
J1224+21	KD+K4+K3[a]/UD+U3	0.34	−14.2	5	5
3C 273	KD+K10/UD+U10	0.35	−118.2	6	...
	K9+K8+K7/U9+U8+U7	5.11	−118.2	6	6
	K4+K5/U4+U5	13.2	−111.4	6	6
3C 279	KD+K4/UD+U4	0.32	−119.0	6	6
	K1+K2/U1+U2	18.6	−114.6	6	6
J1310+32	KALL/UALL	2.80	−63.1	6	5
J1512−09	KD+K2/UD+U2	0.25	−32.7	6	5
	K1/U1	7.49	−28.6	6	6
J1751+09	KD/UD+U3	0.09	35.1	6	...
J1927+73	KD+K3/UD+U3	1.12	150.8	6	...
	K2/U2	8.06	157.3	6	5
	K1/U1	9.41	172.9	6	6
J2005+77	KD+K2/UD+U3+U2	0.73	−91.0	6	6
	K1/U1	8.13	−94.1	6	...

NOTES.—The mean radial position of the jet feature is given by $\langle R \rangle$ at a mean structural position angle of $\langle \theta \rangle$ (measured counterclockwise from north). N_I is the number of epochs available for total intensity variability analysis, and N_P is the number of epochs available for polarization variability analysis. Not all features have adequate polarization strength in at least five epochs (at both frequencies) to be used for variability analysis; these cases are indicated by ellipses. See Paper II for a description of our selection criteria.

[a] In epoch 1996.23, component "Kz" in Table 11 is the combination of "K4+K3".

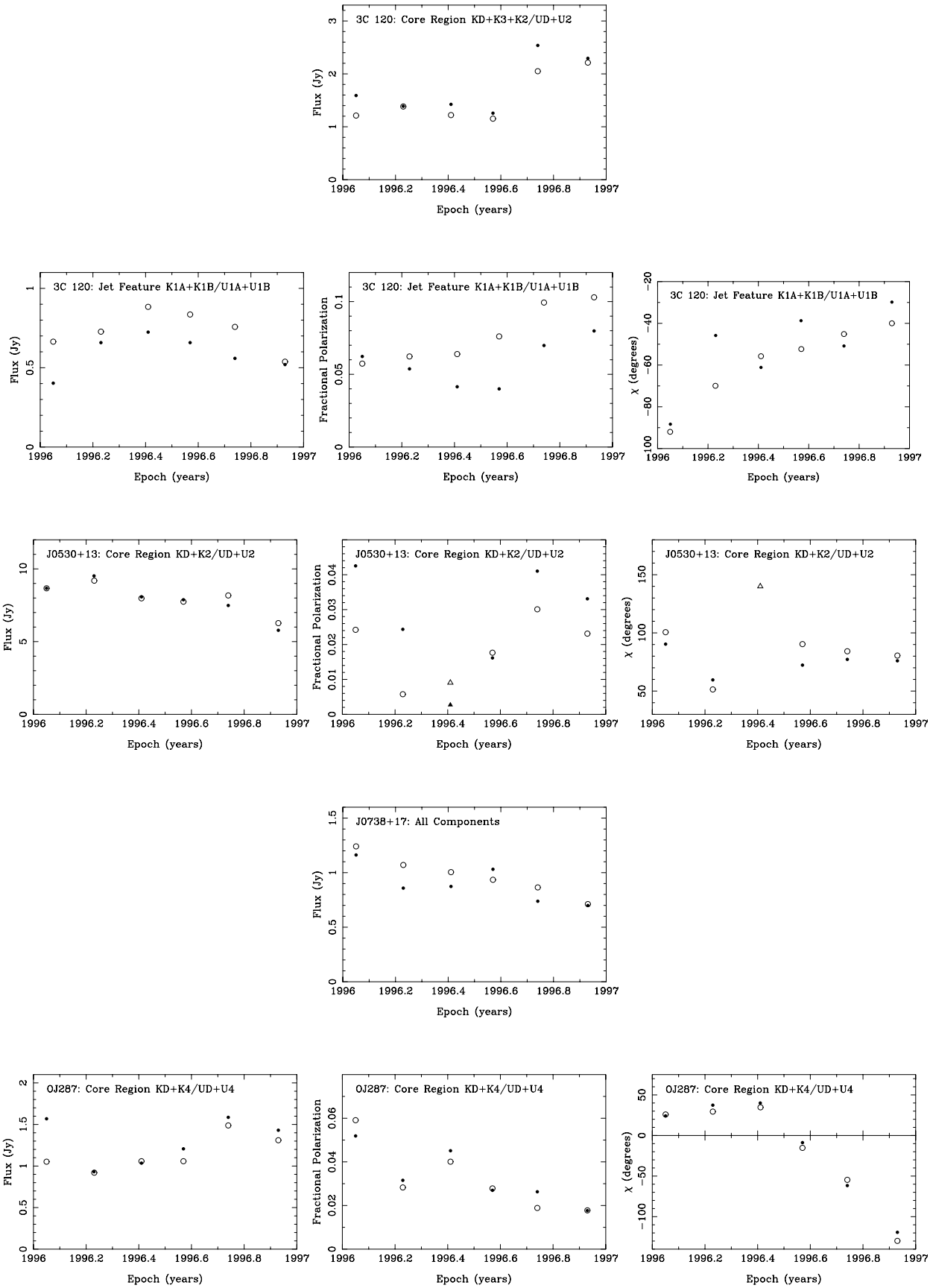

FIG. 39.—Plots of core region and jet feature properties vs. time for the features analyzed in Paper II. One core region or jet feature is plotted on each line with total intensity, fractional polarization, and polarization angle (χ) plotted from left to right. Filled symbols indicate 22 GHz measurements and open symbols indicate 15 GHz measurements. Epochs with sufficient polarization strength to meet the criteria for variability analysis in Paper II are plotted with circles. Triangles represent epochs omitted from the variability analysis in Paper II due to insufficient polarization strength in one or both frequencies. Points with insufficient polarization strength are omitted from the χ plots.

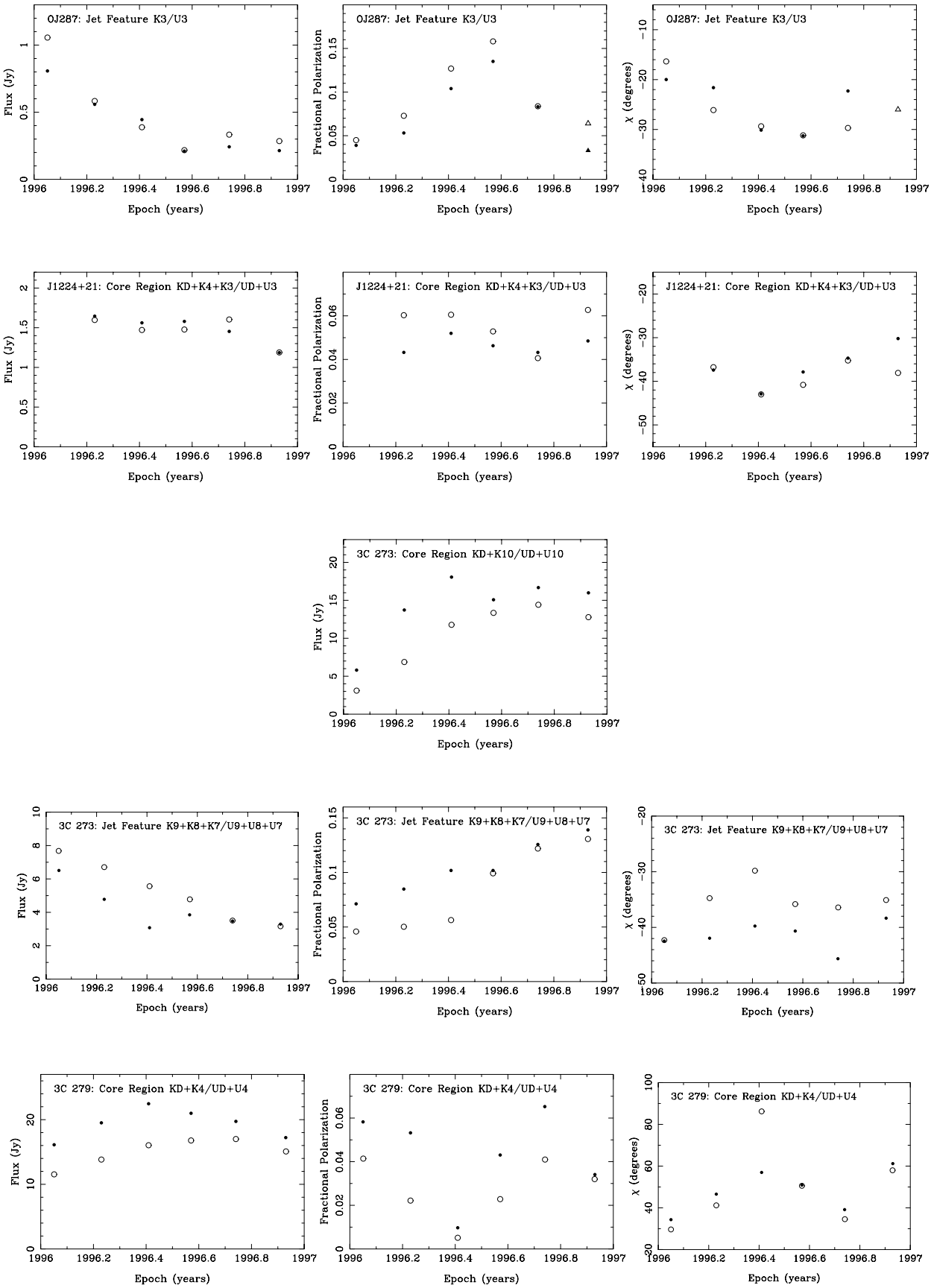

FIG. 39.—*Continued*

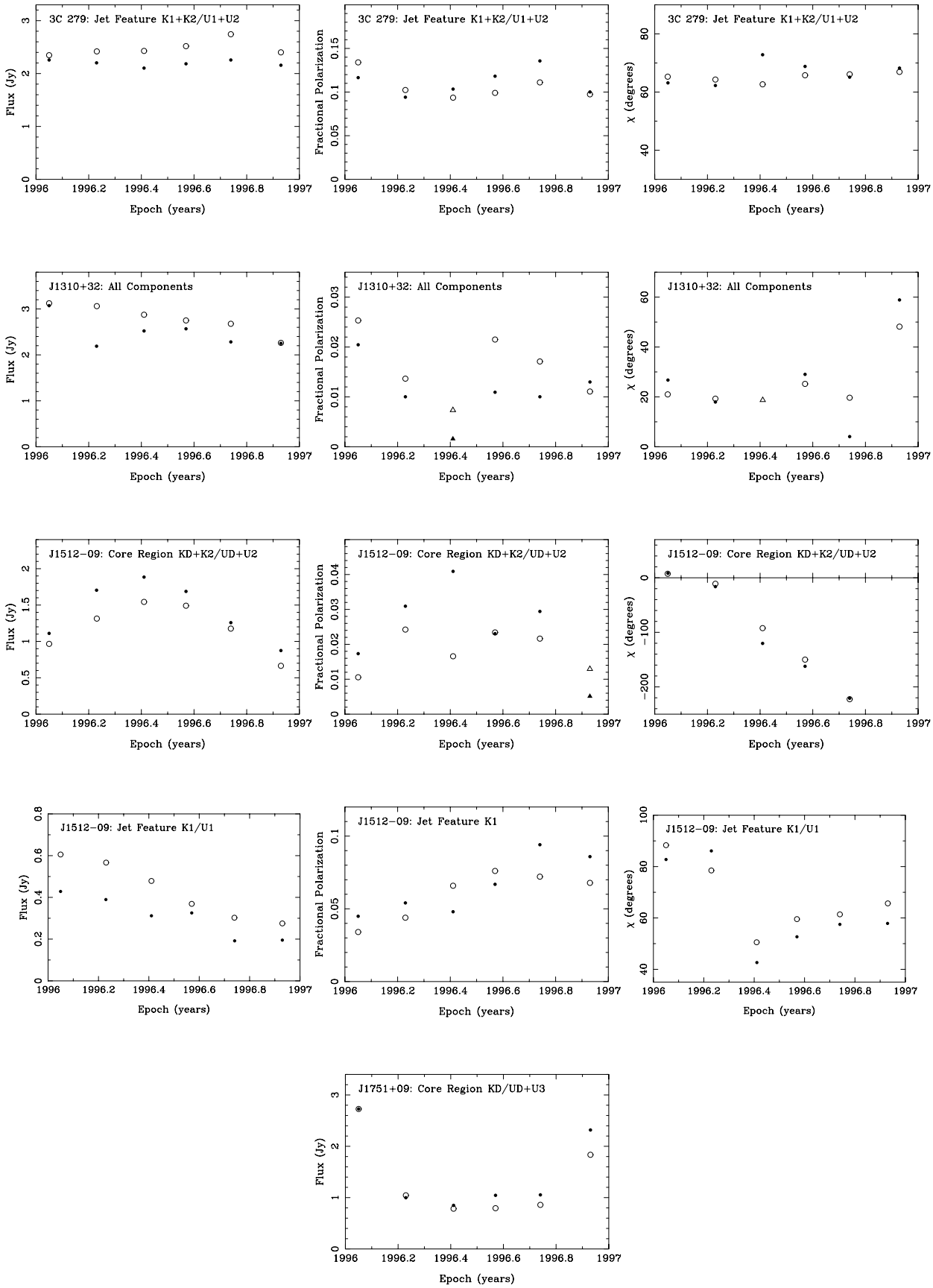

FIG. 39.—*Continued*

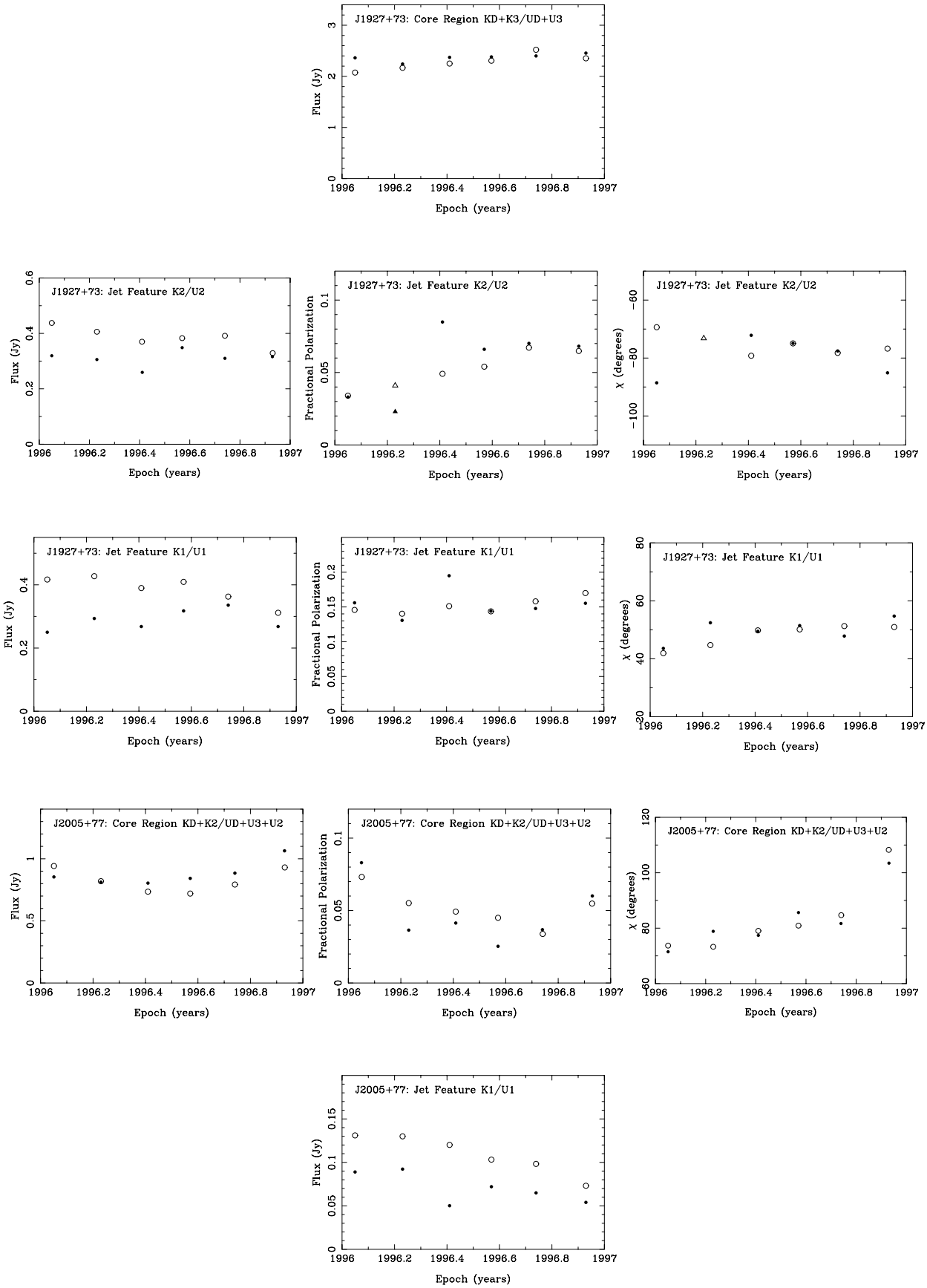

FIG. 39.—*Continued*

REFERENCES

Aller, H. D., Aller, M. F., Latimer, G. E., & Hodge, P. E. 1985, ApJS, 59, 513
Bridle, A. H., & Greisen, E. W. 1994, AIPS Memo 87
Cotton, W. D. 1993, AJ, 106, 1241
Greisen, E. W. 1988, AIPS Memo 61
Homan, D. C., Ojha, R., Wardle, J. F. C. W., Roberts, D. H., Aller, M. F., Aller, H. D., & Hughes, P. A. 2001, ApJ, 549, 840 (Paper I)
———. 2002, ApJ, 568, 99 (Paper II)
Homan, D. C., & Wardle, J. F. C. 1999, AJ, 118, 1942
———. 2000, ApJ, 535, 575
Homan, D. C. 1999, Ph.D. thesis, Brandeis Univ.
Leppänen, K. J., Zensus, J. A., & Diamond, P. J. 1995, AJ, 110, 2479
Ojha, R. 1998, Ph.D. thesis, Brandeis Univ.
Ott, M., Witzel, A., Quirrenbach, A., Kirchbaum, T. P., Schalinski, C. J., & Hummel, C. A. 1994, A&A, 284, 331
Pohl, M., et al. 1995, A&A, 303, 383
Roberts, D. H., Wardle, J. F. C., & Brown, L. F. 1994, ApJ, 427, 718
Shepherd, M. C. 1997, in ASP Conf. Ser. 125, Astronomical Data Analysis Software and Systems VI, ed. Gareth Hunt, & H. E. Payne (San Francisco: ASP), 77
Taylor, G. B. 1998, ApJ, 506, 637
Wardle, J. F. C., Homan, D. C., Ojha, R., & Roberts, D. H. 1998, Nature, 395, 457